

Charge Carrier Formation, Mobility and Microstructure of Sulfonated Polyelectrolytes for Electrochemical Applications

Von der Fakultät Chemie der Universität Stuttgart
zur Erlangung der Würde eines Doktors der Naturwissenschaften
(Dr. rer. nat.) genehmigte Abhandlung

Vorgelegt von

Andreas Wohlfarth

aus Sigmaringen

Hauptberichter: Prof. Dr. J. Maier

Mitberichter: Prof. Dr. S. Ludwigs

Prüfungsvorsitzender: Prof. Dr. T. Schleid

Tag der Einreichung: 24. Februar 2015

Tag der mündlichen Prüfung: 23. April 2015

Max-Planck-Institut für Festkörperforschung

Stuttgart

2015

*Gewidmet
meiner Familie und meiner
Verlobten Anita*

*“What you need as a researcher is
what Napoleon called fortune.
Not luck, but an eye for the right
moment.”*

Manfred Eigen

Erklärung über die Eigenständigkeit der Dissertation

Die vorliegende Doktorarbeit mit dem Titel 'Charge Carrier Formation, Mobility and Microstructure of Sulfonated Polyelectrolytes for Electrochemical Applications' wurde vom Autor selbst in der Abteilung von Prof. Maier am Max-Planck-Institut für Festkörperforschung, im Zeitraum von Oktober 2011 bis Februar 2015 angefertigt. Der Inhalt ist die eigene Arbeit des Autors, Ausnahmen sind gekennzeichnet, und wurde noch nicht zur Erlangung einer Qualifizierung oder eines Titels an einer akademischen Institution eingereicht.

Declaration of Authorship

The work described in this thesis entitled 'Charge Carrier Formation, Mobility and Microstructure of Sulfonated Polyelectrolytes for Electrochemical Applications' was carried out by the author in the Department of Prof. Maier at the Max Planck Institute for Solid State Research from October 2011 to February 2015. The contents are the original work of the author except where indicated otherwise and have not been previously submitted for any other degree or qualification at any academic institution.

Name/Name: _____

Unterschrift/Signed: _____

Ort/Place: _____

Datum/Date: _____

Table of Contents

Abstract	9
Zusammenfassung	12
List of papers	15
Chapter 1 Introduction and motivation	17
1.1 General aspects -----	17
1.2 PEM fuel cell -----	18
1.3 Lithium-ion battery -----	20
1.4 Motivation -----	22
1.5 Materials background-----	23
Chapter 2 Theoretical background	25
2.1 Liquid salt electrolytes-----	25
2.1.1 Electrostatic interactions -----	25
2.1.2 Short range interactions -----	27
2.1.3 Specific chemical interactions -----	28
2.1.4 Solvation -----	29
2.1.5 Ion pairing -----	31
2.2 Polyelectrolytes -----	32
2.2.1 Counterion condensation theory -----	22
2.2.2 Microconformation and microstructure -----	34
Chapter 3 Experimental background	35
3.1 Impedance spectroscopy -----	35
3.2 NMR techniques-----	36
3.2.1 General principle -----	36
3.2.2 Pulsed field gradient (PFG) NMR -----	38
3.2.3 Electrophoretic (E) NMR -----	41
3.2.4 Experimental considerations -----	42

Chapter 4 Results and discussion	45
4.1 Dissociation of sulfonated polyelectrolytes in solution -----	45
4.1.1 Influence of IEC -----	47
4.1.2 Influence of counterions -----	54
4.1.3 Influence of solvent -----	57
4.2 Solvent mixtures in polyelectrolyte solutions -----	64
4.2.1 High and low dielectric solvents -----	64
4.2.2 Lewis acid and base solvent mixtures-----	65
4.3 Dissociation and transport at high concentrations -----	68
4.3.1 Proton form-----	68
4.3.2 Lithium and sodium form-----	70
4.4 Microstructure of sulfonated polyelectrolytes -----	76
4.4.1 Influence of IEC -----	76
4.4.2 Influence of counterions -----	78
4.4.3 Influence of solvents -----	79
4.5 Acid-base blend membranes -----	81
4.5.1 General aspects -----	81
4.5.2 Concept -----	83
4.5.3 Synthesis of pyridine modified UDEL and blend formation -----	85
4.5.4 Acid-base interaction -----	86
4.5.5 Ion transport and water uptake -----	87
4.5.6 Mechanical properties -----	89
4.5.7 Microstructure -----	92
4.5.8 Lithium conducting 'membranes' for battery applications -----	92
Chapter 5 Summary and conclusion	95
Appendix	99
A1. Experimental details -----	99
A2. List of Abbreviations and Symbols -----	103
References	107
Danksagung	111
Curriculum vitae	113

Abstract

Polyelectrolytes are materials consisting of a polymer backbone with covalently attached positively or negatively charge groups including their counterions. Sulfonated polyelectrolytes are a specific class, which is especially interesting for electrochemical application as they can be used to separate the electrodes and mediate the electrochemical reactions taking place at anode and cathode by conducting a specific ion; this ion may be H^+ in the case of PEM-fuel cells or Li^+ and Na^+ in various battery systems. The key challenges for the development of these electrolytes is the combination of good mechanical properties and high ion transport as well as high electrochemical stability.

High ionic conductivity of polyelectrolytes depends on the presence of small polar solvents to ensure efficient dissociation and mobility of the counterions. These processes cannot be understood by merely considering electrostatics (i.e. Deby-Hückel approach) such as in Manning counterion condensation theory. Specific interactions between solvent-ion-polymer and the molecular conformations have to be taken into account as well. This is one of the results of the present work using sulfonated polyelectrolytes, different cations and solvents as model systems with a combined approach of experimental techniques and simulations.

The dissociation behavior of sulfonated polysulfones was investigated by a combined electrophoretic (E) NMR, pulsed magnetic field gradient (PFG) NMR and conductivity approach. Since the results from the NMR experiments, especially from E-NMR which is by far no standard measurement, are crucial for the key conclusions drawn in this thesis, some critical issues of this technique are studied and discussed in detail. E-NMR is essentially a PFG-NMR experiment with an applied electric field; the applied voltage can reach up to 300 V. Therefore, it was necessary to determine a measurement window in which no decomposition or other interfering effects appeared. In addition, polymers generally exhibit some polydispersity with the low molecular weight fraction

showing a higher diffusion coefficients and drift velocities, which had to be taken into account.

By concentrating ionic groups on the polymer, specific polyelectrolyte effects show up. Dissociation is no longer complete, the interaction between ionic charges and the solvent is heavily modified and correlations of ionic motion start to appear. According to a MD-simulation, this very much depends on the polymer conformation and position of the ionic groups as well as the chemical nature of the solvent. Once the density of ionic groups ($-\text{SO}_3\text{H}$) of polysulfones reaches a point where their average separation is of the order of the Bjerrum length of water, the degree of counterion condensation is shown to depend on details of the molecular structure and the accessible conformations of the polymer chain. In this regime, well-defined ionic aggregates occur, i.e. triple-ions form. The conformational details depend on the degrees of freedom and specific interactions between ions and solvent.

When it comes to ion conducting membranes, increasing the ion exchange capacity (decreasing the average separation of ionic groups) is a common measure to increase ionic conductivity. However, the results on dissociation and conductivity of synthesized polysulfones containing octasulfonated units (currently the material with highest known IEC) clearly reveal the limit of this approach. The short separation of ionic charges in such systems at high concentrations additionally leads to electrostatic interactions between neighboring polymer strands. This is the driving force for a nanoscale ordering in polyelectrolyte membranes. Different kinds of solvents, ions and ion exchange capacities directly affect the microstructure formation.

Finally, the effects of acid-base interactions between sulfonic acid-based polyelectrolytes and weakly basic modified polymers were investigated as blending of both is a way to form stable membranes for electrochemical applications. Here, the membrane formation process and the resulting properties, in particular proton conductivity, microstructure and mechanical strength have been studied. The developed polymer blends are the first example in which an improvement of mechanical properties not goes along with a significant decrease of proton conductivity. Key to success was to use a hydrophilic polymer with a high IEC and a hydrophobic polymer with a low number of basic groups.

In summary, this thesis provides insights into the charge carrier formation process, the transport and microstructure of sulfonated polyelectrolytes by identifying the relevant molecular interactions. Together with the superior mechanical properties of the developed blend membranes, this work significantly contributes to solve the key challenges for electrolytes in electrochemical application.

Zusammenfassung

Polyelektrolyte bestehen aus einem Polymerrückgrat mit positiv oder negativ geladenen, kovalent gebundenen Gruppen sowie deren Gegenionen. Eine spezielle Klasse sind sulfonierte Polyelektrolyte, die vor allem Anwendung in elektrochemischen Speichern finden und dort durch den Transport von verschiedenen Ionen die Reaktionen zwischen den Elektroden vermitteln. Die Ionen können Protonen (H^+) im Fall von PEM-Brennstoffzellen oder Lithium- (Li^+) bzw. Natrium-Ionen (Na^+) für verschiedene Batteriesysteme sein. Die größte Herausforderung für solche Elektrolyte ist die Kombination von guten mechanischen Eigenschaften und einem hohen Ionentransport zusammen mit einer hohen elektrochemischen Stabilität.

Die Ionenleitfähigkeit in Polyelektrolyten hängt von der Gegenwart kleiner polarer Moleküle (Lösemittel) ab, die zur Dissoziation und Beweglichkeit der Gegenionen führen. Vor allem die der Dissoziation zugrunde liegenden Mechanismen können nicht allein unter Berücksichtigung von elektrostatischen Wechselwirkungen (Deby-Hückel-Ansatz), wie z.B. in der Manning-Theorie, beschrieben werden. Spezifische Wechselwirkungen zwischen Lösungsmittel, Ionen und Polymer sowie die molekulare Konformation des Polymerrückgrats müssen zusätzlich berücksichtigt werden. Das ist bereits eines der ersten Ergebnisse der vorliegenden Arbeit an sulfonierten Polyelektrolyt-Modellsystemen mit verschiedene Kationen und Lösungsmitteln, die durch experimentelle Befunde zusammen mit Simulationen gewonnen werden konnten.

Ganz konkret wurde das Dissoziationsverhalten von sulfonierten Polysulfonen durch eine kombinierte elektrophoretische und gepulste Magnetfeldgradienten NMR sowie mittels Ionen-Leitfähigkeit Messungen untersucht. Da die Ergebnisse aus den NMR-Experimenten, vor allem aus der E-NMR, bei Weitem keine Standardmessungen sind, jedoch von entscheidender Bedeutung für die Kernaussagen sind, wurden einige kritischen Aspekte dieser NMR Technik im Detail untersucht. Die E-NMR ist im Wesentlichen ein PFG-NMR-Experiment mit bis zu 300 V starkem, angelegten

elektrischen Feld. Um chemische Zersetzung und andere störende Einflüsse durch die hohen Felder zu vermeiden, wurde ein Messfenster bestimmt. Zusätzlich muss berücksichtigt werden, dass Polymere eine Molmassenverteilung mit niedermolekularen Fraktionen zeigen, die höhere Diffusionskoeffizienten und Driftgeschwindigkeiten aufweisen.

Die Erhöhung der Konzentration an ionischen Gruppen auf dem Polymer führt zu spezifischen Polyelektrolyt-Effekten. Das bedeutet: Die Dissoziation ist nicht mehr vollständig und Wechselwirkungen zwischen Ionen und Lösungsmittel werden wichtiger sowie Korrelationen in der Ionenbewegung tauchen auf. Die Ergebnisse von MD-Simulationen zeigen einen sehr starken Einfluss der Polymerkonformation, der Position der ionischen Gruppen auf dem Rückgrat und der chemischen Natur des Lösungsmittels auf das Dissoziationsverhalten. Sobald die Dichte der ionischen Gruppen ($-\text{SO}_3\text{H}$) kleiner wird als die Bjerrum-Länge von Wasser, kommt es zur Gegenionkondensation, die dann wiederum von Details der molekularen Struktur sowie den zugänglichen Konformationen der Polymerkette abhängt. In diesem Bereich treten bestimmte ionische Aggregate, wie z.B. Dreifachionen auf.

Die Erhöhung der Ionenaustauschkapazität (Abnahme des mittleren Abstands der ionischen Gruppen) führt normalerweise bei ionenleitenden Membranen zur Erhöhung der ionischen Leitfähigkeit. Allerdings zeigen die erst kürzlich synthetisierten Polysulfone mit octasulfonylierten Einheiten (derzeit das Material mit der höchsten bekannten IEC) ein anderes Verhalten. Die Erhöhung der Konzentration an Sulfonsäuregruppen führt hier sogar zu einer Erniedrigung der Leitfähigkeit, was Weiterentwicklung dieser Materialien klar limitiert.

Eine unmittelbare Folge der Dissoziation in solchen Systemen ist das Auftreten von ionischen Wechselwirkungen zwischen benachbarten Polymersträngen. Welche die treibende Kraft hinter der Strukturbildung in Polyelektrolytmembranen auf der Nanometerskala sind. Des Weiteren konnte ein Einfluss der Lösungsmittel, der Art der Ionen und der Ionenaustauschkapazitäten auf die Strukturbildung gezeigt werden.

In einem zweiten Teil wurden Säure-Base-Wechselwirkungen zwischen Sulfonsäurebasierten Polyelektrolyten und schwach basisch modifizierten Polymeren ausgenutzt,

um mechanisch stabile Blendmembranen zu erhalten. Die Eigenschaften der so hergestellten Membranen wurden bezüglich Protonenleitfähigkeit, Mikrostruktur und mechanischen Eigenschaften untersucht. Die Ergebnisse dieser Messungen zeigen, dass die Polymerblends das erste Beispiele überhaupt sind, bei dem die Verbesserung der mechanischen Eigenschaften kaum die Protonenleitfähigkeit reduziert. Schlüssel zum Erfolg war die Verwendung von hydrophilen Polymeren mit hohem IEC und schwach basisch modifizierten hydrophoben Polymeren.

Zusammenfassend zeichnet die vorliegende Arbeit ein recht vollständiges Bild der Ladungsträgerbildung, des Transports und der Mikrostrukturbildung von sulfonierten Polyelektrolyten und identifiziert alle relevanten molekularen Wechselwirkungen. In Anbetracht der hervorragenden mechanischen Eigenschaften der entwickelten Polymermembranen liefert diese Arbeit einen Beitrag zu Verbesserung der zentralen Herausforderungen für Elektrolyte in elektrochemischen Anwendungen.

List of papers

This thesis is based on the following publications:

- I. **Wohlfarth, A.**; Smiatek, J.; Kreuer, K.D., Takamuku, S.; Jannasch, P.; Maier, J., Proton Dissociation of Sulfonated Polysulfones: Influence of Molecular Structure and Conformation. *Macromolecules*, 2015, DOI: 10.1021/ma502550f.
- II. **Wohlfarth, A.**; Takamuku, S.; Titvinidze, G.; Marino, M.; Melchior, J.; Kreuer, K.D., Acid-Base blending of highly sulfonated polysulfones. 2015, in preparation.
- III. Takamuku, S.; **Wohlfarth, A.**; Manhart, A.; Räder, P.; Jannasch, P., Hypersulfonated polyelectrolytes: preparation, stability and conductivity. *Polymer Chemistry*, 2015, DOI: 10.1039/C4PY01177E.
- IV. **Wohlfarth, A.**; Titvinidze, G.; Takamuku, S.; Meyer, W. H.; Kreuer K.-D., Polymer blends with high ion-exchange capacity and high ion-conductivity as well as methods for preparing the same *European Patent Application*, 2014, 14000404.5.
- V. Smiatek, J.; **Wohlfarth, A.**; Holm, C., The solvation and ion condensation properties for sulfonated polyelectrolytes in different solvents—a computational study. *New Journal of Physics*, 2014, 16, 025001.
- VI. Titvinidze, G.; **Wohlfarth, A.**; Kreuer, K. D.; Schuster, M.; Meyer, W. H., Reinforcement of Highly Proton Conducting Multi-Block Copolymers by Online Crosslinking. *Fuel Cells*, 2014, 14, 325.
- VII. **Wohlfarth, A.**; Maier, J.; Kreuer, K.-D.; Fuchs, A., Alkaline single ion conductors with high conductivity and transference number and methods for preparing the same *U.S. Patent*, 2013, 20130216936.
- VIII. Kreuer, K. D.; **Wohlfarth, A.**, Limits of proton conductivity. *Angewandte Chemie International Edition*, 2012, 51, 10454.

Chapter 1

Introduction and motivation

1.1 General aspects

Charged polymers appear all over nature and technology, often in solutions or swellable solids. These polymers are commonly named ionomers or polyelectrolytes, depending on the concentration of ionic or ionizable groups attached to the polymer backbone (Figure 1).[1] The term polyelectrolyte (i.e. polymerized electrolyte) describes the unique combination of salt and macromolecular like behavior. Based on the chemical structure, they are classified as polyanions, consisting of a negatively charged polymeric backbone with positively charged counterions, or vice versa as polycations.

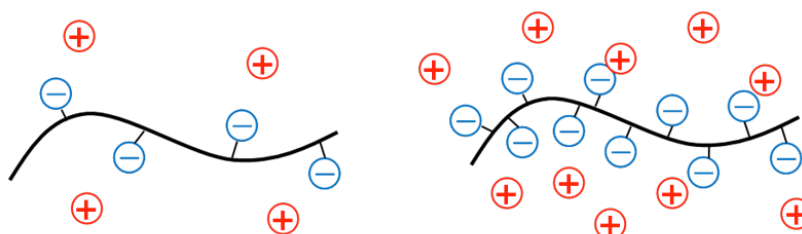


Figure 1: Schematic representation of an ionomer with a small number of functional groups and a polyelectrolyte with a substantial number of functional groups. Polymer backbone (black), fixed anionic group (blue) and counterion (red).

Several electrochemical conversion and storage systems rely on the excellent ion conducting properties of such ionomers or polyelectrolytes as separator and electrolyte material.[2] Depending on the application the mobile counterion can vary from protons or hydroxide ions in the case of polymer-electrolyte-membrane (PEM) fuel cells (FC), Li^+ in lithium-ion/-oxygen batteries, to non-electrochemically active anions or cations

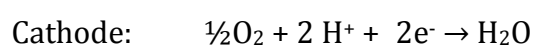
for redox-flow batteries. In the solid phase, the counterions are effectively immobile since they are condensed to the fixed ionic groups. Therefore, high ionic conductivity depends on the presence of small polar (solvent) molecules to ensure efficient dissociation and mobility of the counterions.

The key challenge for all electrolytes in electrochemical applications is the *combination of good mechanical properties and high (sometimes selective) ion transport*. [3] In light of this challenge, polyelectrolytes offer several advantages over classical salt-solutions or polymer electrolytes, such as the covalent attachment of either anion or cation to the polymer backbone resulting in only one kind of mobile charge carrier; often these materials are termed *single-ion conductors*. [4][5] In addition polyelectrolytes intrinsically offer a pronounced mechanical strength due to their macromolecular nature. However, there is a lack of understanding how microscopic features such as chemical structure, specific interactions or microconformation determine the macroscopic transport and mechanical properties.

In the following the principle of two of these applications, a PEM-FC and a lithium-ion battery are given with a special focus on role and development of polyelectrolytes as well as the studied specific class of materials is introduced and a detailed motivation of this work is given at the end of this chapter.

1.2 PEM fuel cell

A fuel cell is an electrochemical device that converts chemical into electrical energy. The commercialization of PEM FCs as power sources for cars is about to start this year, at least in small automotive series productions of Toyota[6] and Daimler[7]. In this type of fuel cell, a polymer membrane is placed between two porous carbon electrodes loaded with platinum (Figure 2). The electrochemical reactions taking place at the electrodes are:



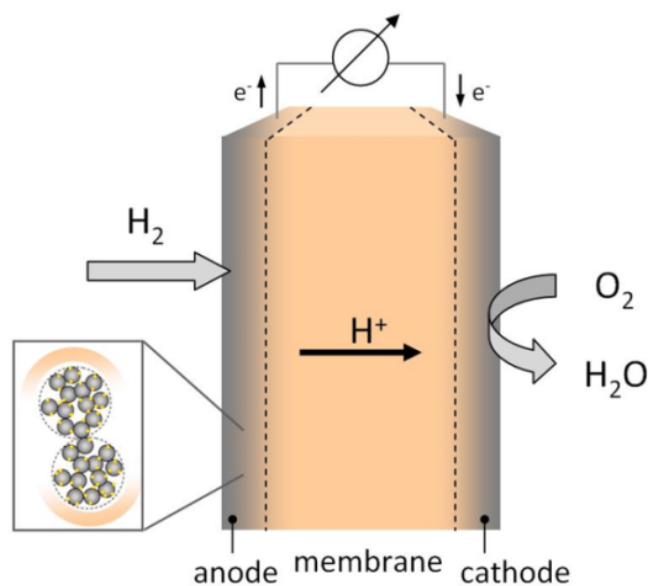
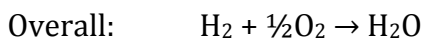


Figure 2: Schematic of a PEM-fuel cell with platinum on carbon electrodes. The membrane (orange) separate the electrodes and mediate the electrochemical reactions by conducting protons.

One of the most critical components in such an FC is the proton conducting membrane which is required to conduct protons while being impermeable to gases and electrically insulating. State of the art membrane materials are perfluorosulfonic acid polymers with Nafion[®] as the most prominent member of this family.[8][9] This material, actually developed for the chlor-alkali electrolysis about 60 years ago, unfortunately shows severe drawbacks in active fuel cells, such as mechanical failure at high temperature, inefficient proton conductivity at low degrees of hydration as well as high cost.

These issues prompted the development of various alternatives mainly based on fluorine free super-acidic sulfonated aromatic hydrocarbon ionomers and polyelectrolytes. A number of different synthetic strategies towards these materials are known: statistical post-sulfonation of polymers[10], polymerization of pre-sulfonated monomers[11][12], sulfonation of radiation-grafted films [13] and more sophisticated block synthesizes [14],[15],[16](e.g. block-copolymers and microblocks). An important finding during this development was the benefit of a high local concentration of ionic groups on the transport properties. Therefore one of the main current trends in the

PEM FC community is to locally increase the concentration of ionic groups on the polymer backbone i.e. going from ionomers to polyelectrolytes.[2][17] Most of these materials already show good or excellent ion conducting properties in the hydrated state but very poor mechanical properties, such as brittleness in the dry state and extensive swelling or dissolution in the wet state. Besides the improvement of mechanical properties the understanding of the physicochemical conductivity limits of such sulfonic acid based systems is of particular interest not only for a fundamental understanding but also for future materials developments.

1.3 Lithium-ion battery

The principle of the lithium-ion battery is based on the reversible insertion and extraction of lithium ions in and out of the electrode materials. The role of the electrolyte is to mediate the electrochemical reactions taking place at the electrode interfaces via the conduction of lithium-ions.[18]

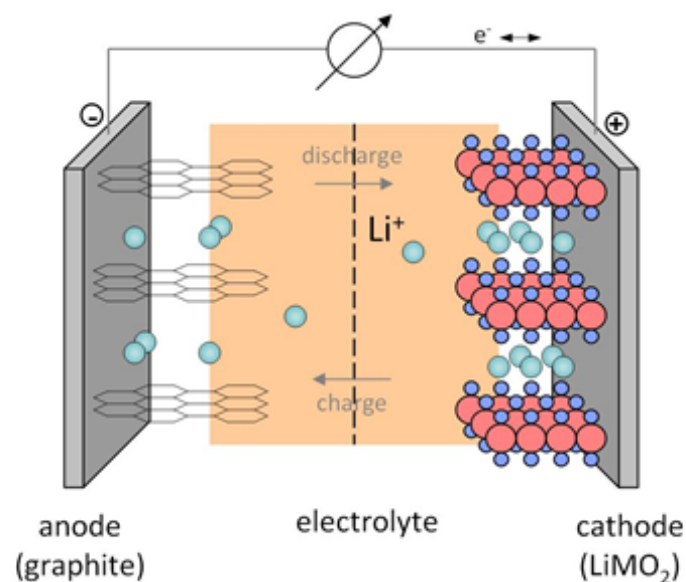
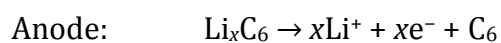


Figure 3: Schematic of a lithium-ion battery with negative graphite and positive LiMO₂ electrodes. Electrolytes (orange) separate the electrodes.

The reactions at the electrodes (discharge) in a conventional lithium-ion battery (Figure 3) made from a carbon anode and a metal oxide cathode are:



The commonly used electrolytes are aprotic, carbonate based solvents with high lithium-salt concentrations. Aqueous and protic electrolytes are not suitable due to their reaction with the electrodes causing immediate decomposition. [19] While aprotic electrolytes also do not show an intrinsically thermodynamic stability, they are kinetically stabilized e.g. by the formation of protective layers on the electrodes. Apart from stability issues also transport aspects have to be considered, i.e. the presence of contact ion pairs and higher aggregates lead to correlations in the ionic motion.[20] Polyelectrolytes offer a significant advantage in this regard as the fixed anionic groups (Figure 4) only allow the cations to diffuse, corresponding to a transference number of $t_+ = 1$. In contrast to conventional salt-containing electrolytes, no significant concentration polarization (anion accumulation close to the electrode over time) and associated decreasing electrical performance is expected in battery application.

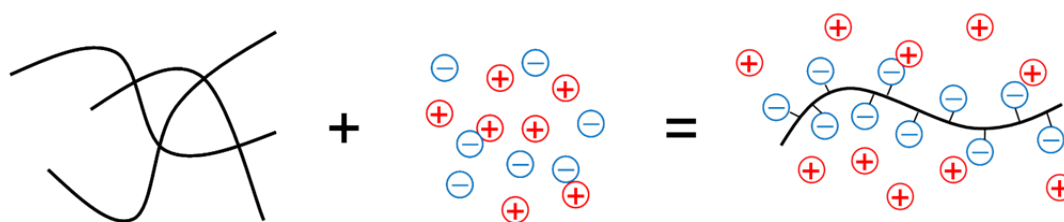


Figure 4: Schematic representation of immobilized anions. Polymer (black), anion (blue) and cation (red).

Polyelectrolytes are a rather new class of electrolytes for battery applications and in contrast to the protonic form, little is known about the properties of such materials in lithium (sodium) form especially in aprotic and apolar solvents. A recent study on lithium exchanged sulfonated poly(phenylene sulfones) showed single ion conductivities

of more than $\sigma = 1 \text{ mS cm}^{-1}$ with dimethylsulfoxide as solvent.[5] The approach was based on ionomers and polyelectrolytes originally developed for PEM fuel cell applications having highly acidic sulfonic acid groups. It was realized that the kind of solvents is critical to obtain efficient dissociation, but there is still no clear understanding of what are the important parameter and interaction between solvents and polyelectrolyte.

1.4 Motivation

The transport and structure formation of polyelectrolytes is influenced by a complex relationship of short-range and long-range interactions. A fundamental understanding of the underlying mechanisms and identifying the relevant interactions is of high importance. Current theoretical descriptions of polyelectrolyte systems rely only on simple electrostatic considerations and do not include influences of molecular conformations and short-range specific chemical interactions between solvent, polymer and counterion.

Aim of this work was to identify and explore the effects of these interactions on the charge carrier formation, the mobility and the microstructure on a class of polyelectrolytes based on different sulfonated poly(phenylene sulfones) (Figure 5). Especially the influence of the kind of solvents, counterion and local ion density is studied using a combined approach of experimental techniques (mainly PFG-/E-NMR, EIS and SAXS) and simulations (in collaboration with the University of Stuttgart).

Additional efforts were made to improve the mechanical properties of highly sulfonated poly(phenylene sulfones) using a novel acid-base blending concept. The influences of blending a weak basic modified polymer with a highly acidic polymer are studied with a special focus on mechanical stability under different conditions (relative humidity and temperature). Finally, all findings are discussed in context of the key challenges for separator materials in fuel cell and battery applications.

1.5 Materials background

The here investigated class of polyelectrolytes is based on sulfonic acid functionalized polysulfones. In principle two main synthetic routes to obtain such materials are known: postsulfonation of poly(arylenes) or the polymerization of pre-sulfonated units[10]. The first approach allows only for low degrees of functionalization up to an IEC of 1.8 - 2.4 meq g⁻¹ and the electrophilic substitution of electron-poor poly(arylenes) is extremely difficult [20]. However, the latter approach e.g. realized by a polycondensation reaction made it possible to obtain a material with each phenylene ring of the backbone mono-sulfonated and exclusively connected by electron-withdrawing sulfone linkages, resulting in extremely high IECs up to 4.55 meq g⁻¹. [12] The maximum functionalization using this strategy is limited to monosubstituted phenyl rings, as still conventional sulfonation procedures e.g., sulfuric acid or chlorosulfonic acid, are used to form the sulfonated monomer. As we will see later, (in close collaboration with MPI for polymer research and Lund University) it was recently even possible to synthesize a polymer having four sulfonic acid groups on a single phenyl ring. Key to success was to form the C-S bonds with an efficient substitution reaction in which highly activated fluorine atoms are displaced by strongly nucleophilic thiolate anions and subsequently oxidized to form the sulfonic acid groups. [22]

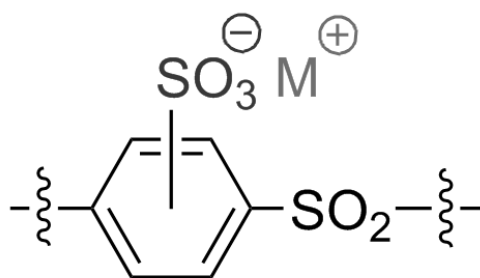


Figure 5: Basic unit of in this thesis investigated polyelectrolytes. A poly(phenylene sulfone) backbone with sulfonic acid group attached to the phenyl ring.

The simple architecture of sulfonated poly(phenylene sulfones) (Figure 5) allows for different local ion densities, polymerization degrees and positioning of the sulfonic acid groups, therefore making it an ideal model. Furthermore, the extremely electron-

deficient aromatic rings make the attached sulfonic acid groups very acidic and lead to high thermal, oxidative and hydrolytic stabilities when compared to other sulfonated poly(arylene)s.[10]

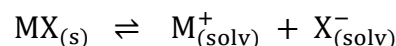
Chapter 2

Theoretical background

In the following some background for the understanding of the results and discussion part is presented. This includes a detailed description of the relevant interactions between solvent and ions in liquid electrolytes and polyelectrolyte solutions.

2.1 Liquid salt electrolytes

Liquid electrolytes are used for many electrochemical applications. The ion-conducting solutions comprise salts in solvents, which can vary from aqueous to nonaqueous and from polar to unpolar. Generally a salt MX will dissolve in a solvent forming ions, according to the dissociation reaction:



The dissolution process of ions is very complex and the dissociation is far from being complete. Especially in organic solvents[23], as we will see later, a high concentration of free ions is one of the keys to obtain high ionic conductivity in electrolytes[24]. Therefore the main interactions between solvents and ions driving dissociation are introduced in this chapter. They can be divided into short range, long range and specific chemical interactions.

2.1.1 Electrostatic interactions

The Coulomb interactions between charged particles occur over comparatively long distances. The potential energy $U(r)$ between two charged particles with charge numbers z_1 and z_2 separated by a distance r is described by the the Coulomb law[25]:

$$U(r) = \frac{e^2}{4\pi\epsilon_0\epsilon_r} \frac{z_1 z_2}{r}$$

where e is the elementary charge ϵ_0 is the vacuum permittivity and ϵ_r the dielectric constant of the solvents. In 1923 Debye and Hückel developed a theory[26] with the basic idea that the ions, since they are free to move in the solution, will arrange in such a way as to lower the potential energy. Thus, an ion of a charge z will always be surrounded by a higher than average density of ions of the opposite charge (see Figure 2.1). The enhanced local density of opposite charges will lead to a partly neutralization of ions.

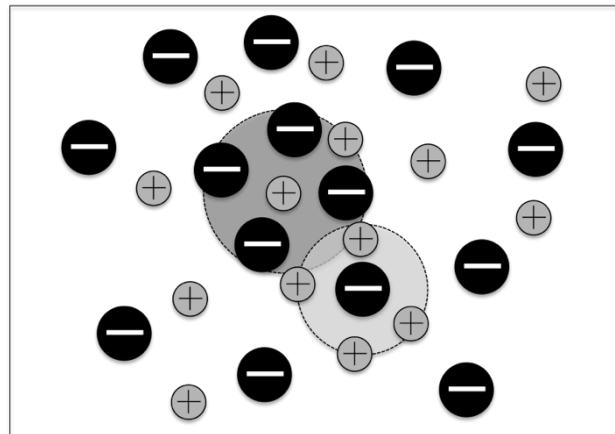


Figure 2.1: Charge distribution in solution.

The Debye-Hückel theory gives the correct Coulomb screening on long-length scales with several assumptions:

- Salts are completely dissociated into ions.
- Ionic interactions are described by the Coulomb law.
- Solvents are treated as continuous dielectric medium.

Especially the treatment of the solvent as continuum neglects important ion-solvent interactions. Additional to intermolecular forces (e.g. Waals forces) other short range

interactions between ions and neutral molecules have to be discussed for a more accurate description of an electrolytes.

2.1.2 Short range interactions

Ion-dipole forces

Solvent molecules with unsymmetrical charge distribution (polar solvents) possess a permanent dipole moment μ_d . Such permanent dipoles orient themselves with respect to an ion in order to minimize the potential energy. The attractive end of the solvent directs toward the ion and the repulsive end orients itself away from the ion. The ion-dipole interaction energy U is given by

$$U_{ion-dipol} = -\frac{1}{4\pi \cdot \epsilon_0} \frac{z \cdot e \cdot \mu_d \cdot \cos\theta}{r^2}$$

where ϵ_0 is the permittivity of a vacuum, $z \cdot e$ the charge on the ion, r the distance from the ion to the center of the dipole, and θ the angle between ion and the dipole. This interaction mainly occurs in the solvation shell of an ion.

Dipole-dipole forces

Solvent molecules with permanent dipole moments not only interact with the ions but also with each other. The positive side of a polar molecule attracts the negative side of another polar molecule. This dipole-dipole orientation is strongly temperature dependent and is described by

$$U_{dipol-dipol} = -\frac{1}{(4\pi \cdot \epsilon_0)^2} \frac{2\mu_{d1}^2 \cdot \mu_{d2}^2}{3k_B \cdot T \cdot r^6}$$

where k_B is the Boltzmann constant, and T is the absolute temperature. The appearance of such an interaction is mainly limited to solvents only.

Dipole-induced dipole forces

A solvent with permanent dipole moment can induce a dipole moment in neighboring solvent molecules. The magnitude of the induced dipole moment depends on the polarizability α_d of the solvents and is defined as

$$\mu_{induced} = 4\pi \cdot \epsilon_0 \cdot \alpha_d \cdot E$$

with E as the electric field strength. The induced moment directs along the dipole moment. The energy of dipole-induced dipole interaction U between solvent molecules is given by the following equation

$$U_{dipole-induced\ dipole} = \frac{1}{(4\pi \cdot \epsilon_0)^2} \frac{\alpha_{d1} \cdot \mu_{d2}^2 + \alpha_{d2} \cdot \mu_{d1}^2}{r^6}$$

Ion-induced dipole forces

In addition to the solvent induced dipole moment, there also can be an induced solvent polarization by ions in the electrolyte. The magnitude of the ion-solvent induced polarization depends on the polarizability α of the solvent molecules. The energy U of ion-induced dipole interaction is

$$U_{ion-induced\ dipole} = \frac{1}{(4\pi \cdot \epsilon_0)^2} \frac{z^2 \cdot e^2 \cdot \alpha}{2r^4}$$

The importance of both the dipole- and ion-induced dipole Forces is limited to situations such as mixtures of dipolar and nonpolar solvents or solutions of ionic compounds in nonpolar solvents.

2.1.3 Specific chemical interactions

Hydrogen bonding

Generally hydrogen bonding is the attraction of a covalently bound hydrogen atom to another atom.[27] A hydrogen bond is a type of polar interaction with the electropositive hydrogen atom located between two electronegative atoms. Such an interaction occurs when a proton donor (electronegative atom with a covalent

hydrogen bond) attracts a lone electron pair of an acceptor group, forming a directional bond to the acceptor group.

The most important electron pair donors (hydrogen bond acceptors) are the oxygen atoms in ethers, and carbonyl compounds, as well as nitrogen atoms, whereas compounds with easily polarizable groups such as acid-, amino-, and amide groups are the most important proton donors. The hydrogen bond formation can be regarded as a first step in a Brønsted acid-base reaction, but the full transfer of the proton requires a higher electronegativity difference between donor and acceptor groups.

Electron donor-acceptor interactions

An electron pair donor-acceptor complex is formed between molecules with occupied orbitals of high energy (donor) and molecules with unoccupied orbitals of sufficiently low energy (acceptor). The strength of this interaction is typically referred to as Lewis basicity (nucleophiles) or Lewis acidity (electrophiles).

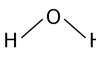
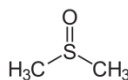
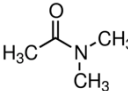
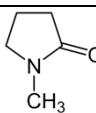
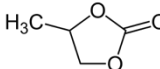
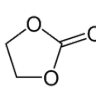
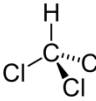
Gutmann et al. have developed a semi-quantitative scale for the Lewis basicity (LB) [28] and acidity (LA) [29] of solvents. The degree of nucleophilicity (LB) of solvents, called the donor number (DN) is defined as the negative ΔH value for 1:1 adduct formation between the antimony pentachloride (SbCl_5) and the solvent molecules in question in a dilute solution of non-coordinating 1,2-dichloroethane. A semi-quantitative electron acceptor ability (accepting number, AN) for electrophilic (LA) solvents has also been developed based on ^{31}P -NMR chemical shift of triethylphosphine oxide ($\text{Et}_3\text{P}=\text{O}$) in presence of the solvents in 1,2-dichloroethane. The chemical shift for n-hexane is as reference. The following table gives the DN, AN and the dielectric constant ϵ for solvents investigated in this thesis:

2.1.4 Solvation

The above described interactions between ions and solvent molecules are involved in the thermodynamics of ion solvation. The free energy of solvation $\Delta G_{\text{solvation}}$ is the

change in Gibbs energy when an ion is transferred from vacuum into a solvent (see Figure 2.2). A salt will dissolve only if the stabilizing interactions of solvents in solution, including entropic effects overcome the free energy of ions in the crystalline state.

Table 2.1: Solvent properties and chemical structure.[23]

solvents	chemical structure	donor-number (DN)	acceptor number (AN)	dielectric constant ϵ
water		18	54.8	80.1
dimethylsulfoxide (DMSO)		29.8	19.3	47.2
N,N-dimethyl-acetamide (DMAc)		27.8	13.6	37.8
N-Methyl-2-pyrrolidone (NMP)		27.3	13.3	32.2
propylene carbonate (PC)		15.1	18.3	64.9
ethylene carbonate (EC)		16.4	-	89.8
Chloroform		0	23.1	2.2

Solvation number

The solvation number is the number of solvent molecules in the primary solvation shell of the ion. The translational and rotational dynamic of solvating molecules is different from those in bulk solution. According to the HSAB concept higher solvation numbers are found for harder ions (small size) compared to softer ions (large size). The alkali

metal-ions solvation number increases in the order $(\text{Cs}^+) < (\text{Rb}^+) < (\text{K}^+) < (\text{Na}^+) < (\text{Li}^+)$. [31]

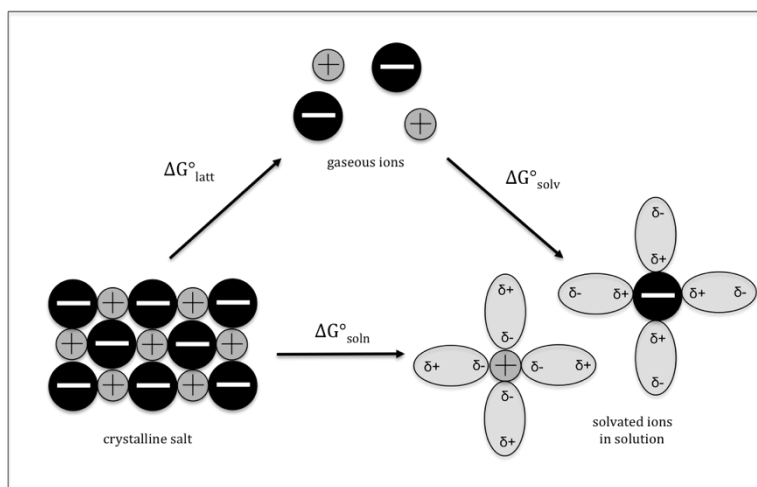


Figure 2.2: Born Haber cycle of dissolution.

2.1.5 Ion pairing

The simple two state model of dissociation introduced in the beginning can be expanded by including different intermediate states between the condensed and dissociated state (see Figure 2.3) as to obtain a more realistic picture. [30][31] Salts in solution will form contact ion pairs without any solvent molecules between anion and cation. Such a contact ion pair possesses an electric dipole moment and has a joined solvation shell for both ions.

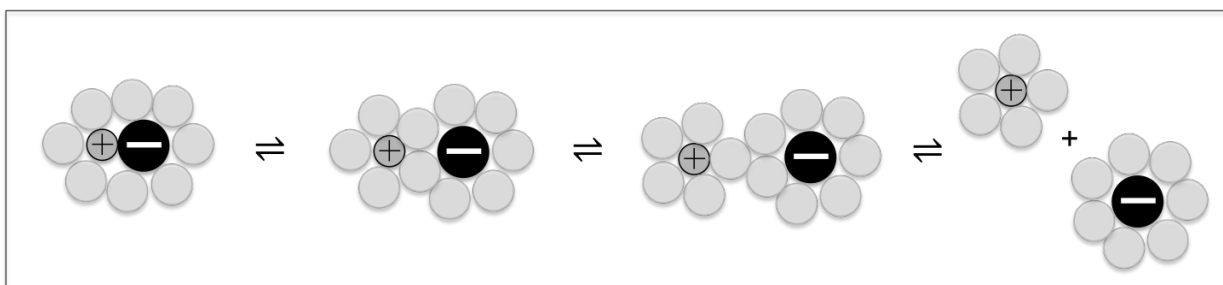


Figure 2.3: Schematic representation from left to right of a solvated contact ion pair, a solvent-shared ion pair and a solvent-separated ion pair and solvated dissociated ions.

In the next step the ion pair is separated by only one solvent molecule and is called a solvent shared ion pair. In such a solvent-shared ion pair, the two ions already have their own primary solvation shells with some overlap. Further dissociation leads to solvent separated ion pairs with a primary solvation shell for each ion separately but the two ions are still close to each other. By further increasing the spatial separation the ions are completely dissociated. All these intermediate states may appear in electrolytes at the same time and depend on the solvation ability of the solvent.

2.2 Polyelectrolytes

Just as the properties of salt solution also polyelectrolyte solutions are governed by an intricate balance of interactions on different length scales but additionally dependent on the polymer chain properties. The macro-ions in polyelectrolyte solutions show both intramolecular and intermolecular interactions. This makes the description of polyelectrolyte systems very complex and the main reason why theoretical models are less developed than for salt solutions.

2.2.1 Counterion condensation theory

In 1969 Manning introduced the concept of counterion condensation[32][33][34], which still is the most often used model to describe the interaction of polyions and their counterions in solution. The model assumes the polyion to be an infinitely long rigid rod with equally spaced charges. The counterions are either electrostatically bound/condensed to the polyelectrolyte backbone or unbound/free.

For a quantification of counterion condensation the electrostatic screening length (Bjerrum length λ_B) is introduced:

$$\lambda_B = \frac{e^2}{4\pi \cdot \epsilon_0 \cdot \epsilon \cdot kT}$$

The Bjerrum length λ_B is a function of the solvent permittivity and gives the distance between two charges, at which the electrostatic energy equals thermal energy kT . The ratio of Bjerrum length and charge spacing b , gives the so-called Manning parameter ξ_M :

$$\xi_M = \frac{\lambda_B}{b}$$

Evaluation of the populations of condensed and free counterions then leads to the simple finding that ξ_M correlates to the fraction of condensed counterions. Counterion condensation is expected to occur for $\xi_M \geq 1$ (see Figure 2.4). Usually, the fraction of condensed counterions f_ξ is expressed as:

$$f_\xi = 1 - \frac{1}{\xi}$$

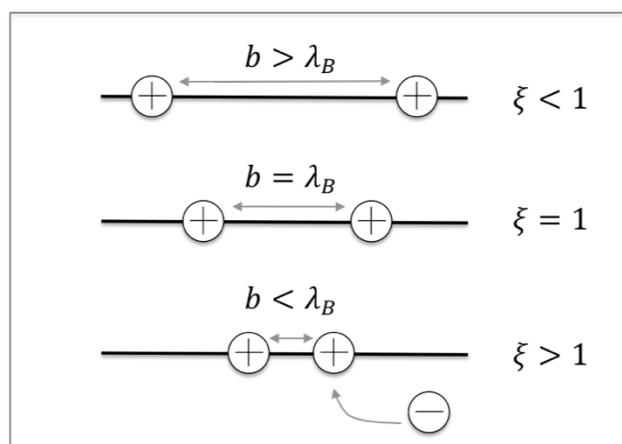


Figure 2.4: Schematic illustration of the concept of Manning counterion condensation for different charge spacing b , black line represents a still linear polyelectrolyte with positive charges.

In recent years further developments of the theoretic description of dissociation in polyelectrolytes have been made. For example, the cylindrical cell model or charged cylindrical cell model[35][36] uses a cylindrical volume around the polyelectrolytes in which counterions are distributed. Another prominent theory developed by Mutukumar [37] even allows for flexible polyelectrolyte backbones. However, these theories entirely treat the surrounding solvents as continuous medium and only interactions within the Debye-Hückel theory are considered. Furthermore all models only rely on

single chains without the possibility of intermolecular interactions. But despite all assumptions made in Mannings counterion condensation theory this simple approach is still the most successfully concept to estimate dissociation in diluted polyelectrolytes.

2.2.2 Microconformation and microstructure

The complex interplay of different interactions in polyelectrolyte solutions (e.g. van-der-Waals forces, ionic, steric and dipole-dipole interactions within the polymer as well as to the surrounding solvents) leads to a structural organization of the polymer chains. Specific stable local conformations, also called microconformations lead to preferred structural organization of single polymer chains into coil or coil-like shape.[38]

At high concentration or in the solid form not only intramolecular but additional intermolecular interactions between different polymer chains need to be considered as well. For example in the membrane form, most polyelectrolytes show a microstructural separation between the polymer and the solvent phase.[39] Both the microconformation and the microstructure of polyelectrolytes influence the transport of solvents and ions as well as the mechanical properties.

Chapter 3

Experimental background

The following chapter gives information for the understanding of the main characterization techniques: pulsed field gradient NMR, electrophoretic NMR and impedance spectroscopy. All experimental details are given in the appendix at the end of this thesis.

3.1 Impedance spectroscopy

The complex AC-Impedance spectroscopy (IS) is one of the standard techniques in determine electrical and ionic conductivities in the solid and the liquid phase, since the use of alternating currents (AC) overcomes all problems related to concentration polarization and stability effects at the electrodes present in direct current experiments. [40][41] The IS measurements can be done non-destructively and close to the thermodynamic equilibrium. Classical direct current measurements only reveal an effective overall resistance while frequency dependent measurements often give more detailed information on specific processes. For example the influence of the electrode/electrolyte interface can be separated from the electrolyte properties.

In an AC-IS experiment the current response I on a sinusoidal applied voltage U is evaluated for different frequencies from the mHz up to the MHz regime. The resulting complex resistance Z (also called impedance) is similar to the ohmic resistance given by:

$$Z = \frac{U}{I} = \frac{U_0 \cdot e^{i\omega t}}{I_0 \cdot e^{i(\omega t + \alpha)}} = \frac{U_0}{I_0} e^{-i\alpha}$$

with α being the phase angle. The impedance Z then can be separated in real and imaginary part.

$$Z = |Z| \cdot \cos \alpha - i|Z| \cdot \sin \alpha$$

The negative imaginary part of the impedance is plotted versus the real part of the impedance resulting in the so-called Nyquist diagram (see Figure 3.6). To evaluate the spectra equivalent circuits are used. In the simplest case of a pure charge transfer reaction it consists of an oscillating circuit containing a parallel connection of an ohmic resistor with a capacitor in series with a capacitor for the electrode polarization. In this work mainly the ohmic resistance of the electrolyte between two platinum electrodes was evaluated. Then the ionic conductivity σ can be calculated from the resistance using a geometrical cell constant ($d(\text{thickness})/A(\text{electrode surface})$)

$$\sigma = \frac{1}{R} \cdot \frac{d}{A}$$

The ionic conductivity is typically strongly temperature dependent and often shows Arrhenius like behavior.[25]

3.2 NMR techniques

Different setups of nuclear magnetic resonance (NMR) spectroscopy are used as techniques for structure determination and studies of molecular dynamics.[42] Thereby a major advantage of NMR is its sensitivity to different nuclei including the influence of their chemical environment.

3.2.1 General principle

A spin of particles with non-zero quantum spin number I will, when placed in an external magnetic field B_0 , split into different energy states E_z (Zeeman splitting). The different magnetic quantum m_I numbers correspond to different energy states

$$E_z = m_I \cdot \gamma \cdot \hbar \cdot B_0$$

with E the energy, B the local magnetic field strength, γ is the gyromagnetic ratio and \hbar the reduced Planck constant. The energy difference ΔE_z between different spin levels depends on the Larmor frequency ω_L and is given by

$$\Delta E_z = \hbar \cdot \omega_L$$

The description of spin systems is commonly done by the Bloch equations[43] using a simplified model of magnetic moment vectors $\vec{\mu}_i$. The net magnetization \vec{M} for a sample is the sum of the individual magnetic moments in the sample volume V .

$$\vec{M} = \frac{\sum_i \vec{\mu}_i}{V}$$

The magnetization of a nucleus in equilibrium rotates along the z-axis. It is possible to change the net magnetization by exposing the sample to energy with a frequency equal to the energy difference between the spin states (equaling to the Larmor precession rate). Enough energy will place the net magnetization in the xy-plane (usually referred to as 90° pulse, see Figure 3.1 left). Here, the net magnetization starts to dephase (rotation at different Larmor frequencies for each spin) with a characteristic time T_2 (spin-spin relaxation) caused by slightly different magnetic field. A spectrum is obtained by acquiring this so called time-dependent free induction decay FID, (see Figure 3.1 left) followed by a Fourier transformation into the frequency domain. NMR spectra (see Figure 3.1 bottom) are usually given in chemical shifts δ , which is the resonant frequency ν of a nucleus relative to a standard:

$$\delta = \frac{\nu_{sample} - \nu_{ref}}{\nu_{ref}}$$

The magnetization in the xy-plane also can be refocused by a 180° pulse. The previously defocusing magnetization is now mirrored in the xy-plane and refocused at the original position. The resulting signal is called spin-echo.

Magnetization can also be stored along the z-axis for some time in between the defocusing and refocusing pulses; the resulting signal is then called a stimulated-echo (see Figure 3.1 right). In such an experiment the conversion of the non-equilibrium to the equilibrium spin population underlies a longitudinal relaxation process with the

characteristic time T_1 affecting the components of \vec{M} parallel to the external magnetic field (also called spin-lattice relaxation). For large and rigid molecules, such as polymers, the longitudinal relaxation typically is slower than transverse relaxation. This is important, as the faster transversal relaxation with characteristic time T_2 would not always allow for long enough experiment times to study molecular motion. Therefore all PFG- and E-NMR experiments in this thesis are carried out using stimulated echo pulse sequences.

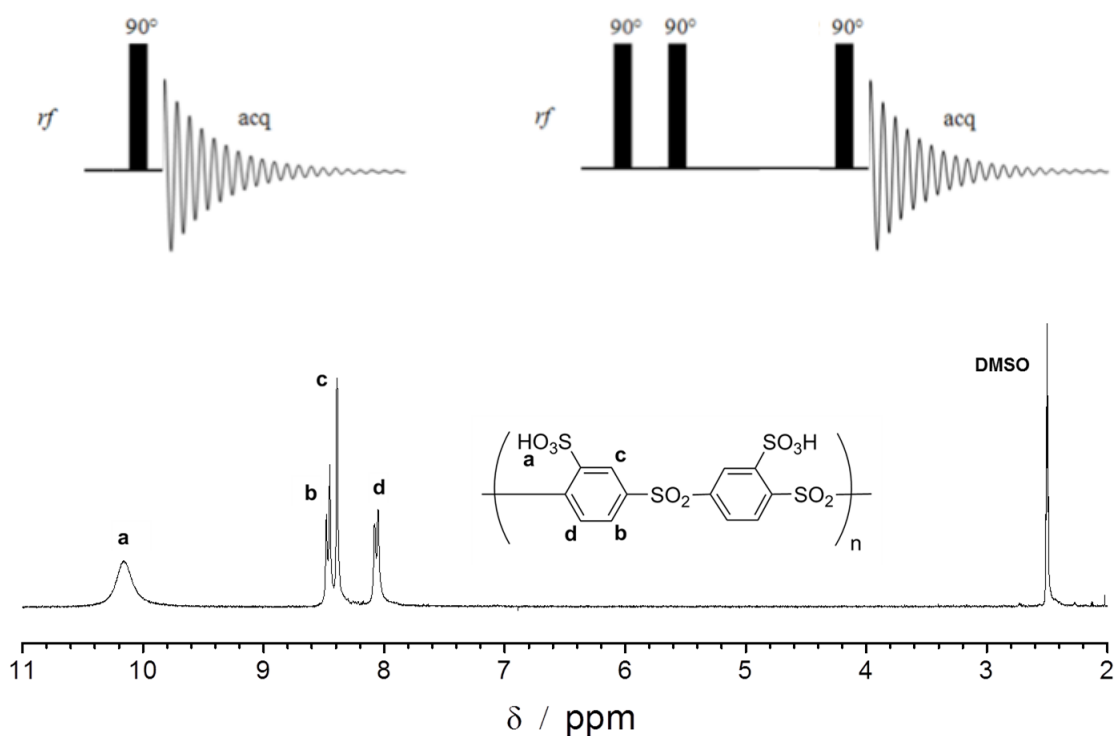


Figure 3.1: top left: 90° RF-pulse and FID. Top right: Stimulated-echo pulse sequence. Bottom typical ^1H -polymer NMR spectra of sulfonated polysulfone dissolved in dimethylsulfoxide.

3.2.2 Pulsed field gradient (PFG) NMR

The addition of controlled magnetic field gradients to the sample space during NMR experiments introduced a way to spatially label and probe the spins at different times. [44][45][46] The combination of spin-echo pulse sequences and short-pulsed magnetic

field gradient makes it possible to probe molecular displacement of both spatially incoherent and coherent nature.

Pulsed field gradient NMR is a modification of a spin echo experiment[47]. Instead of keeping the magnetic field B_0 constant a gradient is applied along the field direction. Nuclei in the sample are spatially labeled by a first gradient pulse and after a defined diffusion time Δ decoded by a second gradient pulse, which is equal in length and duration to the first pulse (see Figure 3.2a).

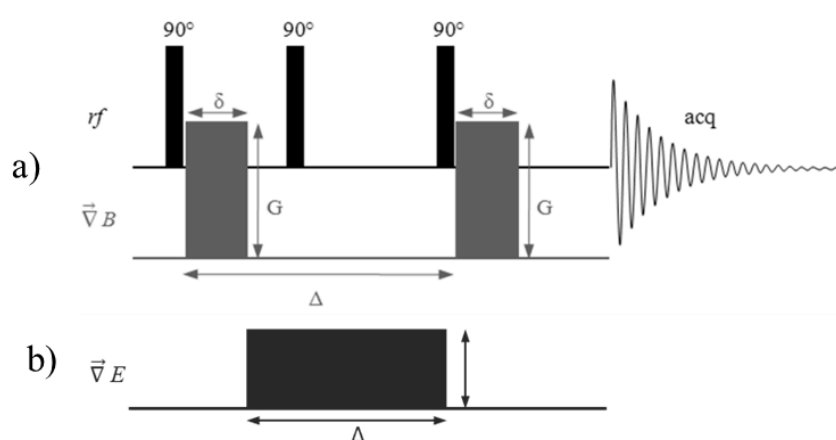


Figure 3.2: a) PFG-stimulated-echo pulse sequence. b) Additional applied electric field of E-NMR pulse sequence.

During the time between the two gradient pulses the nuclei randomly diffuse. After the second pulse each spin shows a phase-error proportional to displacement in z -direction, which depends on the gyromagnetic ratio γ , the gradient field strength g , the duration of the magnetic field pulse δ_m , the time between the two gradient pulses Δ and the particle displacement

$$\Delta\Phi \sim \gamma \cdot g \cdot \Delta \cdot (z_1 - z_2) \cdot \delta_m$$

The inhomogeneous magnetic field spatially modifies the Larmor frequency of nuclei along the gradient direction. Change in position by incoherent, randomly motion (self-diffusion) corresponds to an offset of the Larmor frequency. For all nuclei together this results in a less refocused signal of the overall signal intensity. The signal intensity is

varied by different gradient strengths and can be described by the Stejskal-Tanner equation[46]

$$\ln \frac{I_G}{I_0} = -D_{tr} \cdot \gamma^2 \cdot g^2 \cdot \delta_m^2 \cdot \left(\frac{\Delta - \delta}{3} \right)$$

with I_G is the signal intensity with magnetic field gradient applied, I_0 the signal intensity without magnetic field gradient applied and D_{tr} the diffusion coefficient. By plotting the normalized signal intensity as function of the NMR parameter the diffusion coefficient can be calculated (see Figure 3.3).

Polymeric samples usually show some polydispersity with a low molecular weight fraction showing higher diffusion coefficients and drift velocities. This leads to a multiexponential echo attenuation in the PFG-NMR experiment (see Figure 3.3) making the diffusion coefficient evaluation rather complex.

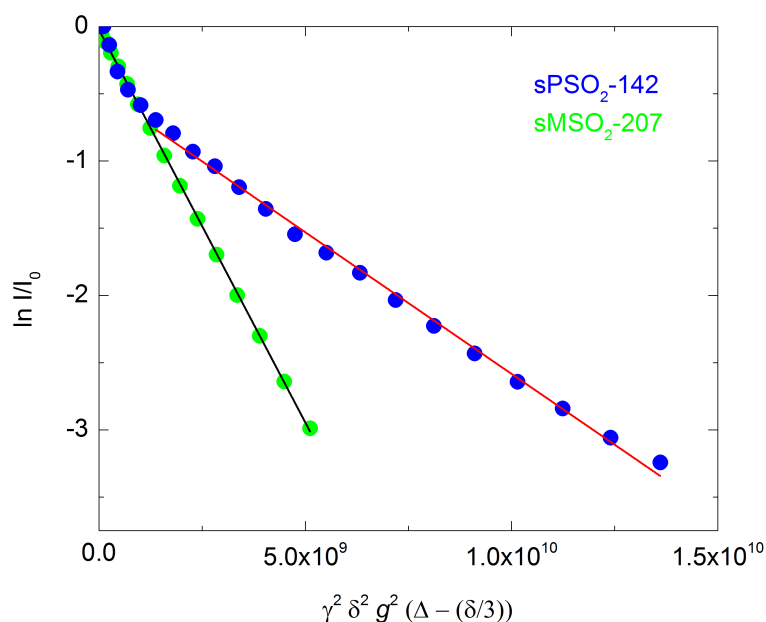


Figure 3.3: PFG-NMR spin-echo ¹H signal attenuation as function of the applied gradient strength for aqueous monomer (green) and polyelectrolyte (blue) solution. Linear regression for high gradient strengths (> 85 G cm⁻¹) is given in red.

An inverse Laplace transformation and nonlinear least-square fitting can be used to describe the distribution function of D_{tr} . [48] Species of low molecular weight diffuse fast compared to high molecular weight species. This leads to a strong signal decay at low gradient strength which flattens for higher gradient strength. This made it possible, at least for the here studied polymeric samples, to only take data at high field gradients leaving a single exponential decay.

3.2.3 Electrophoretic (E) NMR

If an electric field E is applied over a solution with charged particles between two electrodes, the particles i start to move relative to the solution. This movement is called electrophoresis and is proportional to the drift velocity v_i and the electric field strength E . Hence, the electrophoretic mobility μ_i of a particle is given as:

$$\mu_i = \frac{v_i}{E}$$

The mobility μ_i and the diffusion coefficient D_i of a charged mobile particle are related via the Nernst-Einstein relation [25]:

$$D_i = \frac{k_B \cdot T}{z_i \cdot e} \cdot \mu_i$$

where e is the elementary charge, z_i the number of charges per particle, k_B the Boltzmann constant and T the absolute temperature. If the Haven ratio is close to unity this relation also holds for the tracer diffusion coefficient D_{Tr} of a simple particle. However, for various particles or different charged particles the Nernst-Einstein equation only gives an average value for μ/z . Knowing the electrophoretic mobility μ_i and the tracer diffusion coefficient D_{Tr} , therefore, allows one to determine the number of charges per particle. This is only true for diluted solutions where possible correlation effects can be assumed identical for mobility and diffusion processes. Scheler et al. first determined the effective charge of polyelectrolytes in solution by measuring the tracer diffusion coefficient D_{Tr} with PFG-NMR and the mobility μ through an electrophoretic (E) NMR experiment.

E-NMR is a PFG-NMR experiment with applied electric field in the same or opposite direction as the magnetic field gradient (see Figure 3.2 a,b).[49][50][51] Background of this experiment is that superimposed to incoherent thermal motion the coherent drift of charged particles in an electric field leads to a phase shift of the signal (see Figure 3.4). This phase shift depends on the applied electric field strength and contains the information about the displacement per time (drift velocity) of the charged particles.

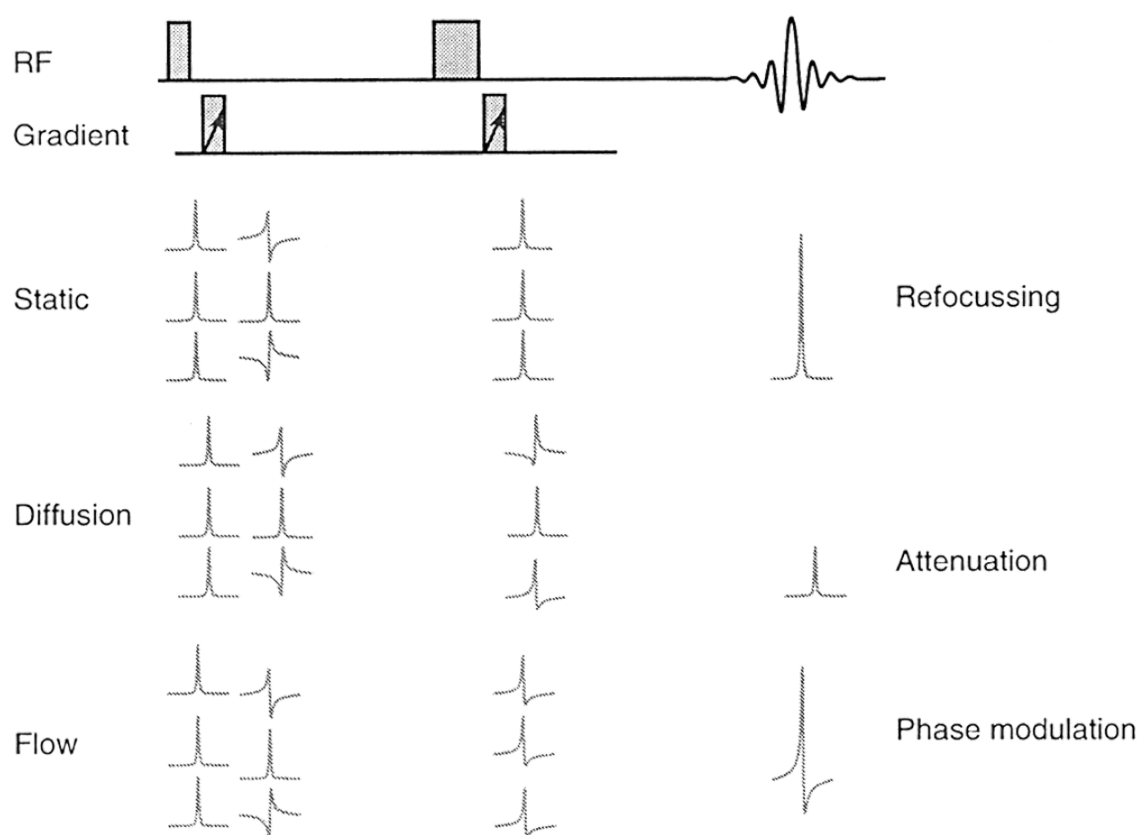


Figure 3.4: Effect of motion in PFG-NMR spin-echo experiments. Static situation showing complete refocussing of transverse magnetization, diffusive motion showing signal of reduced intensity but with the same phase and flow causing a signal of the same amplitude but with shifted phase relation.(from Ref. [52])

3.2.4 Experimental considerations

The basic principle of E-NMR is known for more than 40 years, and measurements were first carried out on electrolytes containing simple ionic species such as quaternary

ammonium ions.[49][50][51] More recently the methodology was adapted to bigger and more complex systems such as ionomers and charged complexes. [53][54][55][57][58][59]

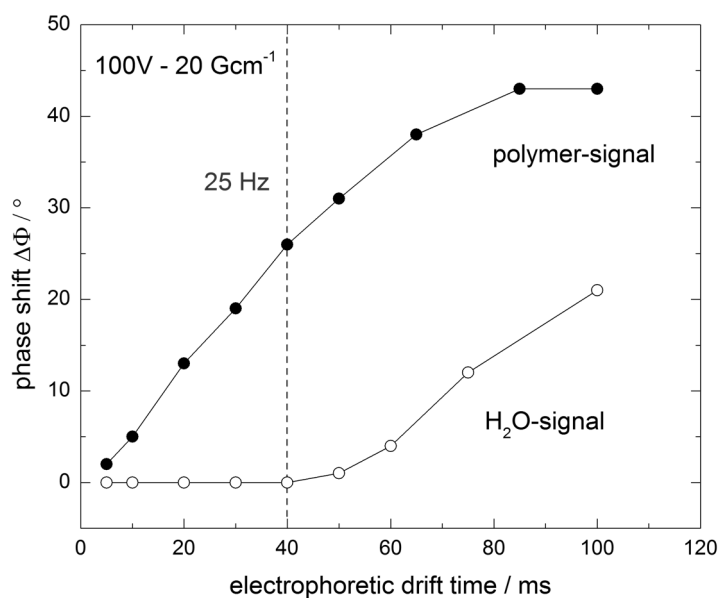
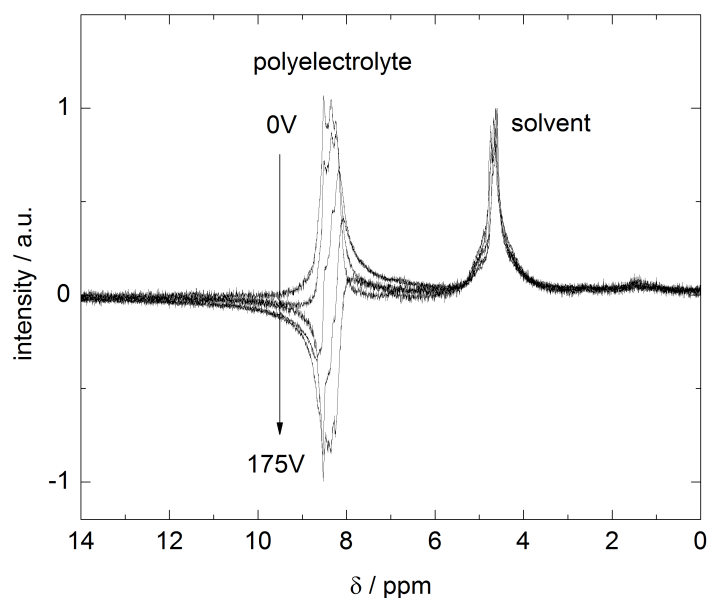


Figure 3.5: Top: ^1H -NMR signal for different applied fields, left peak (polymer) with phase shift, right peak (residual solvents) without phase shift. Bottom: ^1H signal for different magnetic gradient strengths at 100V applied field as function of applied time.

A few points have not been considered in detail so far. In an E-NMR experiment with applied electric field the signal of uncharged diffusing species (e.g. solvent molecules) is expected to show only reduced signal intensity but no phase shift (figure 3.5 top). However, for the here studied polyelectrolyte solutions this is only observed as long as the electric currents and the time, the current is flowing remains in a certain window (figure 3.5 bottom). The applied voltages reach up to $U = 300 \text{ V}$ which is well above the decomposition potential of liquid samples. Nevertheless, a linear increase of the phase shift $\Delta\Phi$ of the polyelectrolyte signals is observed until it reaches a plateau (figure 3.5 right) and a phase shift of the solvent signals is emerging.

There is no clear explanation for this effect. However, the impedance spectrum (figure 3.6) shows the beginning of electrode polarization in the same time regime. This suggests that the current is purely capacitive and no decomposition is occurring at the electrodes. At low frequencies (long times) electrode polarization starts and electrolytic decomposition may lead to the formation of gas bubbles inducing coherent displacements in the sample. Therefore it is important to chose a reasonably short time for E-NMR experiments in the capacitive current regime.

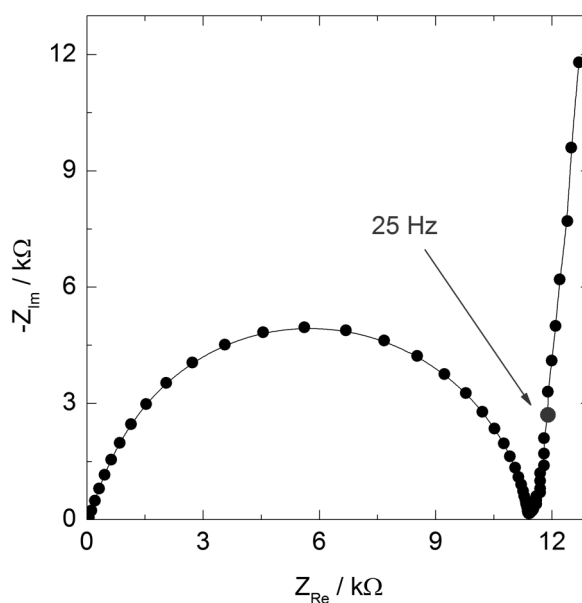


Figure 3.6: Nyquist plot of polymer solution in E-NMR cell, start of electrode polarization around $\nu = 25 \text{ Hz}$ (40 ms).

Chapter 4

Results and discussion

4.1 Dissociation of sulfonated polyelectrolytes in solution

In the last 5 - 10 years, a large number of sulfonated polysulfone materials with different ion exchange capacities IECs (number of sulfonic acid groups on the polymer backbone) have been developed (see Figure 4.1). This was mainly motivated by the quest for higher proton conductivities in PEM-fuel cell membranes. [2]

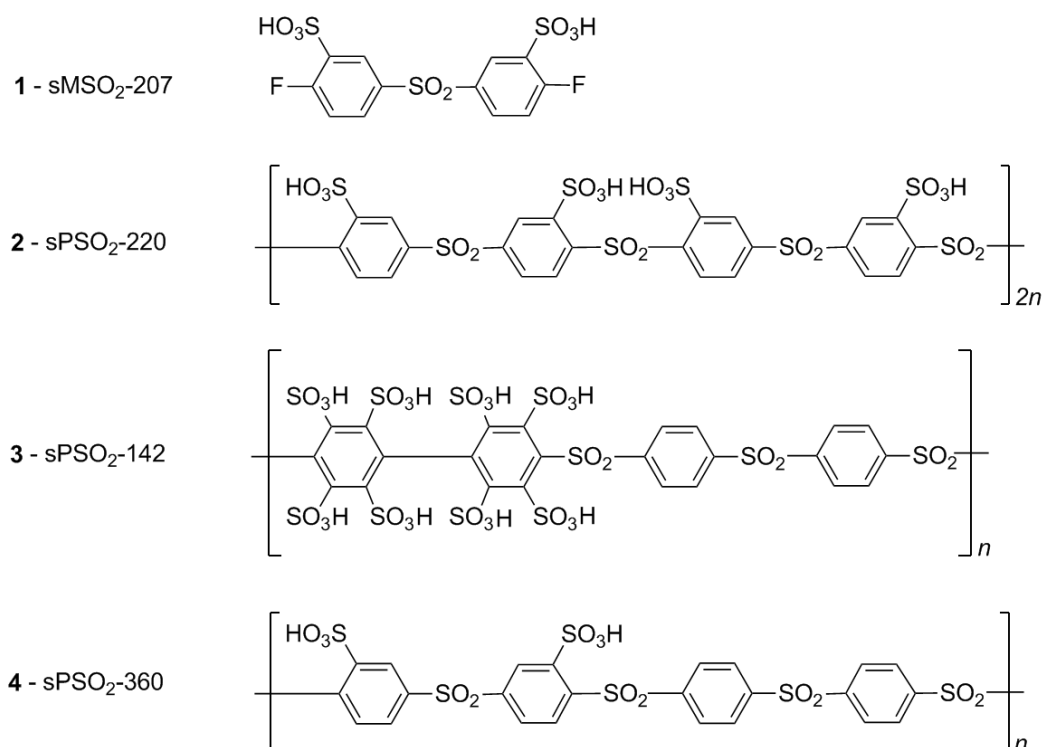


Figure 4.1: Chemical structures of investigated materials. From top to bottom: structure 1: 3,3'-disulfonate-4,4'-difluorodiphenylsulfone sMSO₂-207(M207), *meta* form; structure 2: monosulfonated poly(phenylene sulfone) sPSO₂-220 (S220), *ortho* form; structure 3: hypersulfonated poly(phenylene sulfone) sPSO₂-142 (S142), containing fully octasulfonated biphenyl units and structure 4: half sulfonated poly(phenylene sulfone) sPSO₂-360 (S360). Numbers give the equivalent weight (eq) in g eq⁻¹.

A recently developed material (in close collaboration with a group of the Max-Planck Institute for Polymer Research) is a hypersulfonated poly(phenylene sulfone) sPSO₂-142 (**3**).^[15] This polyelectrolyte contains octasulfonated biphenyl units and currently exhibits the highest IEC of all known sulfonated polymers. Such high concentrations of sulfonic acid groups were obtained by moving away from classical sulfonation reactions (see section 1.5). Instead, a substitution reaction was used, in which reactive fluorine atoms are replaced by strongly nucleophilic thiolate anions, which are subsequently oxidized to sulfonic acid groups. With the right fluorinated starting material, IECs up to 8 meq g⁻¹ were obtained.

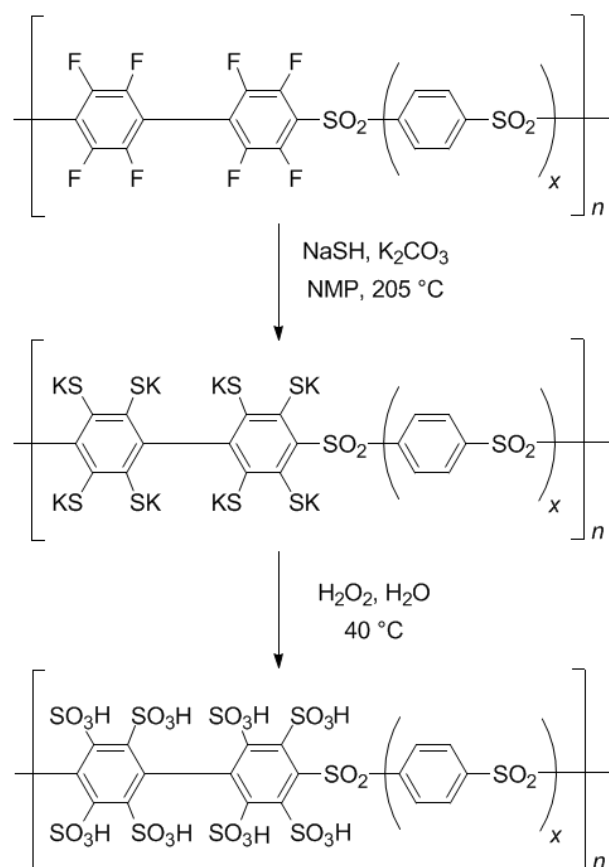


Figure 4.2: Synthetic route to the hypersulfonated polymers.

So far it was observed that the conductivity increases with the concentration of ionic groups in a highly nonlinear fashion. However, the proton conductivity of **3** turned out to be even lower compared to sulfonated polysulfones with only half of the

concentration of sulfonic acid groups (**2**). The reasons for both effects, the nonlinear increase followed by a decrease in conductivity are not yet fully understood. Therefore, one of the main tasks of this thesis was to identify the parameters controlling conductivity in environments with high concentrations of sulfonic acid groups. This includes the charge carrier formation, the transport of ions and solvents as well as microstructural aspects. In the following, results of three aspects influencing the charge carrier formation (dissociation) are presented and discussed separately: The IEC, the kind of counterion (H^+ , Li^+ and Na^+) and the kind of solvent (DMSO and H_2O).

4.1.1 Influence of IEC

In order to study the influence of IEC on the proton dissociation behavior, structure **1** - **3** (Figure 4.1) were used in diluted aqueous solution. The diphenylene sMSO₂-207 **1** has one sulfonic acid functional group per phenyl ring, both in *meta* position with respect to the sulfone (SO₂) linker. This structure is a model system for the polymer structure sPSO₂-360 **4** as the separation (and chemical structure) of the two sulfonic acid groups is the same, while **1** in contrast to **4** still is water soluble (important for the measurements). Different from **1**, the sulfones in the monosulfonated poly(phenylene sulfone) sPSO₂-220 **2** have two nonequivalent sulfone linkers (-SO₂-) with either two sulfonic acid functions in *ortho* or in *meta* position. This means that such a structure has at least two different characteristic separation lengths between neighboring sulfonic acid groups. In hypersulfonated poly(phenylene sulfone) sPSO₂-142 **3** each available position in the 4,4'-diphenylene units is sulfonated. The main difference to **1** and **2** is the fixed minimum separation of sulfonic acid groups in the octasulfonated units, while for **1** and **2** this is affected by conformational changes.

Degrees of dissociation of **1-3** in their protonic form are obtained from combined PFG- and E-NMR experiments as well as from conductivity measurements. The results are then discussed considering electrostatic interactions before including specific chemical interactions and micro conformations with input of MD-simulations (in collaboration with Jens Smiatek from the University of Stuttgart).

Effective charge of polyelectrolytes determined by combined PFG- and E-NMR

The number of charges z_{eff} per polymer object drifting in an electric field is obtained as described in section 3.2.3 according to the Nernst-Einstein equation by the tracer diffusion coefficient D_{tr} (from PFG-NMR) and the electrophoretic mobility μ (from E-NMR, see Figure 4.3). This provides the portion of dissociated ionic groups per object. For the degree of dissociation α , the number of dissociated groups z_{eff} needs to be compared to total number of ionic groups z on the polymer, $\alpha = z_{eff}/z$. The total number z is calculated from the equivalent weight (measured by titration) and the molecular weight M_n (measured by gel permeation chromatography GPC, see Table 4.1) $z = M_n/EW$.

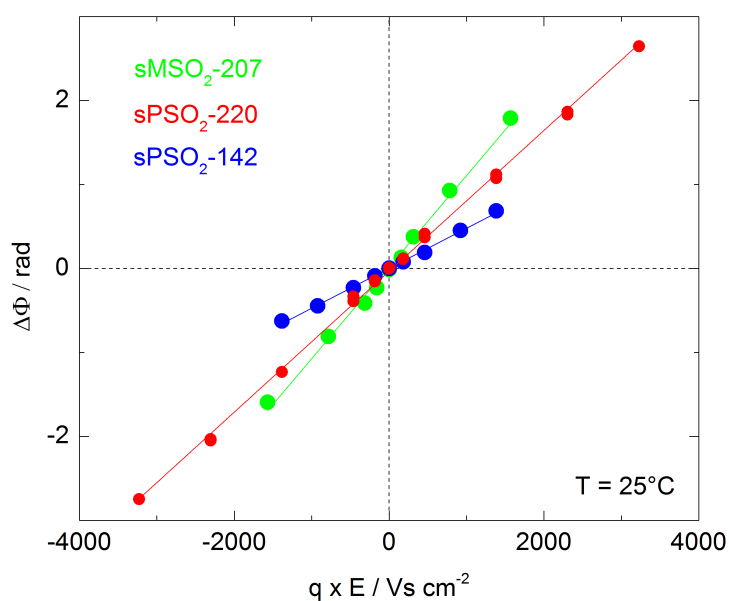


Figure 4.3: Linear trend of the phase angle as function of the applied electric field of **1**, **2** and **3** in protonic form and dissolved in D₂O. Slope gives the electrophoretic mobility μ .

The results for **1** - **3** using the NMR approach are summarized in Table 4.1. The dissociation α shows a trend of decreasing dissociation for an increasing IEC. The diphenylene structure **1** does not show any counterion condensation. For polymer **2** only about half of the ions are dissociated, the other half remains condensed to the sulfonic acid groups. At first glance this observation is quite unexpected as **2** is just a

sequence of several units of **1**. However, only structure **2** has two sulfonic acid groups in *ortho* position to a sulfone group, which causes shorter distances between neighboring sulfonic acid groups. The effects of this will be discussed in more detail in the micro conformation section, with support from MD-simulation. The low degree of dissociation in **3** containing octasulfonated biphenyl units is quite expected, as the separation of neighboring sulfonic acid is fixed and their distance is well below the electrostatic screening length of water (0.71 nm at RT).

Table 4.1: Proton dissociation of sulfonated monomer and polymers by the combined PFG- and E-NMR approach.

	$M_n /$ g mol^{-1}	$EW /$ g eq^{-1}	total number of ionic groups z	$D_T / \text{cm}^2 \text{s}^{-1}$	$\mu / \text{cm}^2 \text{V}^{-1} \text{s}^{-1}$	effective charge z_{eff}	$\alpha / \%$
1 - sMSO ₂ - 207	414	207	2	5.84E-06	4.73E-04	2	104
2 - sPSO ₂ - 220	44000	220	200	1.99E-07	8.30E-04	107	54
3 - sPSO ₂ - 142	5700	142	40	2.05E-06	1.04E-03	13	33

Proton dissociation from conductivity at high dilution

Support for the previous dissociation results was obtained by a different method, which does not require the knowledge of the molecular weight of the polymers as for the combined PFG-/E-NMR approach.

The method is based on the comparison of the apparent proton mobility μ extrapolated to infinite dilution of the polyelectrolyte to the limiting proton mobility μ_∞ (taken from textbooks[60]). For completely dissociated systems, μ approaches μ_∞ . If this is not the case, the ratio between the two values gives the degree of dissociation $\alpha = \mu(\text{H}^+) / \mu(\text{sample})_{\rightarrow\infty}$ (see Figure 4.4). In other words this method determines the number of ionic charge carriers n with known mobility μ from the conductivity $\sigma = n \cdot q \cdot \mu$. This experiment is only applicable for polymers because the anionic conductivity contributions from the polymer backbone are negligible (several orders of magnitude lower) and the overall conductivity stems only from protonic charge

carriers. **1** is not a polymer; therefore the contribution of the anion was separately measured by PFG-NMR and subtracted from the overall mobility μ assuming full dissociation.

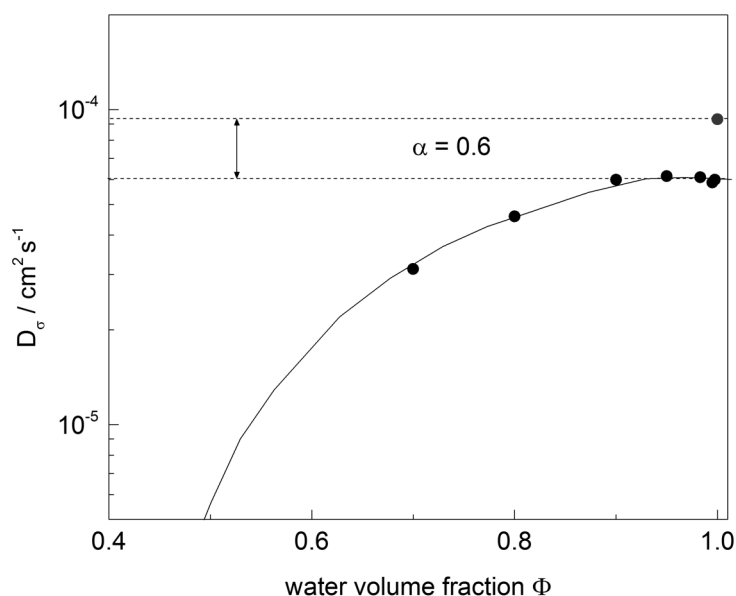


Figure 4.4: Room temperature diffusion coefficients as a function of water volume fraction Φ for poly(phenylene sulfone)-220 (**2**). Black circles: conductivity diffusion coefficients D_σ , calculated via Nernst-Einstein equation from conductivity data assuming complete dissociation. Protonic charge carrier diffusion coefficient at infinite dilution (top) is given as comparison.

Table 4.2: Degree of proton dissociation for different sulfonated materials from the conductivity approach

	$D_\sigma(\text{H}^+)_\infty / \text{cm}^2 \text{s}^{-1}$ lit.	$D_\sigma(\text{H}^+)_{\rightarrow\infty} / \text{cm}^2 \text{s}^{-1}$ exp.	$\alpha / \%$
1 - sMSO ₂ -207	9.31E-05	9.30E-05	100
2 - sPSO ₂ -220		5.72E-05	61
3 - sPSO ₂ -142		2.30E-05	25

The conductivity diffusion coefficient of **2** remains about 40 % below the limiting proton conductivity diffusion coefficient for aqueous media which is $9.31\text{E-}05 \text{ cm}^2 \text{ s}^{-1}$ (see Figure 4.4) suggesting in a degree of dissociation of about $\alpha = 60 \%$. The results (Table 4.2) are in good agreement to the degree of dissociation obtained from NMR for all structures. The small errors may be a result of the difficulty for polyelectrolytes in molecular weight determination by gel permeation chromatography.

Electrostatic considerations

As already mentioned in the experimental background section Manning counterion condensation theory is still the most prominent model to describe polyelectrolyte dissociation in solution. It purely relies on electrostatic interaction between ions in a dielectric continuum. The minimum distance between charges on a polymer backbone in water is according to Manning 0.71 nm, for shorter distances counterion condensation start. Generally, the theory works well in aqueous media for many polyelectrolytes. Implying that the electrostatic forces are the dominant interactions controlling dissociation of polyelectrolytes in polar media. Another simplification of the model is the consideration of the polymer as infinite thread with equidistant point charges. These are very strong assumptions, which are not suitable for the complex structures of sulfonated polyelectrolytes having diverse conformational freedom. Another approach is the consideration of the IEC and the density of the water free polyelectrolytes only, the separation of ionic groups with this can be calculated for equidistant separation (ionic groups on a cubic lattice). This results in distances of 0.59, 0.60 and 0.52 nm for structure **1**, **2**, **3**. All these ion-ion separations are below the Bjerrum length of water and therefore, the experimentally found incomplete dissociation of **2** and **3** is expected even from electrostatics only. In addition, also structure **3** being less dissociated than structure **2** is reproduced.

In the case of structure **1** the situation is more complex and complete dissociation was found experimentally, but the above consideration points already towards counterion condensation. The consideration of the limiting molecular conformations with minimum and maximum distance between the sulfonic acid groups (Figure 4.5 top)

reveals separations larger than the average separation in dry bulk material. This is because the two ionic groups are in *meta* position to the central sulfone group which allows the neighboring sulfonic groups to cover separations in the range (MD-simulation) from 0.53 (*cis* form) to 1.13 nm (*trans* form), which makes the experimentally found complete dissociation more reasonable. The same considerations are true for polymer **2**, however, the sulfonic groups are in *ortho* position to the next sulfone group. This leads to separation between next neighboring sulfonic acid groups (Figure 4.5 bottom) in the range from 0.41 nm (*cis* form) to 0.73 nm (*trans* form), which is in the range of the Bjerrum length. Simple electrostatic repulsion of the sulfonic group would favor the *trans* form, but conformational effects such as electrostatic stabilization of protons between two close sulfonic groups may stabilize the *cis* form.

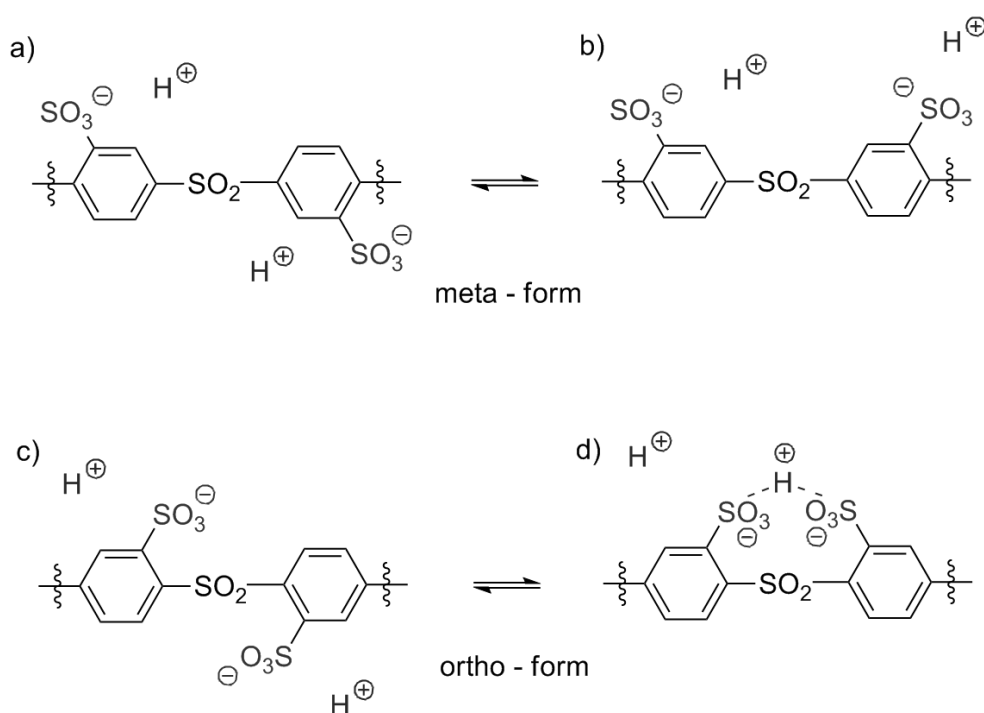


Figure 4.5: Sketch of structural units: limiting conformations, maximum anion-anion distance *trans* conformation of a) *meta* form, c) *ortho* form and bridging *cis* conformation of b) *meta* form, d) *ortho* form.

The bridging of one positive ion between two negative groups corresponds to a partially neutralized situation with a degree of dissociation close to the experimental values of $\alpha = 0.5$ for **2**. For short ion-ion distances simple electrostatic considerations, such as the

Debye-Hückel approaches fail. In addition, details of the water structure and the sulfonic acid group, and also ion-dipole, dipole-dipole, dispersive interactions and the backbone energetics need to be considered as well. To investigate the idea of a bridging conformation in more detail, a molecular dynamics simulation was performed (in collaboration with the University of Stuttgart) which produces all thermally accessible configurations and entropic effects of two model structures, one having the sulfonic acid groups in *ortho* and the other in *meta* position to a sulfone linker.

Specific interactions – micro conformation

To gain a more detailed insight into the effects of micro conformation on the dissociation behavior of **1** and **2**, small model systems (sulfonated diphenylene in *meta* and *ortho* form) in a large number of explicit water molecules were investigated. Since simulation of protons as counterions is very difficult, sodium was chosen for the model systems. The distance between the sulfur atoms of neighboring sulfonic groups was chosen as reaction coordinate in the metadynamics evaluation.

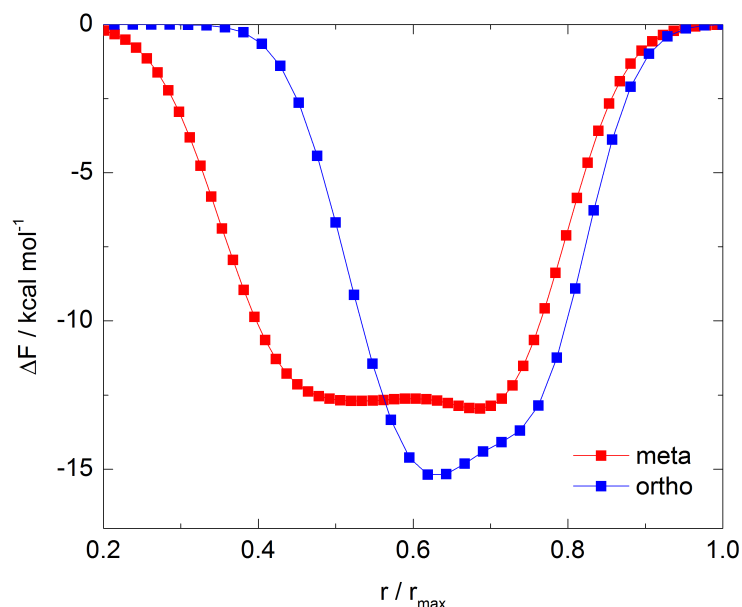


Figure 4.6: Free energy landscapes evaluated by well-tempered metadynamics of *ortho* form (blue) and *meta* form (red) of sulfonic acid dimer for different sulfur-sulfur distances of the sulfonic acid groups. Wide and flat distribution for the *meta* form, narrow distribution at lower energies for the *ortho* form.

In other words, the total free energy change for different angles between the two sulfonic acid groups for a rotation around the sulfone linker were evaluated. For more simulation details see [61][62].

The total free energy change ΔF shows a higher configurational freedom in the region $r/r_{\max} \sim 0.5$ to 0.7 for the *meta* form whereas the *ortho* form shows a conformation which is constrained by the presence of a global minimum at $r/r_{\max} \sim 0.62$ (Figure 4.6). This exactly corresponds to the conformation in which both sulfonic groups interact with a single ion, i.e. a triple-ion is formed (Figure 4.7 left). On the other hand the *meta* form shows no such stable explicit conformation (Figure 4.6), because the molecular structure can not take any conformation where the two sulfonic acid groups are close enough to form such triple-ions (Figure 4.7 right).

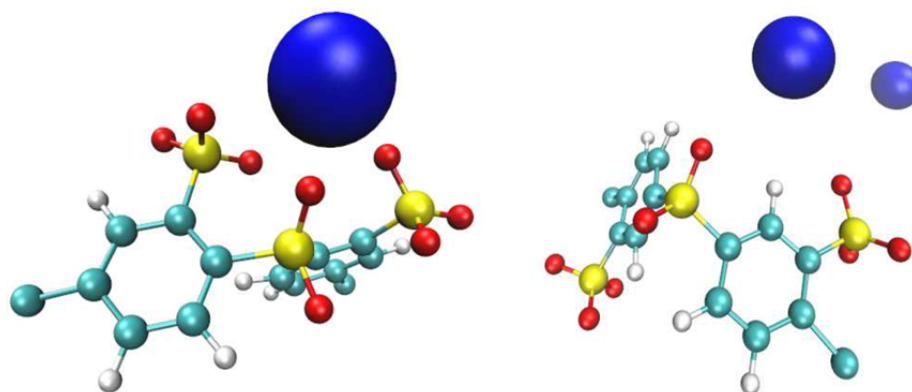


Figure 4.7: Snapshots of the well-tempered metadynamics simulation at the global energetic minima of the *ortho* (left) dimer at $r/r_{\max} \sim 0.62$ (left side) and the *meta* dimer (right) at $r/r_{\max} \sim 0.72$ (right side). Only sodium ions (blue) within a distance of 0.7 nm to the dimer center are illustrated. [61]

4.1.2 Influence of counterions

A high concentration of mobile charge carrier is crucial to obtain high ionic conductivities not only for the protonic form but also for sodium and lithium exchanged

polyelectrolytes. Therefore also the dissociation behavior of different ionic forms especially lithium and sodium is of importance.

The polyelectrolytes were ion-exchanged into the different forms by ion-exchange resins or submerging the polymer in corresponding salt solutions and subsequent dialysis (further details can be found in the experimental appendix A1). To separate the solvent effect from properties of the kind of counterion only aqueous solutions are considered in this chapter, while the influence of the solvent is discussed in the next section.

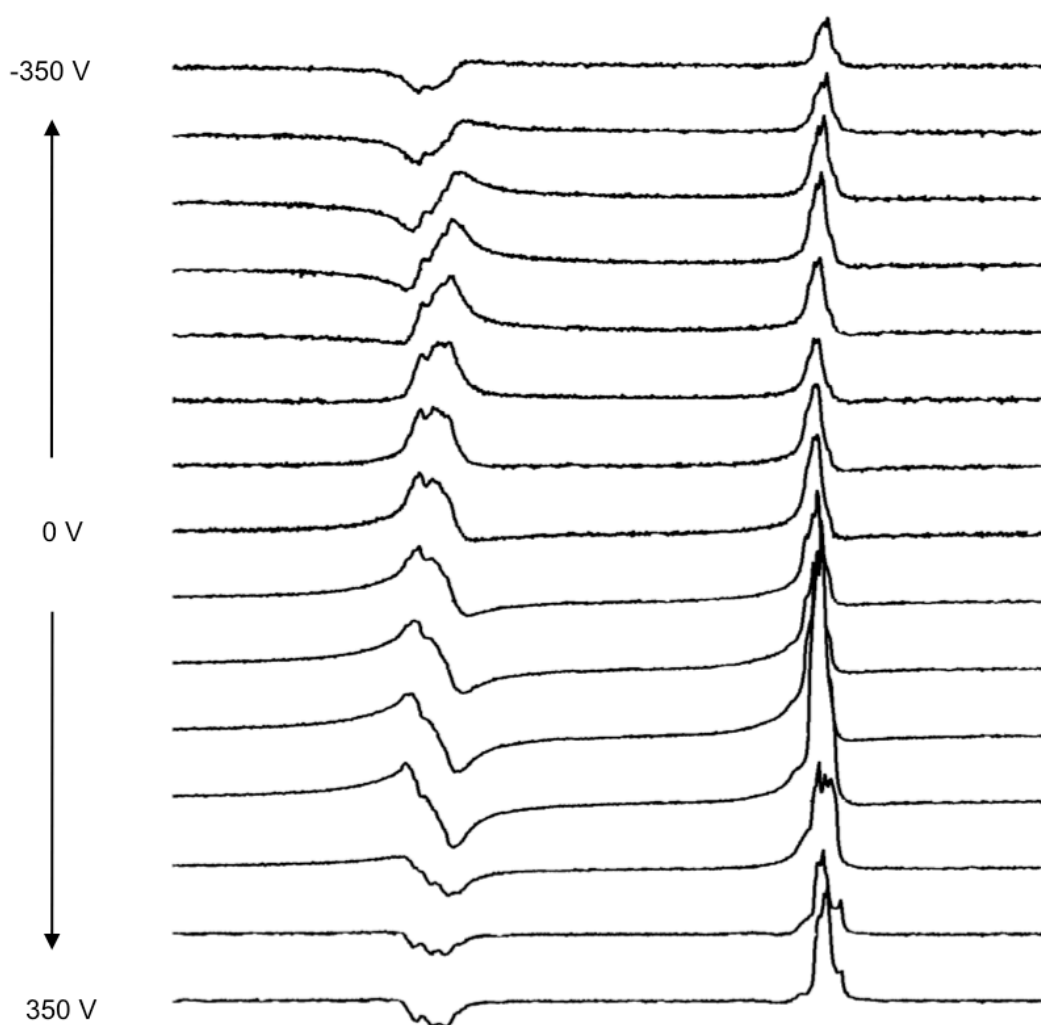


Figure 4.8: ¹H-NMR signal (without ppm scale) for different applied fields between +350 and -350V, left peak: sulfonated poly(phenylene sulfone)-220 **2** in lithium form with phase shift, right peak: residual solvents without phase shift.

Effective charge of polyelectrolytes determined by combined PFG- and E-NMR

The effective charge is determined by the phase shift of an E-NMR experiment and the signal attenuation in a PFG-NMR experiment. The phase shift for different applied electric field strengths are shown in Figure 4.8 for the lithium form of structure **2** in water. It shows a 360° phase shift for the polyelectrolyte signal, whereas the solvent (water) signal phase remains the same for all applied electric fields. The degree of dissociation (Table 4.3) decreases in the order (H⁺) > (Li⁺) > (Na⁺). In the protonic form about half of the counterions are involved in condensation to the sulfonic acid groups, while in the lithium form around two third, and for the sodium form slightly more counterions are found to be condensed to the polyelectrolyte.

Table 4.3: Dissociation of sulfonated poly(phenylene sulfone)-220 (**2**) in water and different ionic forms by NMR

	total number of ionic groups z	D_T / cm² s⁻¹	μ / cm² V⁻¹ s⁻¹	effective charge z_{eff}	α / %
2 - sPSO ₂ -220 H ⁺ -form	200	1.99E-7	8.30E-04	107	54
2 - sPSO ₂ -220 Li ⁺ -form		1.89E-7	5.10E-04	69	34
2 - sPSO ₂ -220 Na ⁺ -form		3.26E-7	7.70E-04	61	30

The trend in the dissociation behavior of the different counterions in the same solvent is quite expected as the ionic radius increases, while the hardness (according to the HSAB concept) of the ions decreases in the same manner, as the effective charge on the polymer decreases from proton to sodium. This leads to less solvent coordinating the counterions, resulting in lower solvation energies from solvent-ion interactions. In addition, the observed stabilizing bridging conformation of ions between two sulfonic acid groups (previous section 4.1.1) is involved in reducing the dissociation.

4.1.3 Influence of solvent

The ionic conductivity of structure **2** in lithium form solvated with DMSO (Figure 4.9) shows a more than an order of magnitude lower conductivity compared to water (at the same lambda values). This effect can not only be explained by the different solvent dynamics as the mobility for water ($D_{Tr} = 2.29 \cdot 10^{-5} \text{ cm}^2\text{s}^{-1}$) since it is only a factor of 2 higher compared to DMSO ($D_{Tr} = 1 \cdot 10^{-5} \text{ cm}^2 \text{ s}^{-1}$). The additional discrepancy may also result from a reduced dissociation for DMSO, because the dielectric constant of water is about 2 times higher. It is generally assumed that a higher dielectric solvent more efficiently screens the charges leading to higher degrees of dissociation.

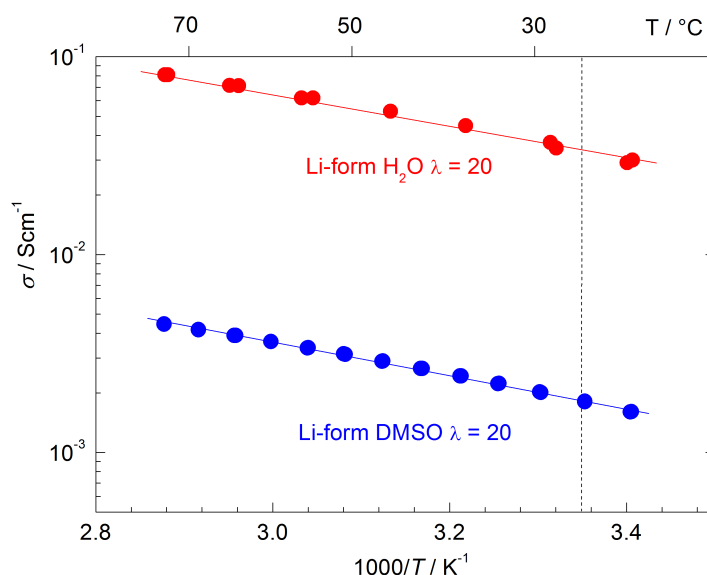


Figure 4.9: Lithium conductivity at $\lambda = 20$ water (red) and DMSO (blue) as a function of temperature.

Effective charge of polyelectrolytes determined by combined PFG- and E-NMR

In contrast the above considerations, a higher effective charge of the polyelectrolyte in lithium form was observed with DMSO ($\alpha = 46 \%$) compared to water ($\alpha = 34 \%$). The effective charge determined by the electrophoretic mobility (Figure 4.10) and the tracer diffusion coefficient of the polyelectrolyte in different solvents is given in Table 4.4.

Table 4.4: Lithium dissociation of sulfonated poly(phenylene sulfone)-220 (2) in different solvents by NMR

	total number of ionic groups z	$D_T / \text{cm}^2 \text{s}^{-1}$	$\mu / \text{cm}^2 \text{V}^{-1} \text{s}^{-1}$	effective charge z_{eff}	$\alpha / \%$
2 - sPSO ₂ -220 Li ⁺ -form in H ₂ O	200	1.89E-7	5.10E-04	69	34
2 - sPSO ₂ -220 Li ⁺ -form in DMSO		6.94E-8	2.50E-04	93	46

The result suggests that the assumption of solvents as continuous dielectric medium does not hold here; additional local molecular interactions between the solvent and ions need to be considered. A number of additional experimental observations further support this finding. For example, neither high dielectric solvents such as ethylene carbonate ($\epsilon = 89.8$) and propylene carbonate ($\epsilon = 64.9$) nor low dielectric solvents such as chloroform ($\epsilon = 2.2$) did lead to the dissolution of the polyelectrolyte. To further investigate this, MD-simulations (in collaboration with the University of Stuttgart) using a model sulfonated polyelectrolyte were performed in different solvents.

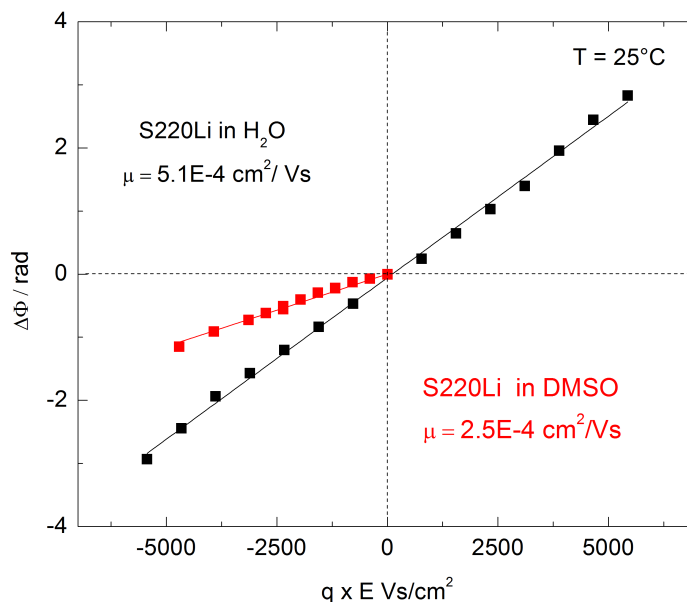


Figure 4.10: Linear trend of the phase angle as function of the applied electric field of poly(phenylene sulfone)-220 (2) in lithium form dissolved in water (black) and DMSO (red) at room temperature.

MD-simulation of a sulfonated polysulfone model structure

The model polyelectrolyte **mod**-sPSO₂-220 (Figure 4.11) has a similar chemical structure to the sulfonated poly(phenylene sulfone)-220 (**2**) with the same main chain equivalent weight of 220 g eq⁻¹. Structure **2** has two nonequivalent sulfone linkers with either two sulfonic acid functions in *ortho* or in *meta* position. Different from that, the model polyelectrolyte has only equivalent sulfone linkers with always one sulfonic acid function in *ortho* and another in *meta* position.

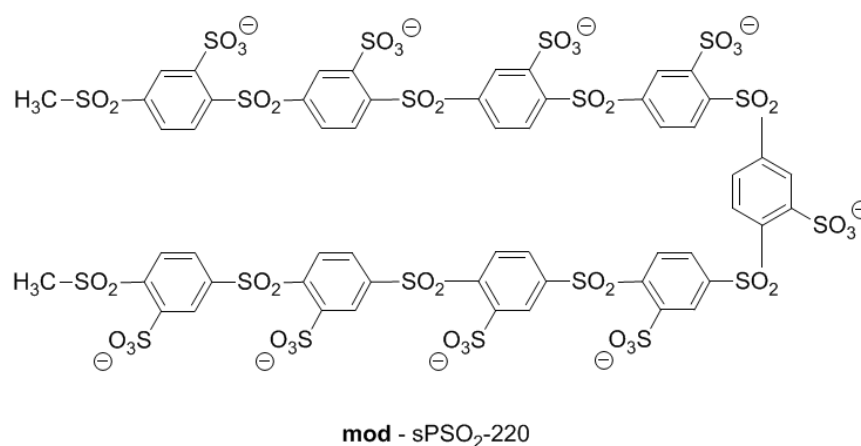


Figure 4.11: Structure of simulated polysulfone **mod**-sPSO₂-220.

The number of repeating units in **mod**-sPSO₂-220 is $n = 9$, which is in the order of the sulfonated subunits in recently developed block copolymers [Titvinidze 2012]. Two methyl groups form the ends of the model polyelectrolyte, to avoid any influence of the end capping on the solvation properties. For electroneutrality, 9 sodium counterions were randomly placed in the simulation box.

The molecular dynamics simulations were performed in water, chloroform and DMSO at room temperature ($T = 300\text{K}$) with the topologies and force field parameters included in GROMOS53A6[64]. The box sizes were chosen to contain 4691 explicit solvent molecules for water, 4756 for DMSO and 4704 molecules for chloroform. This corresponds to a cation concentrations between 0.02 mol l⁻¹ and 0.03 mol l⁻¹, which is in the range of the experimental studied concentrations and matches to $\lambda = 521$ for

water, $\lambda = 528$ for DMSO and $\lambda = 523$ for chloroform. For further simulation details see reference [61].

Electrostatic considerations

Figure 4.12 shows typical simulation snapshots for conformations of **mod**-sPSO₂-220Na in water, DMSO and chloroform. The snapshots show variations in the polymer conformation for the different solvents. DMSO and water lead to elongated (stretched) conformations while chloroform forms a coil-like (collapsed) configuration. The fraction of condensed counterions can be analyzed by the cumulative number distribution function (Figure 4.13).

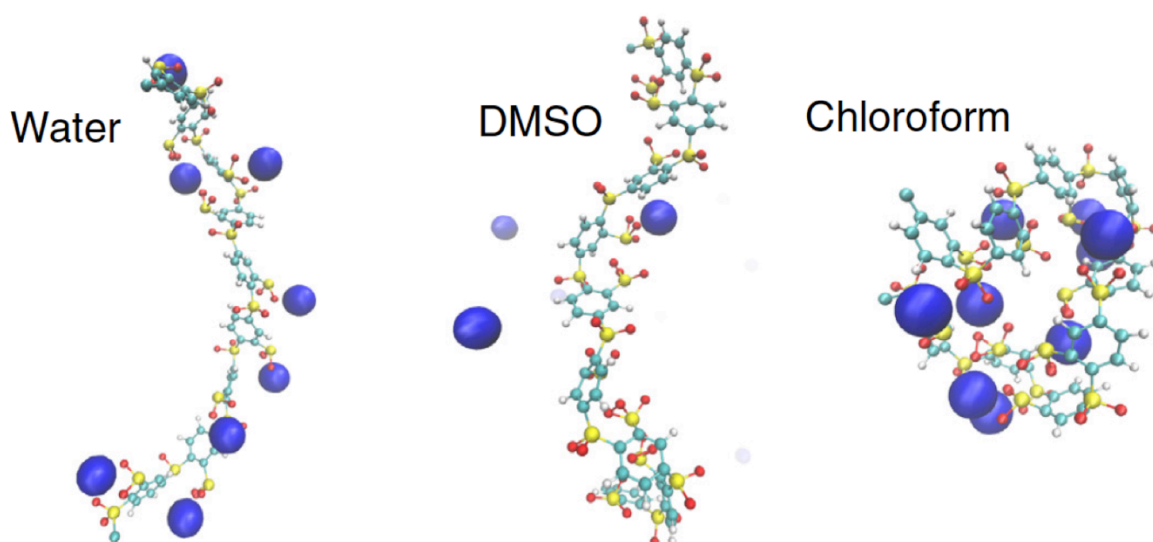


Figure 4.12: Simulation snapshots of mod-sPSO₂-220 Na⁺ in water (left), DMSO (middle) and chloroform (right). The sodium ions are shown as blue spheres. [61]

Almost no dissociation of sodium ions is found in chloroform in accordance with Manning theory. Since the larger Bjerrum length of chloroform leads to a Manning parameter ξ_M significantly larger 1. The situation is less clear for the condensation behavior in DMSO and water. Figure 4.13 shows that more ions are close to the polymer backbone for water compared to DMSO, although water has a smaller Bjerrum length.

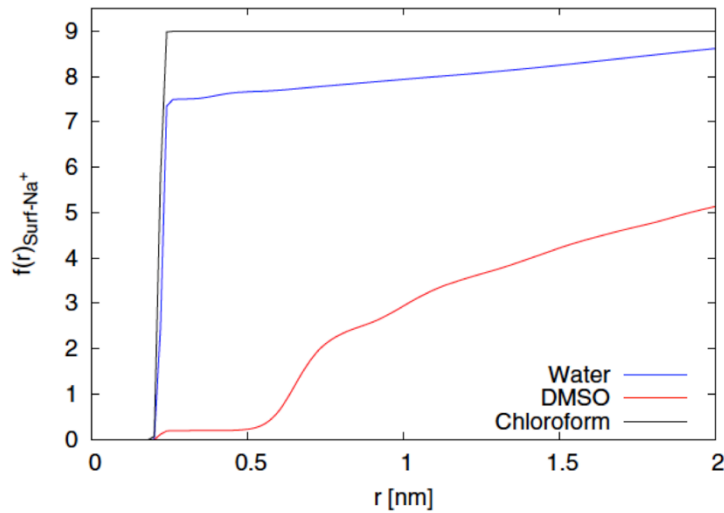


Figure 4.13: The cumulative number distribution function for sodium ions around the molecular surface of **mod-sPSO₂-220Na** for water, DMSO and chloroform as solvents ($f(r) = 9$ comprises all counterions of the model polyelectrolyte). [61]

The fraction of condensed ions f_c can be obtained by dividing the number of counterions within the distance of the Bjerrum length N_{λ_B} the total number of counterions N

$$f_c = \frac{N_{\lambda_B}}{N}$$

For water $f_c = 0.86$, while DMSO leads to a constant of $f_c = 0.38$ (chloroform $f_c = 1$).

So far only electrostatic aspects were discussed but the situation is more complex and the detailed chemical structure of the polyelectrolyte and the solvents has to be taken into account.

Chemical structure of polyelectrolyte and solvent

The binding free energy between solvent molecules and the different groups of the polyelectrolyte is shown in Figure 4.14. The overall binding energy of DMSO to the SO_3^- group is larger than water but both form explicit solvation shells, while the binding of chloroform is unfavorable for all distances. A nearly identical behavior is observed for the SO_2 -group. This means that the solvent not only interacts to the charged ionic

groups alone, also neighboring functional groups are involved. The binding properties of the different solvents to the phenyl ring were also analyzed (not shown) and a small free energy minimum was observed for chloroform while the other two solvents show no interaction. The strong dipole–dipole interactions between DMSO and the polar groups (SO_3^- and SO_2) of the polyelectrolyte are found to be the main driving forces for the good solvation properties of DMSO. Therefore, the DMSO orientation was analyzed between the sulfur atoms of the SO_3^- and SO_2 -groups and the corresponding carbon and oxygen atoms of DMSO. The results are presented on the right side of Figure 4.15. The spatial distribution function illustrates a well-ordered orientation for the methyl groups (carbon atoms) of DMSO toward the sulfur atoms of the polyelectrolyte with a preferred position of the methyl group between SO_3^- and SO_2 -groups.

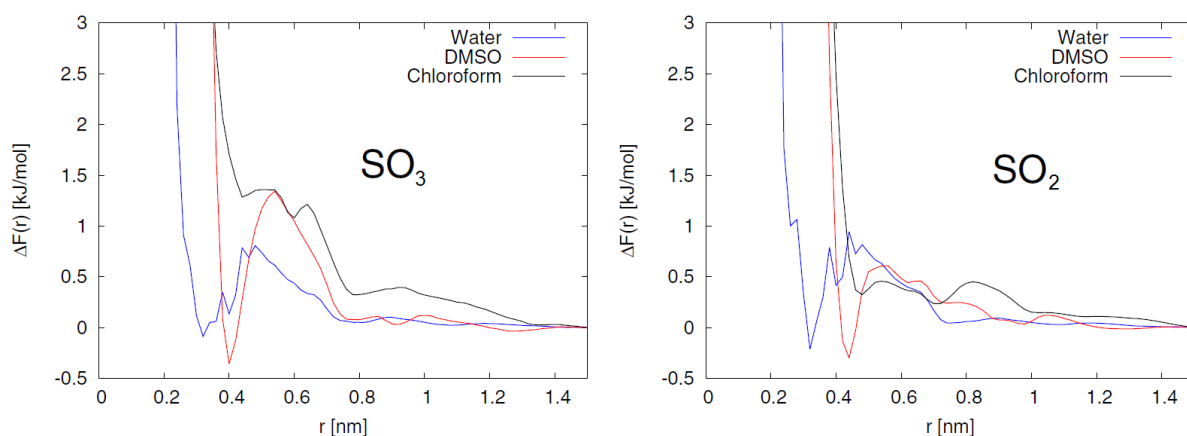


Figure 4.14: Binding free energy for solvent molecules around SO_3 (left) and SO_2 (right) of **mod-sPSO₂-220**. The distance r is defined by the sulfur atom of the DMSO molecules, the carbon atom of the chloroform molecules and the oxygen atom of the water molecules, to the corresponding sulfur atoms of the sulfonic acid groups on the polymer. [61]

The solvation behavior for the sodium ions was also evaluated by pair radial distribution function. The number of solvent molecules in the first shell for DMSO was found to be 5.9 and for water 4.5. Furthermore the binding free energy of sodium ions to solvent molecules was around 1 kJ mol^{-1} larger for DMSO ($\Delta G = -5.3 \text{ kJ mol}^{-1}$) compared to water ($\Delta G = -4.2 \text{ kJ mol}^{-1}$). Therefore, DMSO can be considered as a strong coordinating solvent. This is expressed by the donor numbers, which is the electron

donor strength and is for water $DN = 18 \text{ kcal mol}^{-1}$ and for DMSO $DN = 29.8 \text{ kcal mol}^{-1}$, whereas chloroform shows a small donor number of $DN = 4 \text{ kcal mol}^{-1}$.

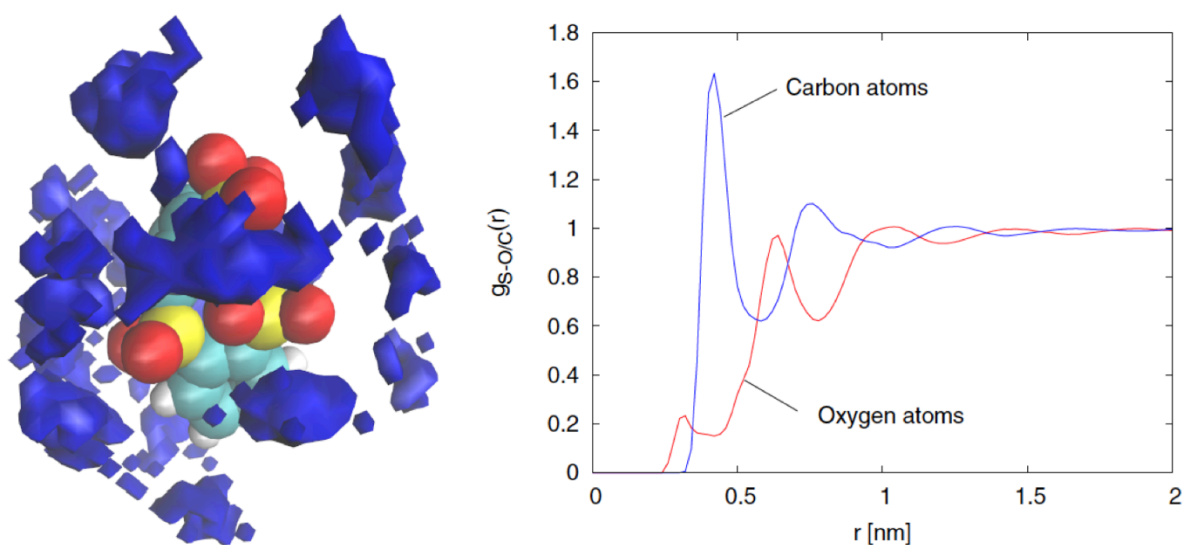


Figure 4.15: Left: DMSO molecules (center-of-mass in blue) around the monomers of **mod-sPSO₂-220** ($\leq 0.8 \text{ nm}$ from the macromolecular surface). The sulfur-oxygen atoms (red) on the left side belong to a SO_2 group. The two groups are SO_3 -groups. Right side: the radial distribution function between the sulfur atoms of the SO_3 -group and the carbon and oxygen side (atoms) of DMSO.[61]

The found fractions of condensed ions f_c are in good agreement to the donor number concept. However, this does not explain the higher sodium conductivity for water compared to DMSO. Most probably, the strong coordination of solvent molecules leads to less mobility of the free counterions and together with the higher diffusion coefficient for water this results in the observed conductivities.

4.2 Solvent mixtures in polyelectrolyte solutions

The experimentally observed conductivities of solvated polyelectrolytes in lithium (and sodium) form are extremely high due to the high concentration of super acidic sulfonic acid groups[5], but the previous results revealed low degrees of dissociation, which still allows for further conductivity enhancement by increasing the number of mobile charge carriers. This may be achieved by using solvent mixtures, which provide the freedom of specifically solvating cation, immobilized anion and even polymer backbone by different but still miscible solvents. In the following two approaches are presented, the first uses mixtures of high and low dielectric constant and the second mixtures of high donor and acceptor solvents.

4.2.1 High and low dielectric solvents

It was shown (section 4.1), that a high dielectric constant alone is not enough to ensure efficient solvation. Especially carbonate based solvents, which are commonly used in salt electrolytes for battery applications, did not dissolve the polymer.

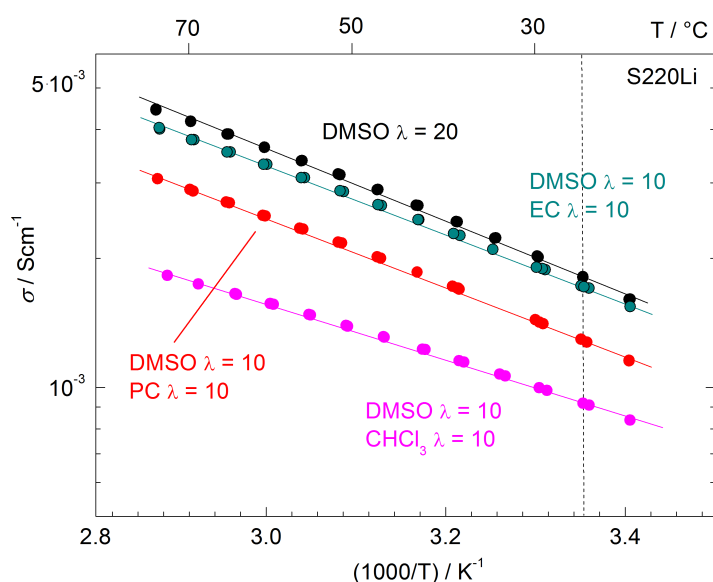


Figure 4.16: Ionic conductivity of **2** in lithium form with solvents mixtures as a function of temperature. Pure DMSO with $\lambda = 20$ and 10 DMSO molecules per lithium ion (black, open symbols), DMSO/EC mixture (green), DMSO/PC mixtures and DMSO/chloroform mixtures (pink).

Instead a high Lewis acidity and basicity of the solvent appeared to be necessary for an efficient interaction between solvent and ions. In order to verify if this is also true for solvent mixtures, the conductivity of a number of different solvent combinations was investigated. All studied mixtures (see Figure 4.16) contained $\lambda = 10$ DMSO, which allowed the dissolution of the solvent, and $\lambda = 10$ of solvents with high and very low dielectric constants. The resulting conductivities were always below the conductivity of the same amount (λ) of pure DMSO and no positive effect of the high dielectric solvents was observed.

4.2.2 Lewis acid and base solvent mixtures

The following approach is based on the result of section 4.1 that electron pair donor and acceptor interactions play a major role in the charge carrier formation process of polyelectrolytes. On the one hand electron acceptor solvents strongly coordinate to anions, while electron donor solvent on the other hand favorably binds to cations.

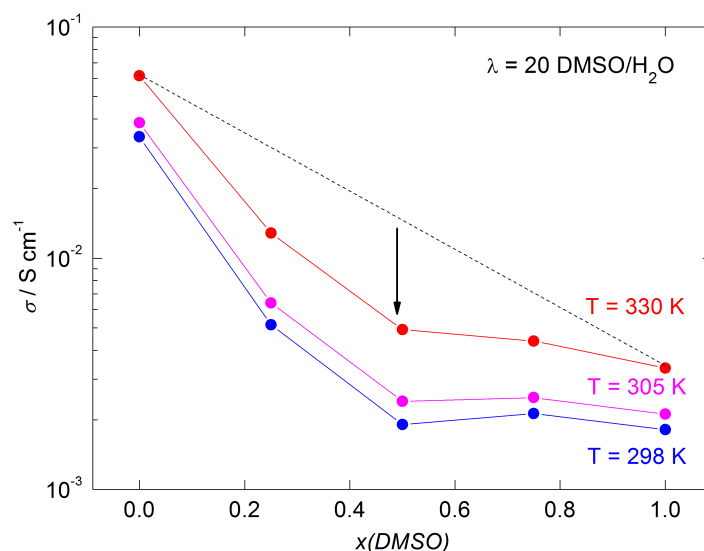


Figure 4.17: Ionic conductivity of sulfonated poly(phenylene sulfone)-220 (**2**) in lithium form in water-DMSO mixtures with fixed $\lambda = 20$ as a function of mole fraction of DMSO for different temperatures. The values increase from pure DMSO (right) to pure water (left) in a nonlinear fashion.

The idea is to use a combination of both in a solvent mixture, leading to a strong coordination of anions and cations is expected to result in increased degree of dissociation and, as a consequence, a higher ionic conductivity. As a model system water and DMSO exactly match the requirements of high donor (DMSO) and high acceptor (water) solvent. For the sulfonated polyelectrolyte this means the sulfonic acid group is coordinated by water and the counterion by DMSO. The conductivity data for different mole fractions and of the pure solvents are shown in Figure 4.17. A decreased conductivity, lower than the linear extrapolation between the pure solvents, is observed, which is opposite to the expected behavior. This finding points even towards reduced dissociation in the mixture. To clarify this in more detail the solvent dynamics were investigated with PFG-NMR.

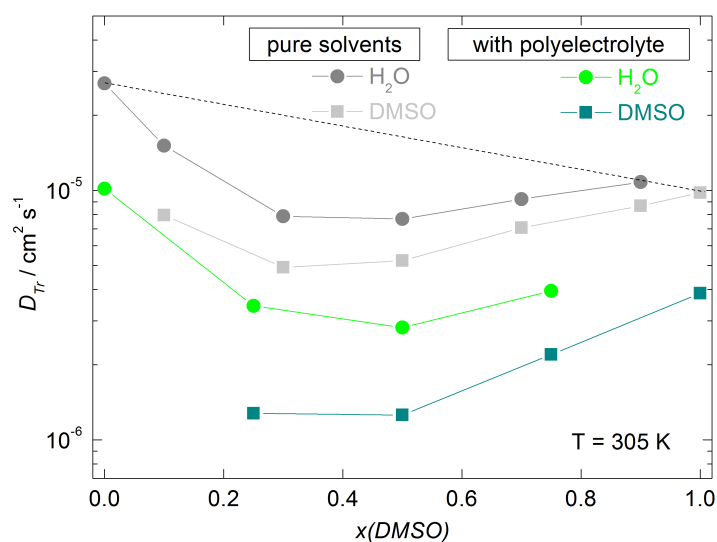


Figure 4.18: ¹H-tracer diffusion coefficient of water and solvent mixtures with and without added polyelectrolytes as a function of mole fraction of DMSO for at T = 305 K. A distinct minimum at a 2:1 mixture (~ 33 mol% DMSO) of water and DMSO is observed for both solvents.

This technique allows the determination of the tracer diffusion coefficient D_{Tr} of each solvent in the mixture simultaneously. The results (Figure 4.18) show a decrease in the solvent mobility both in water and DMSO, even without added polyelectrolyte, implying the effect is due to the solvents alone. A minimum in D_{Tr} for both solvents can be found

at a water:DMSO ratio of 2:1. This corresponds to a situation where two water molecules coordinate to one DMSO molecule (see Figure 4.19).

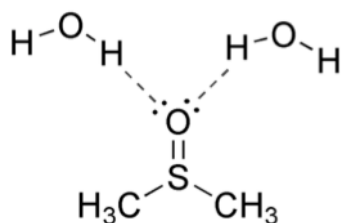


Figure 4.19: Schematic representation of water-DMSO complex with a 2:1 ratio.

Selective solvation in a mixture of high donor and acceptor solvents leads to a reduced overall solvent mobility due to donor-acceptor interactions between the solvents. Although some increased dissociation need to be present at high DMSO contents as the conductivity stays constant (see Figure 4.17) until a water:DMSO ratio of 1:1 while the solvent mobility already decreases. Therefore a higher mobile charge carrier concentration needs to be present in order to compensate for the decreasing mobility.

4.3 Dissociation and transport at high concentrations of sulfonated polyelectrolytes

4.3.1 Proton form

The proton conductivity in the membrane form at low water contents ($T = 120\text{ }^{\circ}\text{C}$, $\text{RH} = 50\%$) varies non-monotonically with increasing IEC (see Figure 4.20). The hypersulfonated polymer (**3**) shows a reduced conductivity under these conditions compared to **2**, which only has about half of the sulfonic acid concentration. The major cause of such a finding only can be explained by a reduced charge carrier concentration because of counterion condensation, although other effects such as microstructural organization may play a minor role.

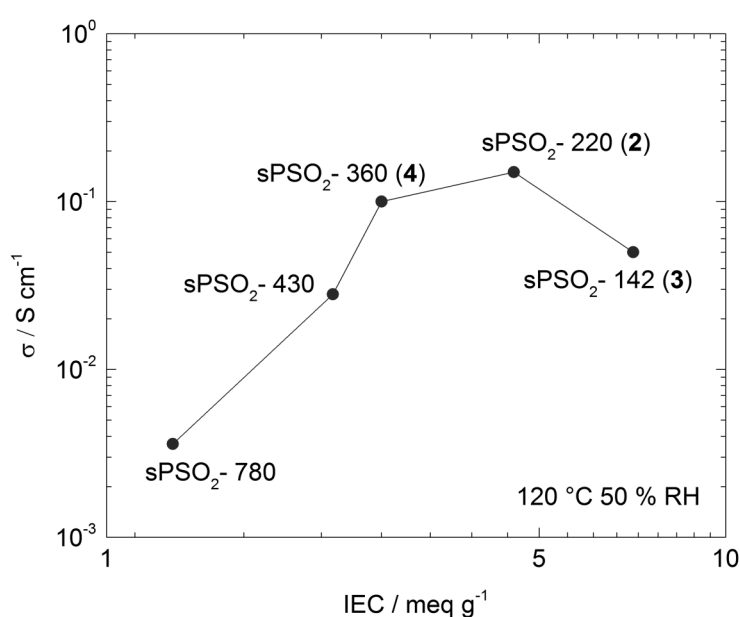


Figure 4.20: Proton conductivity of sulfonated poly(phenylene sulfones) at $T = 120\text{ }^{\circ}\text{C}$, $\text{RH} = 50\%$ as a function of IEC, lines are shown to guide the eye.

Additional indications for reduced dissociation come from the water tracer diffusion coefficient D_{H_2O} and the diffusion coefficient D_{σ} (mobility of protonic charge carriers as obtained from the conductivity via the Nernst–Einstein relationship) recorded down to low water concentrations (see Figure 4.21). D_{σ} is expected to closely follow the water

diffusion coefficient at least for low water volume fractions, because here proton conductivity essentially takes place via the vehicle mechanism without significant contributions from structure diffusion (Grotthuss mechanism[9]). For high water contents D_σ exceeds D_{H_2O} since sufficient amount of water allows for additional intermolecular proton transfer between water molecules. However, in sPSO₂-220 (**2**) the mobility of protonic charge carriers at low water contents falls below the solvent diffusion coefficient, which also points towards incomplete dissociation.

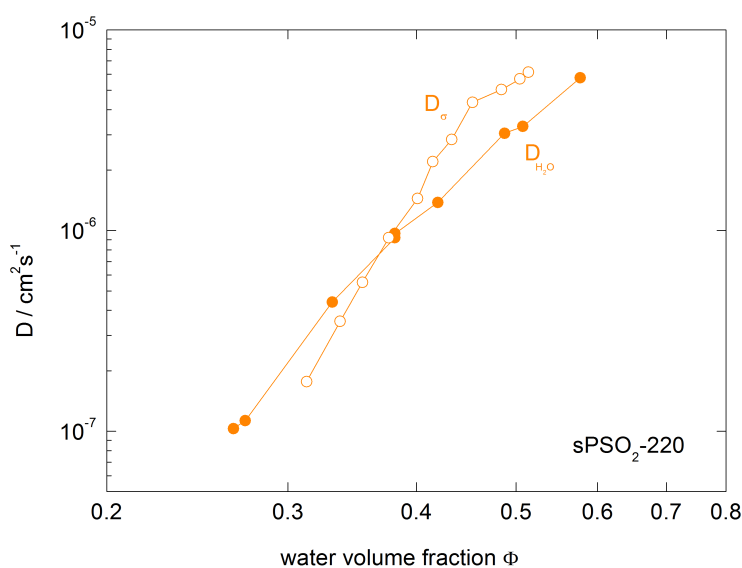


Figure 4.21: Room temperature diffusion coefficients as a function of water volume fraction for sPSO₂-220 (**2**). Open symbols: conductivity diffusion coefficients D_σ , calculated via Nernst-Einstein equation from conductivity data assuming complete dissociation. Filled symbols: water diffusion coefficients D_{H_2O} from PFG-NMR (data taken from [17]).

The incomplete dissociation of protons is also reflected in the hygroscopicity. The reduced dissociation is expected to reduce the water uptake because a large part of the heat of hydration stems from the hydration of dissociated protons. The hydration number λ is usually similar for most of the sulfonated polyelectrolytes especially at moderate relative humidity, but the water content of the highest sulfonated polymer **3** is only about half of that of all the other ionomers and polyelectrolytes (see Figure 4.22). Important to note is that at higher water contents, where the hydration is mainly of entropic nature (osmosis), **2** and **3** dissolve.

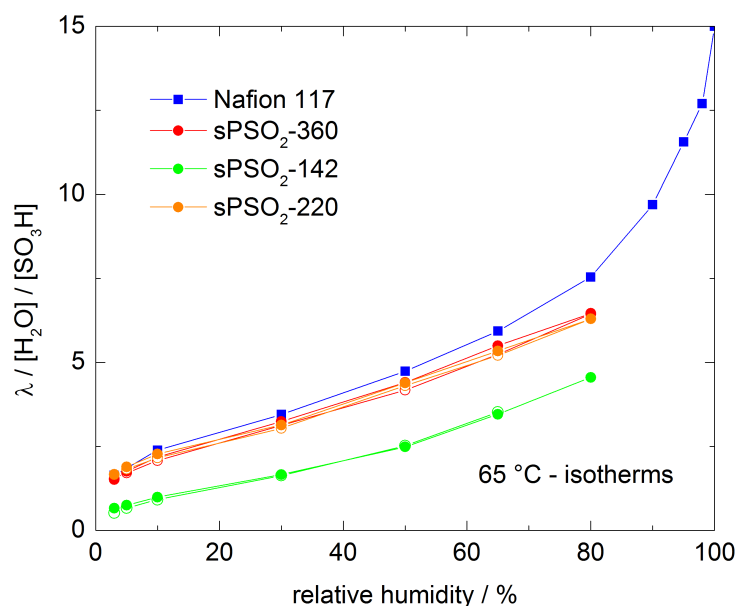


Figure 4.22: Hydration isotherms of Nafion (data taken from [65]) and of sulfonated polyelectrolytes of different equivalent weights (IECs) at $T = 65\text{ }^{\circ}\text{C}$. Number of water molecules per sulfonic acid as a function of relative humidity. (detailed experimental description see ref. [65]).

4.3.2 Lithium and sodium form

Lithium conductivity in the sulfonated polyelectrolytes **2** and **4** was shown to be a single ion conductivity as the comparison of ^7Li tracer diffusion coefficient D_{tr} (by PFG-NMR) fully matches the conductivity diffusions D_{σ} (via the Nernst–Einstein relationship with the total Li-concentration as the charge carrier concentration) measured by impedance spectroscopy.[5] In other words only positive (Li^+) charge carriers contribute to the overall conductivity.

The comparison between lithium and sodium conductivity (see Figure 4.23) shows only a small difference, which most probably stems from the different degrees of dissociation. The concentration dependence of the conductivity (see Figure 4.24) shows an increase with increasing solvent content for polyelectrolytes with the same IEC until a maximum. At the beginning not enough solvent is present to efficiently solvate all ions, but with decreasing concentration of lithium (increasing solvent content) also

dissociation increases. Along with faster solvent dynamics caused by less interaction with the polymer, this explains the increasing in conductivity.

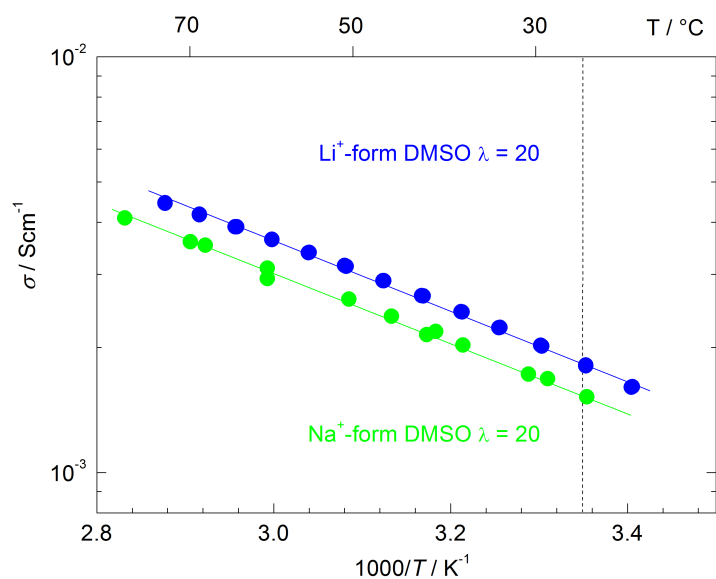


Figure 4.23: Ionic conductivity of sPSO₂-220 (**2**) with $\lambda = 20$ DMSO in lithium and sodium form as a function of temperature.

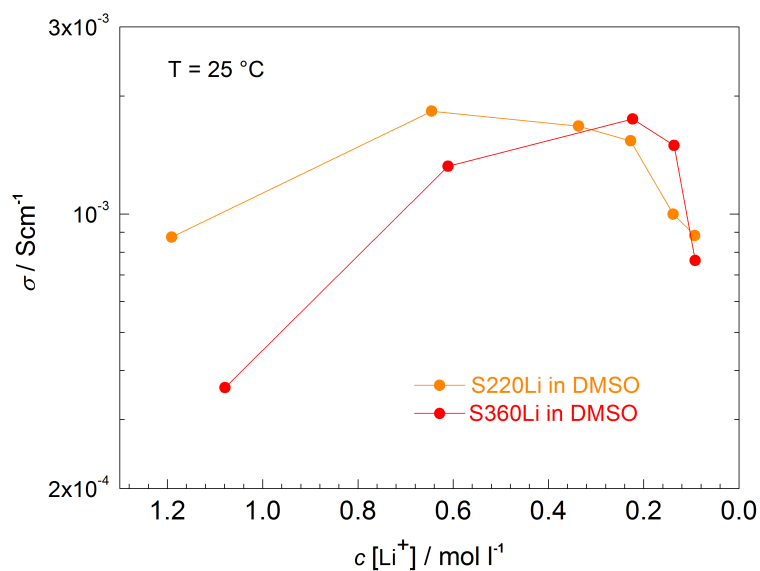


Figure 4.24: Ionic conductivity of sulfonated poly(phenylene sulfone)-S220 (**2**) and -360 (**4**) in lithium form solvated with DMSO as a function of lithium concentration (calculated from the polyelectrolyte) at $T = 25$ °C. High ionic conductivities are observed even for concentration below 1 mol l^{-1} lithium.

The conductivity decrease is simply caused by the dilution of the systems; the maximum mobility of the charge carrier is already reached but the concentration decreases. It should be specially noted that high conductivities are found for a wide concentration range, which strongly affects the viscosity of the solution.

Most lithium based batteries use salt solutions (e.g. LiPF_6 in carbonate solvents) as electrolytes. They are known to show extremely high ionic conductivities of more than 10 mS cm^{-1} at RT.[66] In comparison, sulfonated polyelectrolytes in lithium form exhibit conductivities an order of magnitude lower (see Figure 4.25).

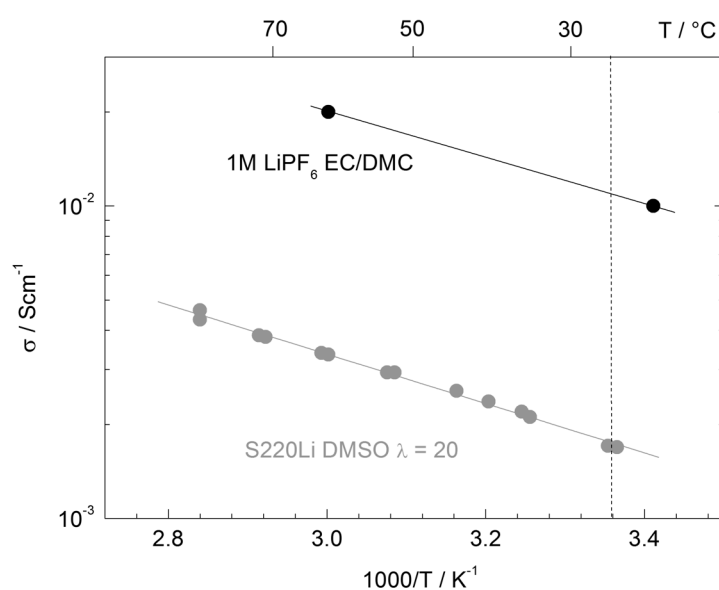


Figure 4.25: Ionic conductivity of sulfonated poly(phenylene sulfone)-220 (2) in lithium form with $\lambda = 20$ DMSO compared to 1 M LiPF_6 in a EC/DMC (commonly used Li-battery electrolyte) as a function of temperature.

The solvating properties of common battery solvents (EC, PC, DMC, PEO) for lithium salts are rather poor and dissociation in such systems is far from complete. The residual ionic interactions lead to correlations of the ionic motion of cations and anions by the formation of contact ion pairs, triple ions and higher aggregates. Such electrolytes are more efficient anion than cation conductors, which translates into a lithium transference number even below $t_+ = 0.5$. The lithium conductivity of such polyelectrolyte solutions in lithium form is found to be similar to salt solutions.(see Figure 4.26).

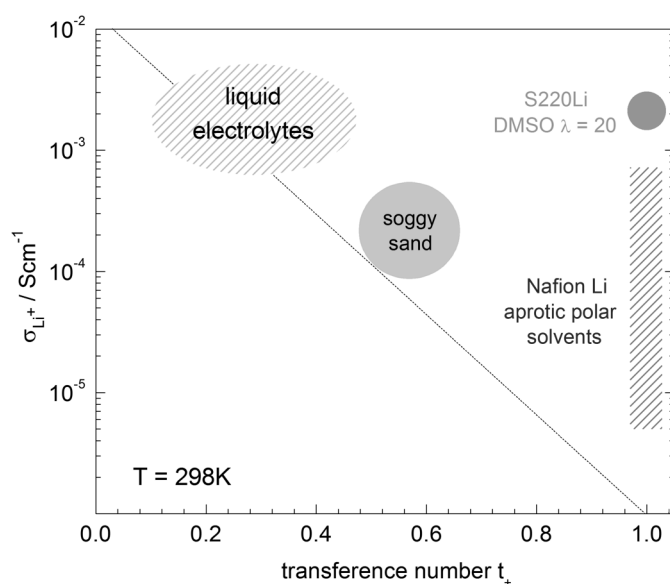


Figure 4.26: Lithium ion conductivity fraction from the total conductivity as a function of transference number at room temperature for different lithium electrolytes.

Apart from that, the transference number of $t_+ = 1$ for polyelectrolyte solutions reduces polarization effects within the electrolyte, which allows for high power batteries with extremely fast charge and discharge rates (see section 1.3). Most other approaches toward high transference numbers either obtain a transference number clearly below unity [67] or a tremendously reduced conductivity[68].

Although conductivities of the polyelectrolytes are extremely high, more than half of the lithium-ions in DMSO remain condensed to the fixed anionic groups. This still leaves some space for a conductivity enhancement by increasing the degree of dissociation. Unfortunately, solvents with higher dielectric constants and also mixtures of high Lewis basic and acidic solvent could not increase the conductivity.

When it comes to the application of such electrolytes in real electrochemical cells, the tunability of viscosities makes them very interesting for filling porous separator or electrode structures, such as in Li-O₂ batteries[69]. These batteries have extremely high specific energies, but an efficient electrolyte for the gas diffusion cathode is needed. The electrode structure needs to accommodate substantial amounts of LiO₂ and Li₂O₂ without blocking the solid, liquid and gaseous interface or the supporting catalyst. To

allow efficient ion transport, liquid salt electrolytes based on carbonates have been used, however, recent studies showed a fast decomposition under battery conditions.[70] Two proposed alternative solvents were DMSO and DMAc[71][72], which both lead to high conductivities in the polyelectrolyte (see Figure 4.27).

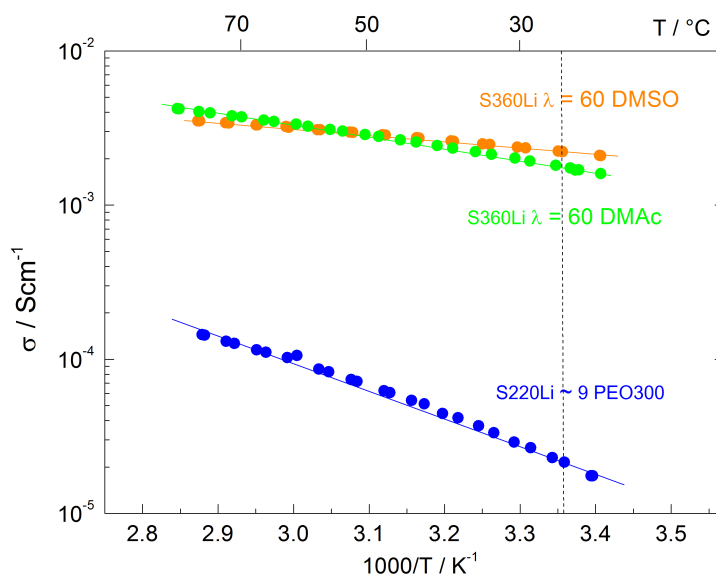


Figure 4.27: Ion conductivity of sulfonated poly(phenylene sulfones)-220 (**2**) Li-form with DMAc (blue) and DMSO (black) as solvents both at $\lambda = 60$ as a function of temperature.

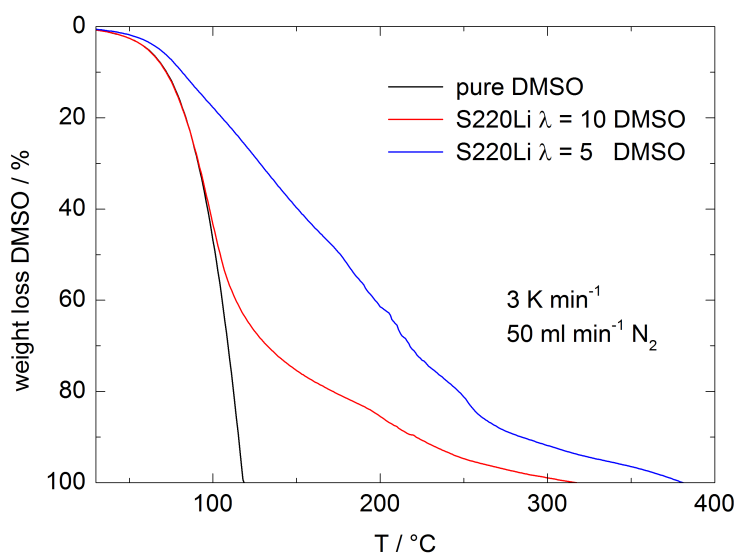


Figure 4.28: Thermo gravimetric weight loss of DMSO in sulfonated poly(phenylene sulfones)-220 (**2**) Li-form with $\lambda = 5$ (red) and 10 (blue) DMSO. Pure DMSO (black) is given for comparison.

Most organic solvents have a high vapor pressure, causing fast evaporation rates in gas diffusion electrodes and less solvent leads to decreased ionic conductivities. Different from that, the evaporation of DMSO in polyelectrolytes is greatly reduced (see Figure 4.28). This finding is probably connected to the strong interaction of the solvent molecules with the counterion and the functional groups on the polymer backbone.

4.4 Microstructure of sulfonated polyelectrolytes

In addition to the microconformation in diluted solution discussed in in section 4.1.1 and 4.1.3 influences of intermolecular interactions between different polymer chains need to be consider at high polyelectrolytes concentrations The formation of distinct microconformations is the first step in the microstructure formation process of membranes, as most of the sulfonated poly(phenylene sulfone) films are prepared by solution casting. In this technique, the evaporation of solvent leads to an increase in polymer concentration causing additional interpolymer interactions. The resulting microstructure depends on the amount of residual solvent. However, the complete microstructure formation is very complex and still poorly understood, especially the relevant interactions are not fully resolved. Therefore, a few aspects (IEC, kind of solvent and counterion) are discussed in this section.

4.4.1 Influence of IEC

Experimentally, a distinct correlation between the IEC of sulfonated polyelectrolytes and the characteristic correlation length of their nanomorphology in the protonic hydrated membrane form is found (see Figure 4.29). The increase in IEC leads to a more dispersed water phase in the membrane corresponding to a decreasing correlation length between primary polymeric objects. The correlation length d (also called ionomer peak) is in the order of a few nanometers and is the characteristic separation length between the polymer and water phase. The width of this peak depends on the disorder between these two phases. For higher IECs narrower and more ordered structures with lower correlations length are found. The narrower and more distinct morphological evolution with increasing IEC of sulfonated poly(phenylene sulfones) is reversed, when moving to the extremely high IEC of sPSO₂-142 (**3**) (see Figure 4.30). This is actually quite expected because of the severe counterion condensation in structure **3** with around 70 % of the ions condensed to the sulfonic acid groups. The found correlation therefore gives additional support for counterion condensation in the solid membrane form and suggests the formation of a well-ordered Coulomb “lattice” through electrostatic interaction.

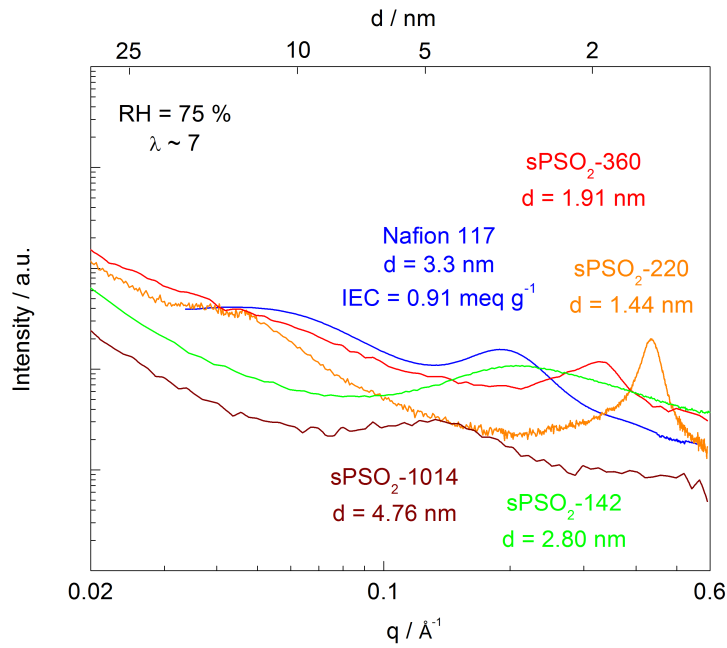


Figure 4.29: Small angle X-ray diffraction patterns of sulfonated poly(phenylene sulfones) and Nafion of different equivalent weights (IEC) at RH = 75 % ($\lambda \sim 7$). The polyelectrolytes show a distinct correlation d (so called ionomer peak) at high q values. Data for Nafion, sPSO₂-360 and sPSO₂-1014 are taken from ref [17].

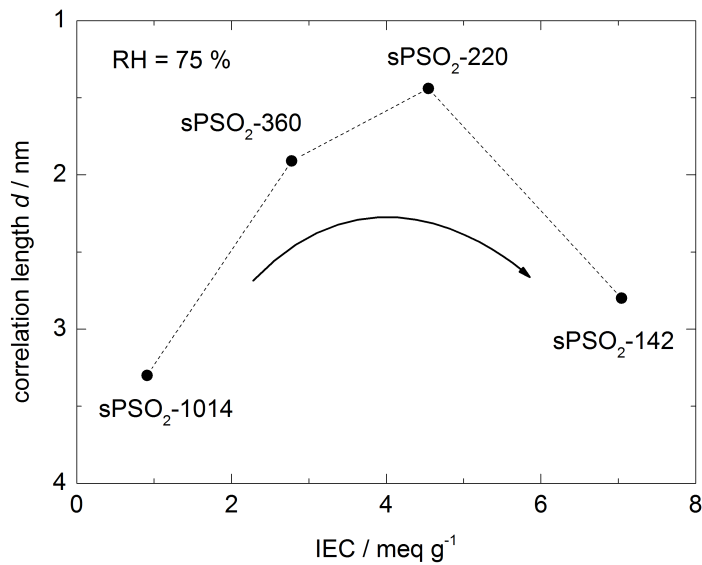


Figure 4.30: Evolution of the correlation length d in SAXS of sulfonated poly(phenylene sulfones) as a function of ion exchange capacity (IEC) at RH = 75 % ($\lambda \sim 7$).

Microstructural features are also expected to affect solvent (water) and ion transport. The percolation and tortuosity on the nanometer scale reduces the absolute

(macroscopic) value of the diffusion coefficient, but more important is that an increasing concentration of dissociated sulfonic acid groups for constant λ is expected to decrease the local water diffusion coefficient because an increasing amount of water molecules are involved in the solvation of the immobilized groups (SO_2 and SO_3).

4.4.2 Influence of counterions

The influence of the kind of counterion on the small angle X-ray scattering pattern of sPSO₂-220 (**2**) at a relative humidity of 75 % is shown in Figure 4.31. A few features are immediately visible in the scattering pattern; a pronounced correlation peak is present for all ion forms, which decrease to lower d values in the order (H^+) < (Li^+) < (Na^+).

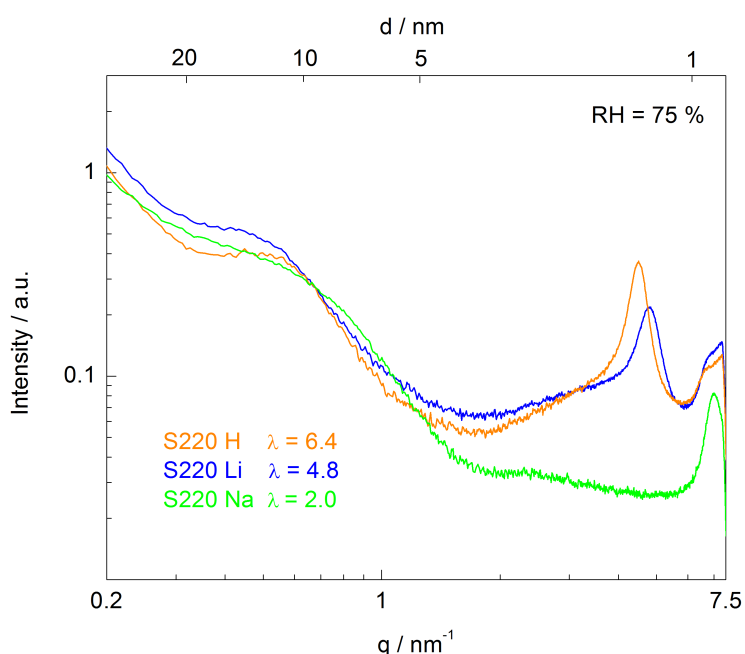


Figure 4.31: Small angle X-ray diffraction patterns of sulfonated poly(phenylene sulfones)-220 (**2**) in different ionic forms (orange: protonic form, blue: lithium form and green: sodium form at RH = 75 %). The ionomer peak is shifting towards lower d from H^+ to Na^+ (decreasing correlation length), which correlates to the water uptake.

The trend of decreasing correlation length d mainly is caused by different amounts of water, causing shorter distances between primary polymeric objects. The different water contents reflect the decreasing hydration enthalpy in the order $\text{H}^+ > \text{Li}^+ > \text{Na}^+$.

Another feature (peak) in the SAXS pattern is visible at larger correlation length of $d = 10 - 20$ nm. Up to now there is no clear explanation for such a correlation, but one may speculate that it is related to the size of single polymer coils which are preformed in casting process.

4.4.3 Influence of solvents

Dissociation strongly depends on the kind of solvents. Therefore, also the influence of different solvents and solvent mixtures on the microstructure formation was investigated. Figure 4.32 shows the SAXS patterns of **2** in lithium-form for water, DMSO, and mixtures of both. The comparison of pure water and DMSO as solvents shows a big difference for low and high correlation length.

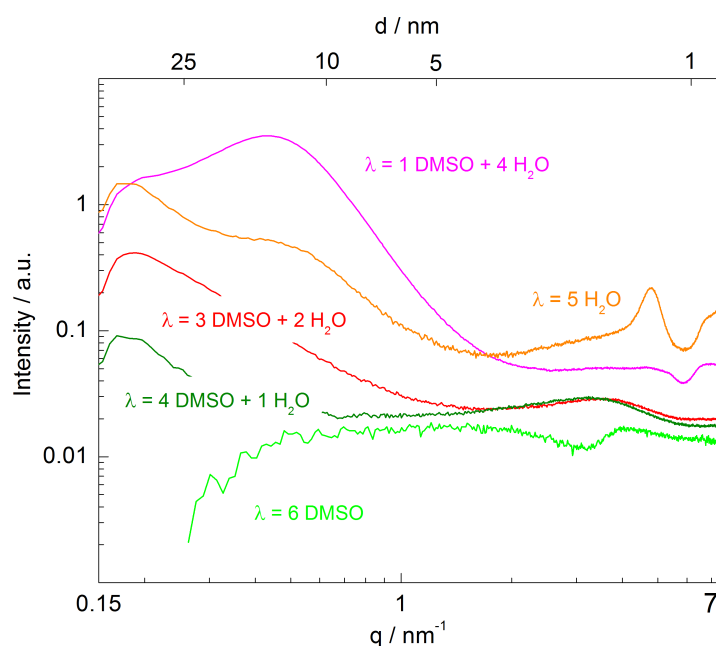


Figure 4.32: Small angle X-ray diffraction patterns of sulfonated poly(phenylene sulfones)-220 (**2**) in lithium form with different fixed λ of DMSO exposed to RH = 75 %. For comparison also pure DMSO $\lambda = 6$ and water $\lambda = 5$ are shown. From high to low DMSO contents a correlation at high d is appearing and shifting towards lower d for increasing amount of water. At the same time a so called ionomer peak is appearing, getting sharper and is shifting towards lower d for increasing water content.

Almost no ionomer peak is observed for DMSO while water causes a very distinct correlation around $d = 2$ nm. The previous results suggest a higher dissociation constant for DMSO compared to water as solvent. On a first glance, this contradicts the dissociation results as more pronounced electrostatic interactions are expected for high degrees of dissociation. However, it was also shown, that DMSO strongly coordinates to the counterion and this may be unfavorable for the formation of a well-ordered Coulomb "lattice".

For solvent mixtures an additional very pronounced correlation is emerging for increasing water: DMSO ratios. Again no clear explanation for such a correlation can be given. In addition an ionomer peak is appearing which gets sharper and moves towards lower correlation length for higher water contents.

4.5 Acid-base blend membranes

4.5.1 General aspects

The state-of-the-art perfluorosulfonic acid based PEMs have severe drawbacks, such as high cost, high fuel crossover, limited chemical stability and most importantly limited operating temperature (below $T = 90\text{ }^{\circ}\text{C}$) because of membrane softening. To overcome these drawbacks, in recent years a number of alternative membranes have been developed based on sulfonated aromatic polymers. A major trend focused on hydrophilic–hydrophobic multiblock copolymers to combine a hydrophilic proton conducting phase and a hydrophobic phase responsible for the mechanical stability of the membrane. The synthesis of these multiblock copolymers, however, is typically very costly, difficult to reproduce and extremely complex since it involves several synthetic steps.[14][15][16]

Another approach towards hydrocarbon-based membranes makes use of classical polymer blending. The goal here, similar to multiblocks, is to achieve a bi-continuous phase separation (see Figure 4.33 middle) between a hydrophilic, proton conducting polymer and a hydrophobic, membrane forming polymer.

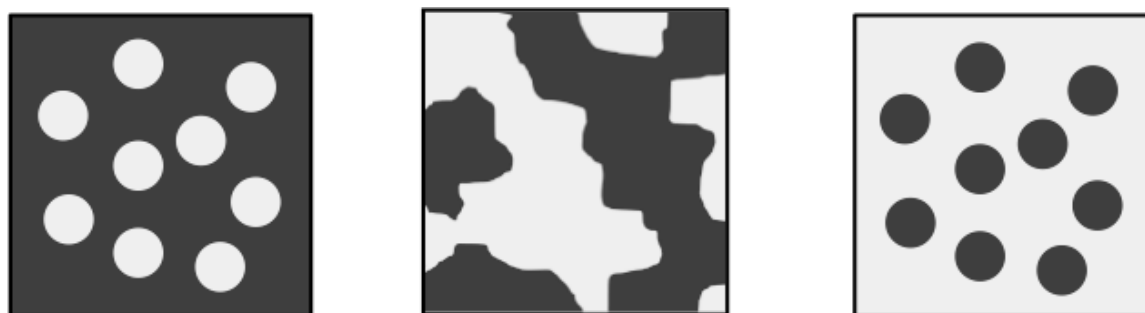


Figure 4.33: Schematic of hydrophilic (bright) and hydrophobic (dark) phase separation in polymer blends for different ratios of hydrophilic to hydrophobic polymer. Left and right picture show a dope like separation without any connectivity of one phase. The center picture illustrates a bi-continuous phase-separation between the two polymers.

A film formed from a common solution of hydrophilic and hydrophobic polymer inherently tends to separate in a drop like manner (see Figure 4.33 left and right) to decrease the contact area indicating a high interfacial energy. In order to reduce the

interface energy, interactions between the two polymers are introduced. One approach uses strongly basic groups on the hydrophobic polymer, which lead to acid-base interactions to sulfonic acid groups of the hydrophilic polymer (ionic crosslinking). The use of sulfonated polyether ketones with ion exchange capacities of less than 1.8 meq g^{-1} didn't allow for sufficient proton transport.[73]

In contrast to this, sulfonated poly(phenylene sulfones) show excellent proton conductivities (see previous 4.4). However, membranes made of such polymers suffer from low mechanical stability. The high concentration of sulfonic acid groups on the polymer backbone (important for the conductivity) leads to dissolution of the polyelectrolyte at high water contents and appears to be responsible for the brittleness in the dry state. The aim is to preserve the transport properties but introduce a viscoelastic behavior that allows for deformation without mechanical failure of the membrane, in particular at high temperatures ($T > 100 \text{ }^\circ\text{C}$) under dry conditions ($RH < 50\%$) and decrease the water uptake at high water activities (no dissolution or extensive swelling). Such operating conditions are believed to need less catalyst loading in the electrodes, and smaller cooling and humidification systems.

Similar to the above concept, also sulfonated poly(phenylene sulfones) were blended with polybenzimidazole (PBI). In these polymer blends, the interaction between the strong basic benzimidazol ($\text{pK}_B = 1 - 2$) [74] and the highly acidic sulfonic acid group leads to the formation of strong ionic cross-links. Therefore, the formation of a common casting solution without precipitation is only possible if the protons of the sulfonic acid group are exchanged by larger cations (neutralized). PBI is a stiff polymer which suppresses the microstructure formation in sulfonated poly(phenylene sulfones) and the high concentration of basic sites in polybenzimidazole leads to a severe decrease in IEC. The proton conductivity of the blended material is more than two orders of magnitude lower as for the pure polyelectrolyte and additionally shows a severe decrease with decreasing relative humidity (see Figure 4.34).

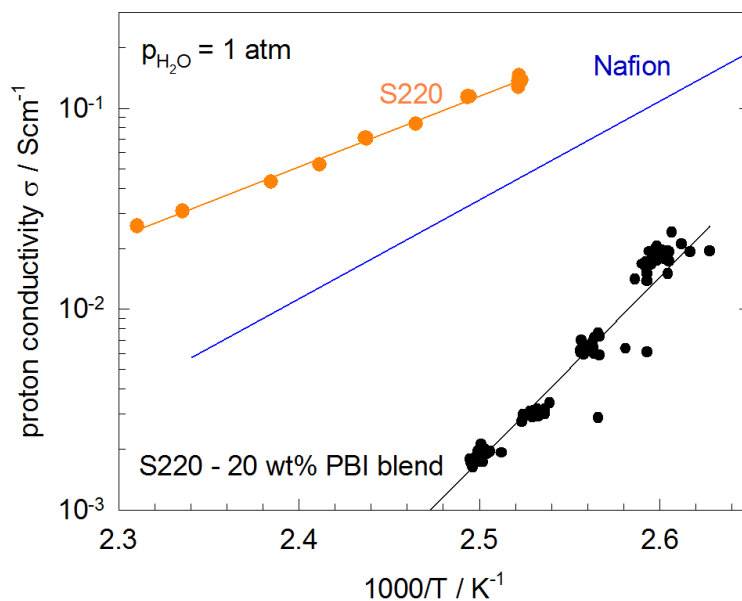


Figure 4.34: Proton conductivity of sulfonated poly(phenylene sulfones)-220 (2) (orange) and blend with 20 wt% polybenzimidazole (black) at given water pressure of $p = 1$ atm as a function of temperature (data taken from HiPEM project report). Data of Nafion are given for comparison (blue).

4.5.2 Concept

Different from all previous blend concepts, the here introduced approach uses sulfonated poly(phenylene sulfone)-360 (4), with an intermediate IEC of 2.8 meq g^{-1} which heavily swells in water but does not dissolve. The blending with an unsulfonated polysulfone needs to reduce the swelling and has to introduce mechanical stability without significantly decreasing transport. The blend membrane should show a phase separation in the order of a few nanometers to preserve the local structure of the sulfonated polysulfone, which is responsible for the excellent transport characteristics. First pretest with pristine UDEL, a polysulfone as blend component (detailed structure see Figure 4.37 top), known for its high chemical stability, flexibility and good film forming properties resulted in an unfavorable drop-like separation (see Figure 4.35) even for various common solvents and different ratios of hydrophilic-to-hydrophobic polymer. A general observation was that this phase separation takes place at the end of the film forming process. Therefore the idea was to introduce a weak interaction

between the two polymers to overcome this separation at high polymer concentrations. For such a purpose an acid-base interaction is ideal as its strength can be controlled by the acidity and basicity of the involved groups. The sulfonic acid group on the hydrophilic polymer can not be changed but different basic functionalities can be introduced into the hydrophobic polymer without to much experimental effort.

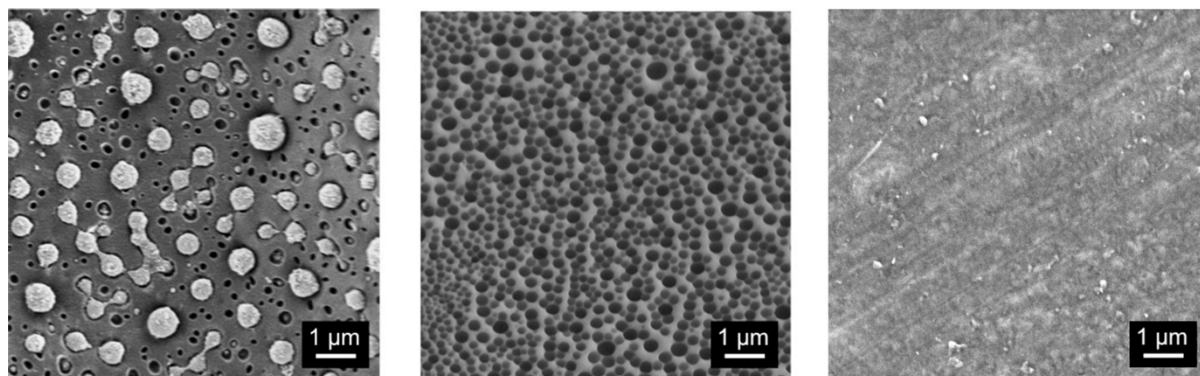


Figure 4.35: Scanning electron microscopy pictures of polymer blends between sulfonated poly(phenylene sulfone)-360 (**4**) (bright regions – silver stained) and UDEL (dark regions) cast from a common solution (DMSO) at different polyelectrolyte/polymer ratios (left 30/70, middle 70/30). Both ratios show a drop like separation. Right picture: blend with Py-UDEL (30 mol%, 20 wt%) with no separation in the μm -scale

The work on PBI blend membranes showed a very strong interaction between benzimidazole and sulfonic acid (Figure 4.36 left). Therefore a weaker base was chosen as basic functional group, namely pyridine with a $\text{pK}_B = 8.75$ [74] (Figure 4.36 right).

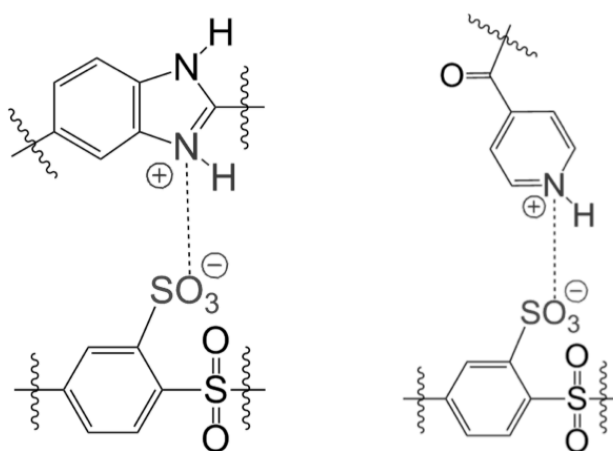


Figure 4.36: Schematic of acid-base interaction between sulfonated polysulfone and PBI (left) and pyridine (right).

In the following a short description of the basic modification procedures of UDEL and a detailed study of the corresponding acid-base blend membranes is given with a special focus on the mechanical properties.

4.5.3 Synthesis of pyridine modified UDEL and blend formation

The pyridine modified polymer was prepared by substitution reaction. In a first step, the polysulfone material (UDEL) was lithiated by *n*-butyllithium at low temperatures ($T = -70\text{ }^{\circ}\text{C}$) followed by the substitution of a ethylether having a pyridine residue (see Figure 4.37).[75] The substitution degree was varied from 16 mol% eg^{-1} to more than 100 mol% (multiple functionalization per equivalent (repeating unit) by using different amounts of lithiation agent. The actual obtained degree of modification could be precisely determined by $^1\text{H-NMR}$ (the final product is in the following named Py-UDEL).

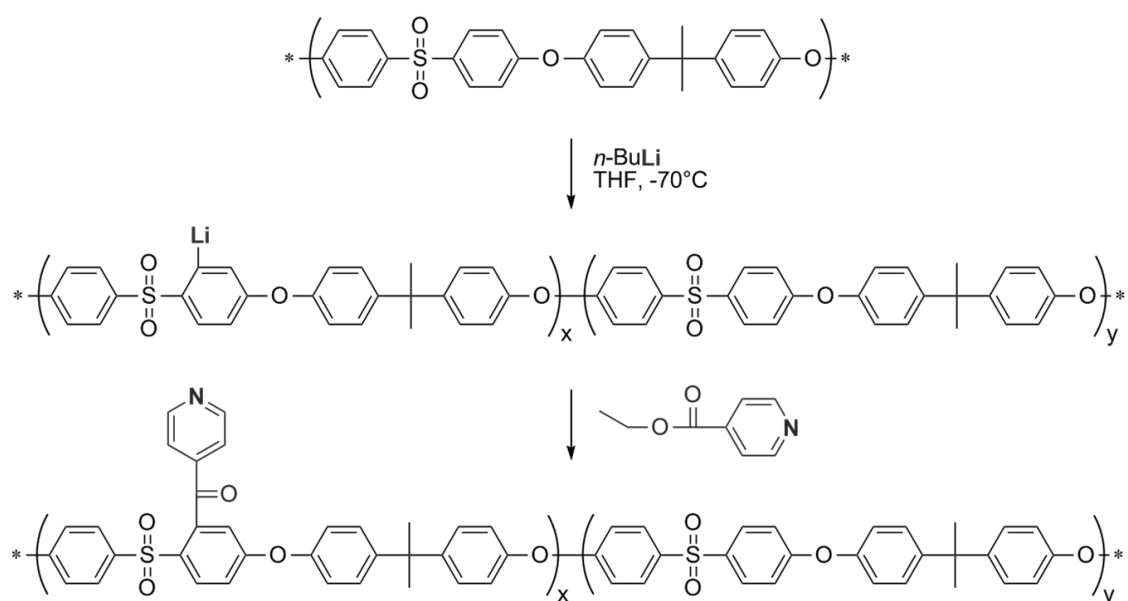


Figure 4.37: Synthesis of pyridine modified UDEL. First step lithiation by *n*-butyllithium followed by a second substitution step.

The Py-UDEL and sPSO₂-360 blend membranes were formed by solution casting from a common solution (DMAc) and did not show any phase separation in the μm scale (see

Figure 4.35 right). The fraction of hydrophilic to hydrophobic polymer was varied between 10 - 30 wt% for the basic polymer.

4.5.4 Acid-base interaction

The acid-base interaction between sPSO₂-360 and Py-UDEL already needs to be present in solution in order to support the film forming process by avoiding phase separation in the μm scale. In order to preserve the properties of the two components in a blend membrane a bi-continuous phase separation is needed.

To study the presence of the acid-base interaction in solution, E-NMR measurements on dilute DMSO solution of the polymers were performed. In the E-NMR measurement charged particles will show a phase shift. Figure 4.38 presents ¹H-NMR spectra of three different samples, pure Py-UDEL, sPSO₂-360 and a 1:2 mixture of both, for different applied electric field.

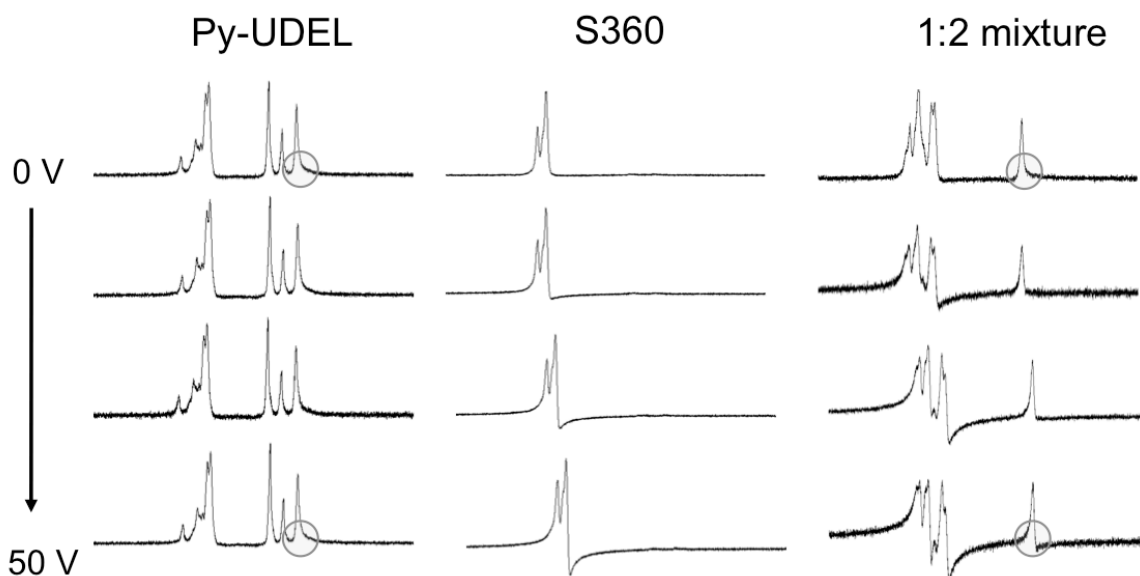


Figure 4.38: ¹H NMR-spectra in DMSO-d₆ (without ppm scale) of 109 mol% pyridine modified UDEL (left), pure sulfonated poly(phenylene sulfone)-360 (4) (middle) and 1:2 mixture of both at different applied electric fields in an PFG-NMR experiment.

Pure Py-UDEL shows no phase shift in the NMR signal. This is expected as the weak basic pyridine group, even with traces of water, should not be charged. Different from this observation is the result for sPSO₂-360, here a clear phase shift is present, corresponding to dissociated sulfonic acid groups. The mixture of both shows the same phase shift for the NMR signal related to sPSO₂-360 but interestingly also a phase shift, in the same direction in the signal of Py-UDEL appeared. Most probably the interaction between the two polymers leads to a coupling of the Py-UDEL to the sPSO₂-360, neutralizing the sulfonic acid group. The residual charged sulfonic acid groups on the sPSO₂-360 leads to a movement in the applied electric field, pulling along the basic UDEL. Of course, these results are not a quantitative measure but at least they show the presence of acid-base interaction in solution.

4.5.5 Ion transport and water uptake

Ionic conductivity

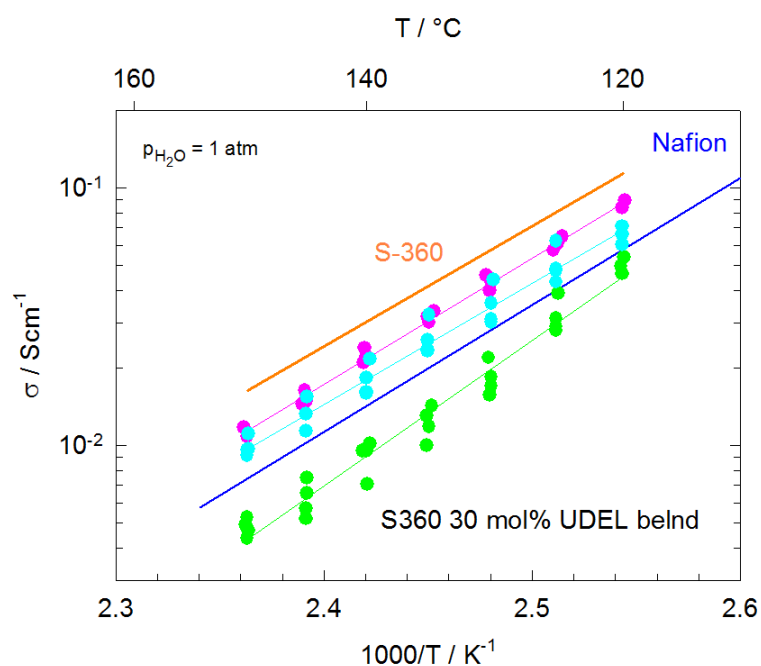


Figure 4.39: Proton conductivity of sulfonated poly(phenylene sulfones)-360 (4) blends pure (orange) and of different wt% of 30 mol% pyridine modified UDEL (10 wt% pink, 20 wt% light blue and 30 wt% green) at a given water pressure of 1 atm as a function of temperature. Data of Nafion are given for comparison (dark blue).

The proton conductivities of 30 mol% Py-UDEL sPSO₂-360 blends only slightly decrease with increasing weight percent (wt%) compared to pure sulfonated polysulfone of basic polymer (see Figure 4.39). For 10 and 20 wt% Py-UDEL the conductivity values are still far above that of Nafion. The temperature dependence at given water pressure of the blends, different for PBI blends, is similar to pure sPSO₂-360, which is a first indication for the preserved structure within the hydrophilic domain.

The same trend is observed for different degrees of modification (see Figure 4.40). The conductivity decrease for different modification degrees by constant weight percent of basic polymer is not reflected in the experimental determined IECs. This is most likely caused by acid-base interactions; by trapping the mobile protons of the sulfonic acid groups, the mobile charge carrier concentration is decreased and the “trapped” protons no longer take part in the conduction mechanism. However, the protons in an acid-base interaction seem to be accessible for hydroxide ions of the titration base.

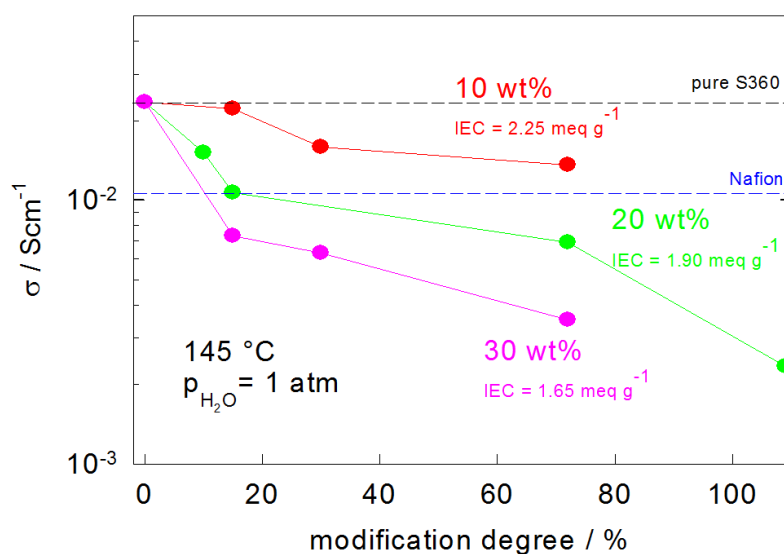


Figure 4.40: Proton conductivity of different wt% blended sulfonated poly(phenylene sulfones)-360 (4) with at a given water pressure of $p = 1$ atm and $T = 145$ °C as a function of pyridine modification degree. Values of Nafion and pure sPSO₂-360 are given for comparison (dark blue).

Membrane Swelling

One of the main purposes of blending is to reduced swelling at high water activities. This was determined by measuring the weight gain of in water immersed membrane pieces. The water uptake (see Figure 4.41) expressed as hydration number λ is significantly reduced in the blend membranes compared to pure sPSO₂-360 and is in the order of that of Nafion. Expressed as water volume fraction this still is about 2 times higher as for Nafion, however, the narrower microstructure (see section 4.5) in the sulfonated polysulfones leads to higher dispersed water film.

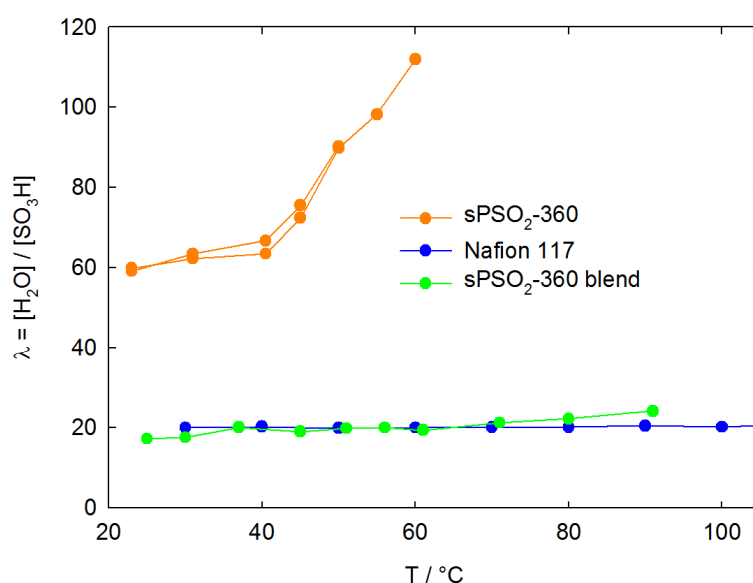


Figure 4.41: Water uptake expressed as hydration number $\lambda = [\text{H}_2\text{O}]/[-\text{SO}_3\text{H}]$ of sPSO₂-360 (4) blend membrane with 20 wt% of 30 mol% pyridine modified UDEL as a function of temperature. For comparison also the water uptake of pure sPSO₂-360 (4) and Nafion are given. sPSO₂-360 (4) shows extreme swelling while the water uptake of the blend membrane is reduced to around $\lambda = 25$.

4.5.6 Mechanical properties

The mechanical properties of pristine sPSO₂-360 are practically not measurable due to its extreme brittleness. Therefore all following results on blend membranes are compared to Nafion. An extremely high storage modulus was observed for the blend membranes up to temperatures of $T = 220$ °C and a relative humidity of $\text{RH} = 1$ %,

whereas Nafion already softens under moderate conditions of around $T = 100\text{ }^{\circ}\text{C}$ (see Figure 4.42). Surprisingly, no hysteresis was found for sulfonated polysulfones.

Apart from the storage modulus, an important parameter for practical use is the fracture toughness. The stress-strain behavior of blends for different conditions (T , RH) and two modification degrees are shown in Figure 4.43. The elongation at break as well as the elastic and plastic deformation critically depends on temperature and relative humidity. In particular, the maximum elongation at break decreases with increasing temperature and lower water activities while the force at break scales inversely. This can be attributed mainly to an increased elastic behavior. At $80\text{ }^{\circ}\text{C}$ and 80% RH blended membranes show an elongation at break $>70\%$, which is to the best of my knowledge the highest value for hydrocarbon base PEM membranes.

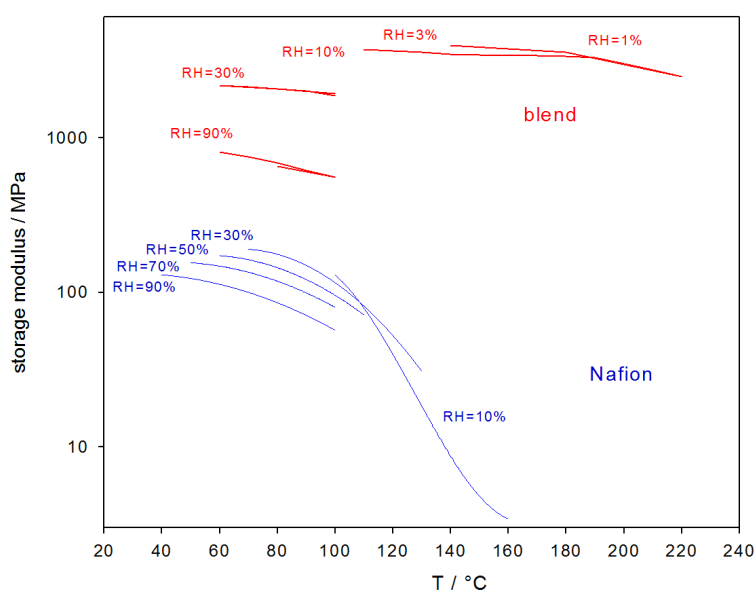


Figure 4.42: Dynamic mechanical analysis: Storage modulus of a blend membrane (sPSO₂-360 (4) 20 wt% 16 mol% Py-Udel) as a function of temperature for different RHs (red). Data for Nafion are given for comparison (blue). The blend membrane shows no softening even at very low RH and high temperatures.

The increasing degree of basic modification (Figure 4.44) revealed a more brittle (shorter elongation at break) behavior for higher concentrations of pyridine groups. However, it is not clear whether the maximum elongation is somewhere between the two studied materials or even at lower degrees of modification.

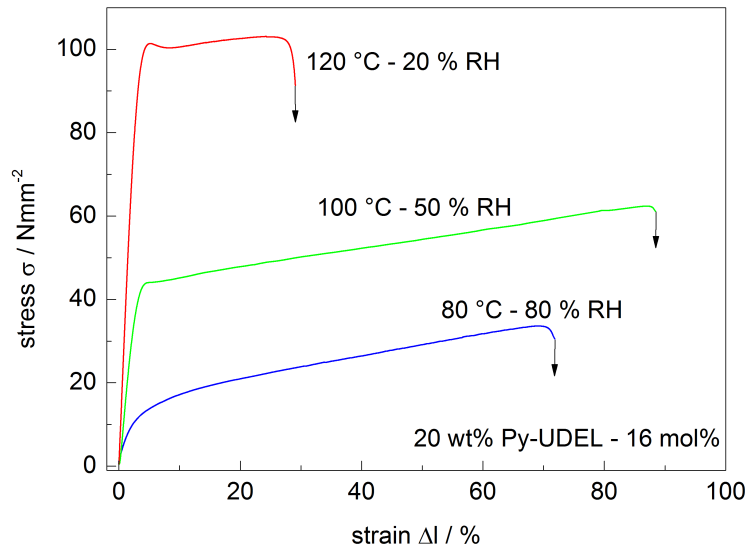


Figure 4.43: Stress-strain curves for different sPSO₂-360 (4) Py-Udel blends with 20 wt% of 16 mol% Py-Udel at different temperatures and RHs showing an increase in stress at break and a decrease of the elongation at break.

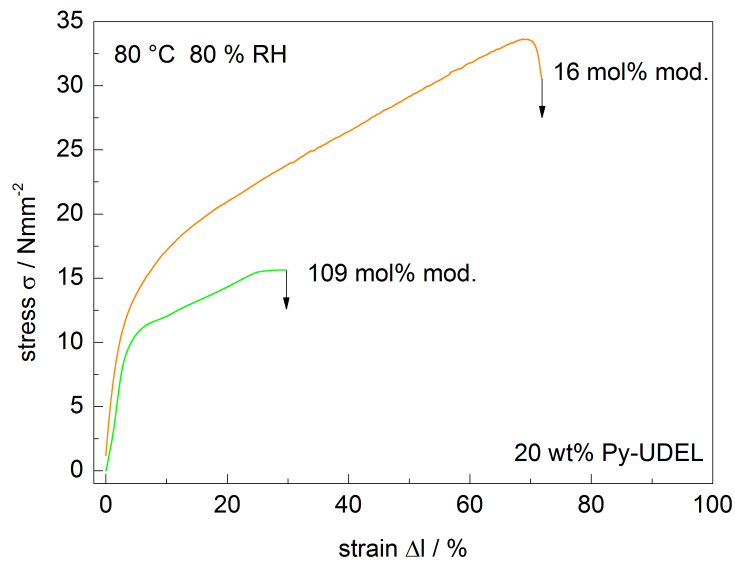


Figure 4.44: Stress-strain curves of sPSO₂-360 (4) 20wt% Py-Udel at T = 80 °C and RH = 80 % for 16 und 109 mol% modification degree. The increase of modification results in more brittle mechanical properties.

4.5.7 Microstructure

From SAXS data (Figure 4.45) it is evident that the microstructural features found in pristine sPSO₂-360 (**4**) (see Figure 4.29) are preserved within the hydrophilic phase in blend membranes. Although the ionomer peak intensity is decreasing with increasing amount of basic polymer, it is still clearly visible for weight percent.

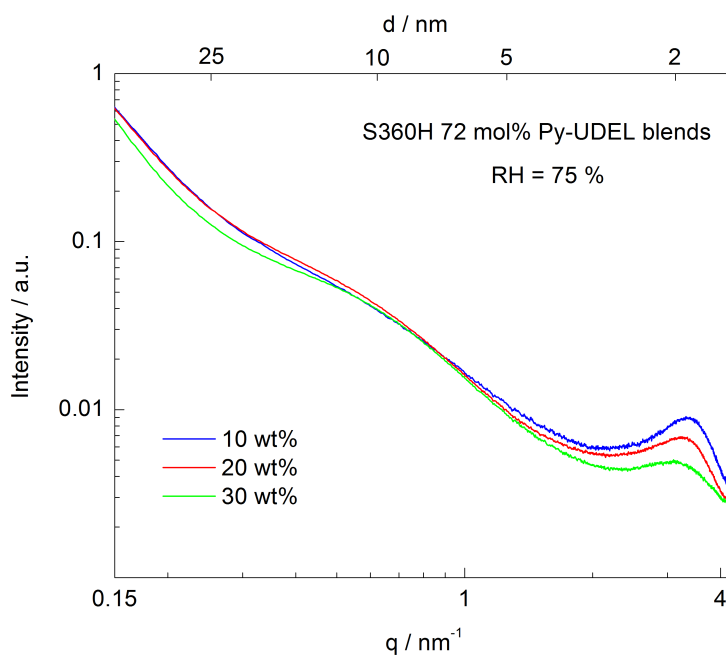


Figure 4.45: Small angle x-ray scattering patterns of sPSO₂-360 (**4**) with 72 mol% pyridine functionalization.

Generally, the presented polymer blends are the first examples wherein an increase in mechanical properties only barely reduces proton conductivity. The combination of high ion-exchange capacity, high ion-conductivity as well as high chemical and mechanical stability is unique and makes these materials a real alternative for fuel cell and other electrochemical applications.

4.5.8 Lithium conducting membranes for battery applications

Liquid or viscous electrolytes are mostly used in battery applications but a solid, lithium conducting membrane would have some advantage as it could be used as electrolyte

and separator at the same time. However, the previously described blend concept is not suitable for the application with organic solvents used in batteries, because such solvents dissolved the blend membranes. Therefore, two approaches to overcome this problem are presented in the following.

Polybenzimidazole sulfonated polysulfone blends

The ion exchange (with LiCl) of PBI/sPSO₂-220 blends (Figure 4.46) from the proton to the lithium form, leads to membranes stable in DMSO. The reason for this may be the still remaining, strong acid-base interaction between the two polymers, where H⁺ can not be exchanged by LiCl. However, the blends only allows for small amounts of solvent to enter the membrane, which results in lithium ion conductivities in the order of 10⁻⁵ S cm⁻¹.

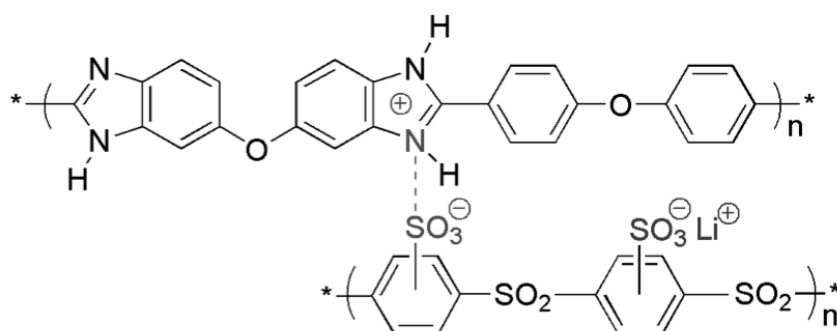


Figure 4.46: Schematic representation of acid-base blend between polybenzimidazole and sulfonated poly(phenylene sulfone)-220 (2). Note, only the sulfonic acid groups not involved in the acid-base interaction are exchanged by lithium ions.

Addition of fumed silica particles

Another approach is the addition of a small fraction of fumed silica nanoparticles (7 nm) to the polyelectrolyte solutions. Small amounts (1 - 5 wt%) of added particles already lead to solid like behavior without losing much of the conductivity (Figure 4.47).

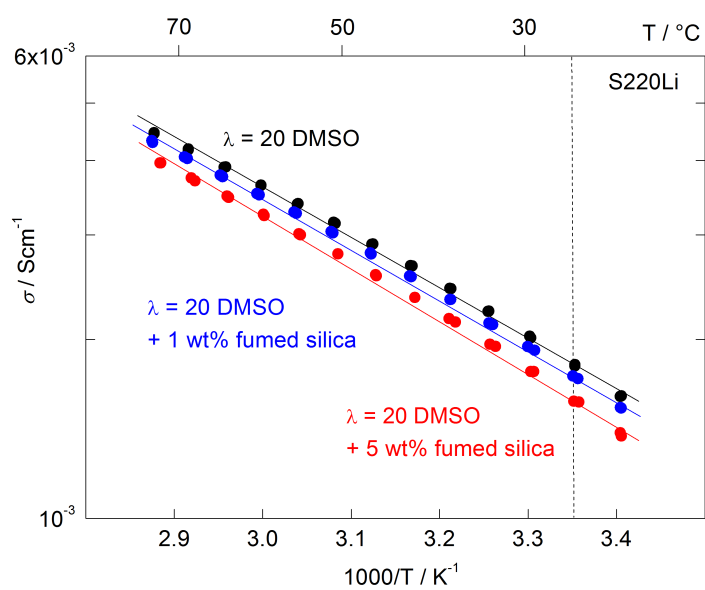


Figure 4.47: Lithium conductivity as a function of temperature for sulfonated poly(phenylene sulfone)-220 (**2**) in lithium form solvated with $\lambda = 20$ DMSO molecules per lithium ion, pure (black), with 1 wt% (green) and 5 wt% (red) of fumed silica. The addition of silica particle leads only to a slight decrease of conductivity.

Chapter 5

Summary and conclusion

The present thesis describes dissociation behavior, nanoscale ordering and transport properties of sulfonated polyelectrolytes with diverse molecular architectures. Different ionic forms solvated with different solvents (polar and unpolar as well as protic and aprotic solvents) are investigated with polyelectrolyte/solvent ratios varying in a wide range. Dilute solutions in which the polymer chains are well separated are studied as well as membranes where interactions between individual polymer strands become increasingly important. Residual ionic interactions, specific directional interactions and the importance of local conformations are identified and studied under conditions close to those of electrochemical applications.

Signatures of residual ionic interactions are observed in the dissociation behavior of high ion exchange capacity polyelectrolytes in diluted solution. If the density of ionic groups on the polymer backbone reaches a point where the average separation is of the order of the Bjerrum length of the surrounding solvent, the degree of counterion condensation starts to depend on details of the molecular structure as well as accessible conformations of the polymer chain. In the protonic form of sulfonated poly(phenylene sulfones) sPSO₂-220 (**2**) the residual ionic interactions even lead to well-defined ionic-aggregates with pair-wise neutralization of sulfonic groups, i.e. triple ions in form of a bridging conformation. For polyelectrolyte architectures with fixed distances between neighboring ionic groups (e.g. sPSO₂-142 (**3**)) reduced dissociation depends on the screening potential of the solvent alone. Indications for residual ionic interactions are not only found for well-separated polyelectrolytes in solution but also between polymer chains at high polyelectrolyte concentrations. As a result, the proton conductivity of hydrated solid polyelectrolytes decreases for high IECs where severe counterion condensation was found. The nanoscale ordering follows the same trend, i.e. with

increasing IEC the characteristic correlation length, corresponding to the separation of primary polymeric objects and aqueous films, again increases as a consequence of reduced dissociation.

The molecular conformation of the polymer backbone strongly influences the dissociation behavior as well as the formation of the nanomorphology. Classical all-atom MD simulations reveal elongated (stretched) polymer conformations for DMSO and water as solvents while chloroform leads to a coil-like (collapsed) configuration. The possible coordination sites and the different affinities of the solvents to coordinate to polar and unpolar groups on the polymer is the reason for the observed conformations. Locally, distinct configurations of the sulfonic acid groups are particularly stabilized by a balance of electrostatic, solvation and configurational free energies.

For different solvents, specific short-range interactions lead to strong variations in the dissociation behavior and polyelectrolyte conformations for water, dimethyl sulfoxide, and chloroform. The nanoscale ordering of the membrane form shows different correlations depending on the kind of solvent and counterion. Surprisingly, a higher fraction of condensed counterion was found in polyelectrolytes solvated with water compared to DMSO, both experimentally and in simulations. These values do not follow the solvent dielectric constants as expected from Manning's counterion condensation theory. Nevertheless, the conductivity of DMSO solvated polyelectrolytes still remains below that of water solvated polyelectrolytes. It was shown that local, directional properties such as electron pair donor and acceptor abilities between solvent and ions are the main reason for the stronger solvation properties of DMSO leading to large solvation shells. The solvated lithium with its larger solvation shell shows a reduced mobility as compared to the average mobility of DMSO. Directional, short-range interactions are also present between different solvents in solvent mixtures. In water-DMSO mixtures, Lewis acid-base interactions lead to the formation of solvent aggregates, which reduce the solvent mobility. Therefore, counterion condensation in polyelectrolytes is not only controlled by the solvent dielectric constant, but also by the chemical nature of the solvent, the immobilized ionic group, and the corresponding counterion. For pure solvents, such as DMSO and DMAc, ionic conductivities in the

lithium form of sPSO₂-220 (2) of more than 1 mS cm⁻¹ (at 25 °C) are obtained even for low polyelectrolyte concentrations. Most important is the finding that this conductivity is a single ion conductivity with an alkaline ion transference number close to unity, leading one to expect the absence of any concentration polarization effects for the use of this class of electrolytes in battery applications.

Besides the transport properties also the investigation of the mechanical properties was part of this thesis. For this, a new polymer blending concept was introduced, which relies on the compatibilization of the blend components through weak acid-base interactions in solution. Membranes cast from such solutions show high proton conductivity and good mechanical properties. Key to success was the use of a hydrophilic polymer with a high IEC and a sparsely basic modified hydrophobic polymer. In the blend membranes the water uptake was reduced, the microstructure of the hydrophilic polymer was retained and the conductivities were only slightly reduced. Such pure hydrocarbon materials usually show very poor mechanical properties. However, the acid base blends show an excellent stress-stain behavior together with very high strength up to temperatures of T = 200 °C. These properties are strongly affected by the degree of modification rather than by the individual polymers alone.

Generally, the polymer blends are the first example wherein an increase in mechanical properties is not on the expense of high proton conductivity. The combination of high ion-exchange capacity, high ion-conductivity also at low RH with high chemical and mechanical stability is unique and makes these materials a real alternative for fuel cell and other electrochemical applications.

Appendix

A1. Experimental details

A1.1 PFG-NMR

PFG-NMR measurements were carried out on a Bruker 400 MHz Avance NMR spectrometer (9.4 T) equipped with a Bruker Diff60 diffusion probe head providing a gradient up to 3000 G cm^{-1} along the z-axis of the polarized field. A selective RF insert for ^1H nuclei with NMR Larmor frequencies of 400.1 MHz was used. Polymer solutions were filled into standard 5 mm NMR tubes, and self-diffusion coefficients of ^1H were measured using pulsed field gradient NMR (PFG-NMR) with the stimulated echo sequence. Self-diffusion coefficients were determined according to the areas of the signals obtained with and without gradient pulses. (see experimental background section) The magnitude of the pulsed magnetic field gradient was varied between 0 and 2300 G cm^{-1} ; the diffusion time Δ between two gradient pulses was fixed to 20 ms, and the pulse duration δ was set to 1 ms. The $\pi/2$ radio frequency pulse length was adjusted to $8.0 \mu\text{s}$. All PFG-NMR experiments were performed at $T = 25 \text{ }^\circ\text{C}$.

A1.2 E-NMR

Studies were carried out in a wide bore Oxford 4.7 T magnet using a Bruker Biospin NMR console operating at 200.1 MHz. Magnetic field gradients were generated using a diff60 diffusion probe and a Great60 gradient amplifier (Bruker Biospin). The diffusion time was typically 20 ms and the gradient pulse width 1 ms. During the E-NMR measurement the gradient strength was kept constant and the applied electric field was varied. The electrophoretic NMR cell is in-house built and similar to the cell described by Hallberg et al.[55]. The electric field is generated in a 3 cm space between two

platinum ring connected to a homebuilt DC amplifier which is driven by TTL-pulses from the spectrometer and controlled with a customized pulse program. The time between two measurements was set to at least 5 s to avoid local sample heating which may lead to convection. All E-NMR experiments were performed at $T = 25\text{ }^{\circ}\text{C}$.

A1.3 Synthesis / materials preparation

Disodium-3,3'-disulfonate-4,4'-difluorodiphenylsulfone was purchased from Fumatech GmbH (Germany) and ion exchanged to its protonic form using Dow cation exchange resin Marathon C. Fully monosulfonated poly(phenylene sulfone) was synthesized according to [11][12][76]. Hypersulfonated phenylene sulfone was synthesized according to Ref. [15]. All materials were dried in a vacuum oven at $120\text{ }^{\circ}\text{C}$ and 10^{-5} bar pressure prior to use. Electrolyte solutions were prepared with double distilled water. Acronyms are used for all materials according to their corresponding equivalent weight (EW). For example, fully monosulfonated poly(phenylene sulfone) (sPSO_2) $\text{EW} = 220\text{ g mol}^{-1}$ is named $\text{sPSO}_2\text{-220}$.

Sulfonated polysulfones in Li^+ and Na^+ -form were prepared by ion exchanging of their acid form either in a tenfold excess of aqueous 1N LiOH or NaOH stirred solution for 4 hours or by ion exchange resins (Marathon C). The products were purified by dialysis until neutrality. After evaporation of the water in a rotary evaporator, the exchanged polyelectrolytes were dried in vacuum ($p < 10^{-5}$ bar) at $T = 120 - 180\text{ }^{\circ}\text{C}$ for 48 hours. The samples were stored under dried Argon gas before elemental analysis. Exchange levels of close to 100 % with an error of $\pm 2\text{ }%$ were found. Swelling or complete dissolution with solvents (purity $\text{H}_2\text{O} < 10\text{ppm}$) was carried out in dry argon atmosphere. The mixtures were sonicated (SONOREX SUPER) in gas tight glass tubes for at least 12 hours at a temperature of $T = 80\text{ }^{\circ}\text{C}$ which led to the formation of gel like or homogeneous highly viscous materials depending on the target concentration.

A1.4 Conductivity

Cylindrical glass cuvettes (length 15 mm, diameter 4 mm) with platinum disc electrodes were used for conductivity measurements of liquid samples. An opening at the top was used for filling and as an exit for residual gas bubbles within the cell. Conductivity measurements in pure water vapor ($p_{\text{H}_2\text{O}} = 10^5 \text{ Pa}$) were carried out in a double-wall temperature-controlled glass chamber with an open outlet at temperatures between $T = 110$ and $150 \text{ }^\circ\text{C}$. Liquid water was continuously evaporated by a heater and injected into the chamber with a constant flow rate using a digital peristaltic pump (Ismatec). Inside the chamber the samples pressed pellets of total thickness of 2 - 4 mm and 6 mm diameter were placed in a porous cylindrical tube gold electrodes. In-plane membrane conductivities were measured in pure water vapor ($p_{\text{H}_2\text{O}} = 10^5 \text{ Pa}$) with a four-electrode set-up between $T = 110 \text{ }^\circ\text{C}$ and $150 \text{ }^\circ\text{C}$ using a modified commercial conductivity cell (Fumatech). Complex impedance spectroscopy was carried out using a HP 4192A LF impedance analyzer in the frequency range $10^{-2} - 10^7 \text{ Hz}$ using a voltage output of 0.1 V. Specific conductivities was obtained from the high-frequency intercept of the complex impedance with the real axis and the dimensions of the stacks.

A1.5 Swelling and water uptake

Swelling in water was measured by immersing a piece of membrane (0.2 – 0.5 g) in liquid water at different temperatures. The water uptake was calculated from the weight difference of hydrated and dried polymer ($T = 120 \text{ }^\circ\text{C}$ and $p < 10^{-5} \text{ bar}$). The water uptake was measured thermogravimetrically by weighing the sample in situ at $T = 65 \text{ }^\circ\text{C}$ as a function of relative humidity (RH). This was possible through a balance (Mettler AT20), which is magnetically coupled (Rubotherm) to a Teflon crucible containing 0.3 – 0.5 g of polymer (the sample is physically decoupled from the balance through a magnetic coupling). The relative humidity was adjusted using a humidifier with a nitrogen flow of 40 ml min^{-1} , the equilibration time at each RH was between 30 – 40 h. The weight gain was calculated with respect to the weight of the dried sample (30 h in pure nitrogen at $T = 180 \text{ }^\circ\text{C}$).

A1.6 Mechanical testing

Dynamical Mechanical Analysis (DMA) was recorded on a DMA Q 800 (TA Instruments) connected to a homebuilt humidifier with temperature and relative humidity (RH) as parameters. For each set of conditions, temperature and RH were kept constant for 5 h while continuously recording data. The measurements were performed by applying oscillatory sinusoidal tensile deformation with a frequency of $\nu = 1$ Hz, an amplitude of $A = 20 \mu\text{m}$ and a preload force of $F = 0.01$ N on a rectangular film sample of $20 \times 5.3 \times 0.05 - 0.2$ mm.

Stress-strain curves were obtained by the same setup described above in a controlled force mode. The samples were equilibrated at the target temperature and RH until a constant storage modulus was reached. Then a force ramp of 1 N min^{-1} with a preload force of 0.001 N was applied and the elongation was monitored. The corresponding stress was normalized to the cross-section of the membrane at ambient conditions.

A1.7 SAXS

SAXS measurements of sPSO₂-220 and sPSO₂-142 in H⁺-form were carried out at 75 % RH equilibrated samples at 25 °C (diameter: 0.6 cm, thickness: 0.02 - 0.03 cm). The scattering experiments were performed by using a SAXSess camera (Kratky, Anton Paar) equipped with a CCD detector. CuK α radiation with a wavelength of 0.1542 nm was generated by a PANalytical PW3830 X-ray generator operating at 40 kV and 50 mA. The other protonic forms and the blends were also equilibrated at RH = 75 % and then transferred into gas tight cell with two thin Mylar sheet windows. For the DMSO containing samples, 30 mg of viscous electrolytes were transferred into the cells. SAXS experiments were performed at the DUBBLE beam line (BM26B) at the European Synchrotron Radiation Facility (ESRF) in Grenoble (France). The data were collected using a 2D multiwire gas-filled detector with pixel array dimensions of 512×512 . The exposure time for each sample was about 60 s and a wavelength of $\lambda = 1.54 \text{ \AA}$ was used. The experimental data were corrected for the background scattering and transformed into 1D-plots by azimuthal angle integration.

A2. List of Abbreviations and Symbols

A2.1 Abbreviations

AC	alternating current
AN	acceptor number
DMAc	N,N-dimethyl-acetamide
DMC	dimethyl carbonate
DMSO	dimethylsulfoxide
DN	donor number
EC	ethylene carbonate
EIS	electrochemical impedance spectroscopy
E-NMR	electrophoretic NMR
FC	fuel cell
FID	free induction decay
HSAB	hard and soft acids and bases (also known as Pearson acid base concept)
IEC	ion exchange capacity
IS	impedance spectroscopy
LA	Lewis acidity
LB	Lewis basicity
MD	molecular dynamics
NMP	N-methyl-2-pyrrolidone
NMR	nuclear magnetic resonance
PBI	polybenzimidazole
PC	propylene carbonate
PEM	polymer-electrolyte-membrane
PEO	polyethylene oxide
PFG-NMR	pulsed field gradient NMR
PFSA	perfluorosulfonic acid
Py	pyridine
RH	relative humidity
SAXS	small-angle X-ray scattering

A2.2 Symbols

$\vec{\mu}_i$	magnetic moment vector
D_{tr}	tracer diffusion coefficient
$I_{0/G}$	NMR signal intensity
\vec{M}	net magnetization vector
M_n	number average molecular weight
f_c	fraction of condensed ion
f_ξ	fraction of condensed counter-ions
k_B	Boltzmann constant
α_d	polarizability
δ_m	duration of magnetic field pulse
ϵ_0	vacuum permittivity
ϵ_r	dielectric constant (of solvent)
μ_d	dipole moment
μ_i	electrophoretic mobility
ξ_M	Manning parameter
ω_L	Larmor frequency
b	charge spacing on polymerbackbone
B	magnetic field strength
d	SAXS correlation length
D_{H2O}	water tracer diffusion coefficient
D_i	diffusion coefficient
D_σ	conductivity diffusion coefficient
E	electric field
e	elementary charge
EW	equivalent weight
E_z	spin energy states
g	magnetic gradient field strength
\hbar	reduced Planck constant
I	electric current
m_l	magnetic quantum numbers
p_{H2O}	water pressure
q	SAXS scattering vector
r	distance

RH	relative humidity
T	absolute temperature
$t_{+/-}$	transference number
T_1	longitudinal relaxation time
T_2	transversal relaxation time
U	voltage
V	sample volume
v_i	drift velocity
γ	gyromagnetic ratio
Δ	NMR diffusion time
ΔG	Gibbs free energy change
ΔF	free energy change (MD-simulation)
λ	solvent molecules per ionic group
λ_B	Debye length
Φ	NMR signal phase shift
α	degree of dissociation
δ	NMR chemical shifts
ν	NMR resonant frequency
σ	ionic conductivity
Z	complex resistance (impedance)
z	number of charges per particle
Z_{eff}	effective charge of a particle in an electric field

References

- [1] Hess, M., et al. *Pure and Applied Chemistry* 2006, 78, 2067.
- [2] Kreuer, K.D. *Chem. Mater.* 2014, 26, 361.
- [3] Page, K.A.; Soles, C.L., Runt, J. *Polymers for Energy Storage and Delivery: Polyelectrolytes for Batteries and Fuel Cells*, ACS Symposium Series, 2013.
- [4] Maier, J. *Advanced Functional Materials* 2011, 21, 1448.
- [5] Kreuer, K. D.; Wohlfarth, A.; de Araujo, C. C.; Fuchs, A.; Maier, J. *ChemPhysChem* 2011, 12, 2558.
- [6] TOYOTA MOTOR CORPORATION, Toyota Delivers First 'Mirai' to Japan's PM, <http://newsroom.toyota.co.jp/en/detail/5249834/>, Web. Jan. 2015
- [7] Daimler AG, daimler.com/technology-and-innovation/drive-technologies/fuel-cell, Web. Jan. 2015
- [8] Hickner, M.; Ghassemi, H.; Kim, Y.; Einsla, B.; McGrath, J. *Chemical Reviews* 2004, 104, 4587.
- [9] Kreuer, K. D.; Paddison, S.; Spohr, E.; Schuster, M. *Chemical Reviews* 2004, 104, 4637.
- [10] Kerres, J. *Journal of Membrane Science* 2001, 185, 3.
- [11] Schuster, M.; Kreuer, K.D.; Andersen, H.T.; Maier, J. *Macromolecules* 2007, 40, 598.
- [12] Schuster, M.; de Araujo, C.C.; Atanasov, V.; Andersen, H.T.; Kreuer, K.D.; Maier, J. *Macromolecules* 2009, 42, 3129.
- [13] Gubler, L. *Advanced Energy Materials* 2014, 4, 3.
- [14] Titvinidze, G.; Kreuer, K.D.; Schuster, M.; de Araujo, C.C.; Melchior, J.P.; Meyer, W.H. *Adv. Funct. Mater.* 2012, 22, 4456.
- [15] Takamuku, S.; Jannasch, P. *Macromolecules* 2012, 45, 6538.
- [16] Ghassemi, H.; Ndip, G.; McGrath, J. *E. Polymer* 2004, 45, 5855.
- [17] de Araujo, C.C.; Kreuer, K.D.; Schuster, M.; Portale, G.; Mendil-Jakani, H.; Gebel, G.; Maier, J. *Phys. Chem. Chem. Phys.* 2009, 11, 3305.

- [18] Maier, J. *Angewandte Chemie* 2013, 52, 4998.
- [19] Xu, K. *Chemical reviews* 2004, 104, 4303.
- [20] Maier, J. *Electrochimica Acta* 2014, 129, 21.
- [21] Do, K.; Kim, D. *J. Power Sources* 2008, 185, 63.
- [22] Takamuku, S.; Wohlfarth, A.; Manhart, A.; Raeder, P.; Jannasch, P. *Polymer Chemistry* 2014, DOI: 10.1039/C4PY01177E
- [23] Reichardt, C., Welton, T. *Solvents and Solvent Effects in Organic Chemistry*, 2011, Wiley.
- [24] Nazri, G.A., Pistoia, G., *Lithium Batteries: Science and Technology*, 2009, Springer.
- [25] Bockris, J.O.M., Reddy, A.K.N. *Modern Electrochemistry*, v. 2, pt. 1, 2000, Springer.
- [26] Debye, P., Hückel, E. *Physik Z.* 1923, 24, 185.
- [27] IUPAC, *Compendium of Chemical Terminology*, 2nd ed., 1997, p. 1123.
- [28] Gutmann, V., Wychera, E. *Inorganic and Nuclear Chemistry Letters* 1966 ,2, 257.
- [29] Mayer, U., Gutmann, V., Gerger, W. *Monatshefte für Chemie* 1975, 106, 1235.
- [30] Marcus, Y., Hefter, G. *Chemical reviews* 2006, 106, 4585.
- [31] Marcus, Y., *Ion solvation*, 1985, Wiley.
- [32] Manning, G.S. *J. Chem. Phys.* 1969, 51, 924.
- [33] Manning, G.S. *J. Chem. Phys.* 1969, 51, 934.
- [34] Manning, G.S. *Acc. Chem. Res.* 1979, 12, 443.
- [35] Deshkovski, A., Obukhov, S., Rubinstein, M. *Phys. Rev. Lett.* 2001, 86, 2341.
- [36] Biesheuvel, P. M., Cohen Stuart, M. A. *Langmuir* 2004, 2011, 4764.
- [37] Muthukumar, M., Wignall, G.D., Melnichenko, Y.B. *J. Chem. Phys.* 2003, 119, 4085.
- [38] Josef, E., Bianco-Peled, H. *Soft Matter* 2012, 8, 9156.
- [39] Kreuer, K. D. *Journal of membrane science* 2001, 185, 29.
- [40] Ende, D.; Mangold, K.M. *Chemie in unserer Zeit* 1993, 3, 134.
- [41] Barsoukov, E.; Macdonald, J.R. *Impedance Spectroscopy Theory, Experiment, and Applications*, Vol. 2, 2005, John Wiley & Sons, Inc., New Jersey

- [42] Berger, S.; Braun, S. *200 and More NMR Experiments* 2004, Wiley
- [43] Slichter, C.P. *Principles of Magnetic Resonance*, Vol. 1 of Springer Series in Solid-State Sciences, 1996, Springer Science & Business Media
- [44] Stilbs, P. *Progress in Nuclear Magnetic Resonance Spectroscopy* 1987, 19, 1.
- [45] Price, W.S. *Concepts in Magnetic Resonance* 1997, 9, 299.
- [46] Stejskal, E.O.; Tanner, J.E. *The journal of chemical physics* 1965, 42, 288.
- [47] Hahn, E. L. *Physical Review* 1950, 80, 580.
- [48] Håkansson, B.; Nydén, M.; Söderman, O. *Colloid. Polym. Sci.* 2000, 278, 399.
- [49] Packer, K.J. *Mol. Phys.* 1969, 17, 355.
- [50] Holz, M.; Lucas, O.; Müller, C.J. *Magn. Reson.* 1984, 58, 294.
- [51] Saarinen, T.R.; Johnson, C.S. *J. Am. Chem. Soc.* 1988, 110, 3332.
- [52] Scheler, U. *Electrophoretic NMR* 2012. eMagRes.
- [53] Ise, M.; Kreuer, K.D.; Maier, J. *Solid State Ionics* 1999, 125, 213.
- [54] Böhme, U.; Scheler, U. *Chem. Phys. Lett.* 2007, 435, 342.
- [55] Hallberg, F.; Weise, C.F.; Yushmanov, P.V.; Pettersson, E.; Stilbs, P.; Furó, I. *J. Am. Chem. Soc.* 2008, 130, 7550.
- [56] Griffiths, P.C.; Paul, A.; Stilbs, P.; Pettersson, E. *Macromolecules* 2005, 38, 3539.
- [57] Zhang, Z.; Madsen L.A. *J. Chem. Phys.* 2014, DOI: 10.1063/1.4865834
- [58] Bielejewski, M.; Giesecke, M.; Furó, I. *Journal of Magnetic Resonance* 2014, 243, 17.
- [59] Hallberg, F.; Furó, I.; Yushmanov, P.V.; Stilbs, P. *J. Magn. Reson.* 2008, 192, 69.
- [60] Linde, D.R. *CRC Handbook of Chemistry & Physics* (88th ed.), 2007, CRC Press.
- [61] Smiatek, J.; Wohlfarth, A.; Holm, C. *New Journal of Physics* 2014, 16, 025001.
- [62] Wohlfarth, A.; Smiatek, J.; Kreuer, K.D.; Takamuku, S.; Jannasch, P.; Maier, J. *Macromolecules* 2015, accepted.
- [63] Titvinidze, G.; Kreuer, K.D.; Schuster, M.; de Araujo, C.C.; Melchior, J.P.; Meyer, W.H. *Adv. Funct. Mater.* 2012, 22, 4456.

- [64] Oostenbrink, C.; Villa, A.; Mark, A.E.; van Gunsteren, W.F. *J. Comput. Chem.* 2004, 25, 1656.
- [65] Kreuer, K.D. *Solid State Ionics* 2013, 252, 93.
- [66] Gores, H.J.; Barthel, J. *Liquid Nonaqueous Electrolytes* in Handbook of Battery Materials, Wiley-VCH Verlag GmbH & Co. KGaA, 2011.
- [67] Pfaffenhuber, C.; Göbel, M.; Popovic, J.; Maier, J. *Physical Chemistry Chemical Physics* 2013, 15, 18318.
- [68] Bouchet, R.; Maria, S.; Meziane, R.; Aboulaich, A.; Lienafa, L.; Bonnet, J.P.; Armand, M. *Nature materials* 2013, 12, 452.
- [69] Choi, N. S.; Chen, Z.; Freunberger, S.A.; Ji, X.; Sun, Y.K.; Amine, K., Bruce, P. G. *Angewandte Chemie Int. Ed.* 2012, 51, 9994.
- [70] Freunberger, S.A.; Chen, Y.; Peng, Z.; Griffin, J.M.; Hardwick, L. J.; Bardé, F.; Bruce, P. G. *Journal of the American Chemical Society* 2011, 133, 8040.
- [71] Peng, Z.; Freunberger, S.A.; Hardwick, L.J.; Chen, Y.; Giordani, V.; Bardé, F.; Bruce, P. G. *Angewandte Chemie Int. Ed.* 2011, 123, 6475.
- [72] Peng, Z.; Freunberger, S.A.; Chen, Y.; Bruce, P. G. *Science* 2012, 337, 563.
- [73] Kerres, J.A. *Journal of Membrane Science* 2001, 185, 3.
- [74] RÖMPP Online – Version 4.0 Thieme Chemistry, Stuttgart, 2015.
- [75] Wohlfarth, A.; Titvinidze, G.; Takamuku, S.; Meyer, W. H.; Kreuer K.-D., *European Patent Application* 2014, 14000404.5.
- [76] Atanasov, V.; Buerger, M.; Wohlfarth, A.; Schuster, M.; Kreuer, K.D.; Maier, J. *Polymer bulletin* 2012, 68, 317.

Danksagung

An dieser Stelle möchte ich mich bei allen bedanken, die mich bei der Anfertigung dieser Arbeit unterstützt haben:

Zuerst danke ich meinem Doktorvater Herrn Prof. Dr. Joachim Maier für die freundliche Aufnahme in seiner Abteilung am Max-Planck-Institut für Festkörperforschung, für die exzellenten Arbeitsmöglichkeiten und sein stets motivierendes Interesse am Fortgang dieser Arbeit.

Ganz besonders möchte ich mich bei Dr. Klaus-Dieter Kreuer bedanken. Die spannende Aufgabenstellung, das immense Fachwissen, die tiefen wissenschaftlichen Diskussionen und der persönliche Kontakt werden mir immer in sehr guter Erinnerung bleiben. Besonders die Freiheit in der Gestaltung der Arbeit und die unermüdliche Motivation, gemeinsam komplexe Zusammenhänge zu verstehen, habe ich sehr genossen.

Ich bedanke mich bei Frau Prof. Dr. Sabine Ludwigs für die freundliche Übernahme des Mitberichts und bei Herrn Prof. Dr. Thomas Schleid für die Übernahme des Prüfungsvorsitzes.

Desweiteren danke ich Sofia Weiglein für den stets verlässlichen Rat rund um Organisation und Bürokratie.

Viele Ideen und Fragestellungen konnten nur Dank hervorragender Kollaborationspartner untersucht werden. Dr. Shogo Takamuku, Dr. Giorgi Titvinidze und Dr. Wolfgang Meyer vom Max-Planck-Institut für Polymerforschung danke ich für die inspirierende Zusammenarbeit bei der Materialsynthese. Dr. Jens Smiatek und Prof. Dr. Christian Holm vom Institut für Computerphysik an der Universität Stuttgart danke ich für die enge Zusammenarbeit und die Durchführung der Simulationen. Prof. Dr. Patric Jannasch von der Lund Universität (Schweden) danke ich für die zahlreichen Diskussionen und SAXS-Messungen. Dr. Guiseppa Portale von der European Synchrotron Radiation Facility Grenoble (Frankreich) danke ich für die Unterstützung

bei zahlreichen SAXS Messungen an der BM26 – DUBBLE beamline. Für die spannenden Einblicke in die großtechnische Membranherstellung danke ich Dr. Michael Schuster von der Fuma-Tech GmbH.

Darüber hinaus bedanke mich bei allen Mitarbeitern und Kollegen der Abteilung Maier, vor allem bei Jan Melchior und Michael Marino, für alle wissenschaftlichen und nicht wissenschaftlichen Beiträge, die zu sehr interessanten und hilfreichen Diskussionen geführt haben. Zusätzlich möchte ich mich bei Jan für seine kompetente und ausdauernde Hilfe bei allen technischen und wissenschaftlichen Fragen rund um die NMR-Spektroskopie bedanken.

Außerdem bedanke ich mich bei allen technischen Mitarbeitern der Abteilung für die experimentelle Unterstützung: Annette Fuchs (REM, IS), Udo Klock (TGA, DMA, Pumpen), Uwe Traub (IT-Unterstützung), Peter Senk (Handschuhboxen) und Ewald Schmitt (mechanisch-technische Hilfe). Desweiteren möchte ich mich bei den Glasbläsern für die Anfertigung zahlreicher Glaszellen und bei der elektronischen Werkstatt für den Bau des benötigten NMR-Equipments bedanken. Insbesondere möchte ich mich auch bei Annette und Babsi für die „kleinen Pausen“ bedanken, durch die ich den Kopf immer wieder frei bekommen habe für neue Gedanken.

Dem Bundesministerium für Wirtschaft und Energie (BMWi) und dem Bundesministerium für Bildung und Forschung (BMBF) danke ich für die zusätzliche finanzielle Unterstützung durch die Projekte PSUMEA I (03ET2004A) und PSUMEA II (03SF0473).

Mein herzlichster Dank gilt meiner Familie und meinen Freunden, ohne ihren Rückhalt und ihr Vertrauen wäre ich heute nicht an diesem Punkt angekommen.

Mein abschließender und tiefster Dank gilt meiner Verlobten Anita für ihre unendliche Unterstützung, ihre Liebe und Motivation.

Danke.

Curriculum Vitae

Andreas Wohlfarth * 02.08.1986 in Sigmaringen
Stöckachstr. 1 | 70190 Stuttgart | 0176 63783190|wohlfarth.andreas@gmail.com

Ausbildung

seit 10/2011 Promotion am Max-Planck-Institut für Festkörperforschung Stuttgart, unter Dr. Kreuer und Prof. Dr. Maier, „New electrolytes for batteries and fuel cells“

10/2006 – 09/2011 Studium der Chemie, Universität Stuttgart, Diplom (Gesamtnote 1.9), Diplomarbeit: „Präparation und Charakterisierung Lithium-leitender Polyelektrolyte“ am Max-Planck-Institut für Festkörperforschung (MPI-FKF), Stuttgart (Gesamtnote 1.0)

09/1997 – 07/2006 Stauferymnasium Pfullendorf, Abitur (Durchschnittsnote 2.3)

Auslandserfahrung

seit 07/2012 mehrere Forschungsaufenthalte am ILL und ESRF in Grenoble, Frankreich

04/2010 – 09/2010 ERASMUS Praktikum an der KTH Stockholm, Schweden, unter Prof. Dr. Franzén, Thema: Highly Effective Stereoselective Synthesis of Quinolizidine-Derivatives

Auszeichnungen

Outstanding young researcher award (International Society of Electrochemistry)

GDCh-Preis für das beste Abitur im Fach Chemie (Gesellschaft Deutscher Chemiker)

Preis für besondere soziale Leistungen (Staufer Gymnasium Pfullendorf)

Sprachkenntnisse

Deutsch (Muttersprache)

Englisch (verhandlungssicher)

Französisch (Schulkenntnisse)

Publikationen, Patente und Vorträge

Wohlfarth A.; Smiatek, J.; Kreuer, K.D.; Takamuku, S.; Jannasch, P.; Holm, C.; Maier, J. (2015) Dissociation of sulfonated polysulfones: importance of molecular structure and conformation, *Macromolecules*

Wohlfarth, A.; Kreuer, K.D., Titvinidze, G.; Takamuku, S.; Meyer, W., (2014) Europäische Patentanmeldung 14000404.5, Polymer blends with high ion-exchange capacity and high ion-conductivity as well as methods for preparing the same

Wohlfarth A.; Takamuku, S.; Titvinidze, G.; Marino, M.; Melchior, J.; Kreuer, K.D. (2015) Acid-Base blending of highly sulfonated polysulfones – in preparation –

Takamuku, S.; Wohlfarth, A.; Manhart, A.; Raeder, P.; Jannasch, P. (2015) Hypersulfonated Polyelectrolytes: Preparation, Stability and Conductivity, *Polymer Chemistry*

Marino, M.; Melchior, J.; Wohlfarth, A.; Kreuer, K.D. (2014) Hydroxide, halide and water transport in a model anion exchange membrane, *Journal of Membrane Science*

Titvinidze, G.; Wohlfarth, A.; Kreuer, K.D.; Schuster, M.; Meyer W.H. (2014) Reinforcement of Highly Proton Conducting Multi-Block Copolymers by Online Crosslinking, *Fuel Cells*

Smiatek, J.; Wohlfarth, A.; Holm, C. (2014) The solvation and ion condensation properties for sulfonated polyelectrolytes in different solvents – a computational study, *New Journal of Physics*

Wohlfarth, A. (2014) Dissociation behavior of highly sulfonated polyelectrolytes in H⁺, Li⁺ and Na⁺ form, Vortrag, 14th International Symposium on Polymer Electrolytes, Geelong, Australia

Wohlfarth, A. (2014) Interactions driving Nafion's nano-morphology and visco-elastic properties, Poster, 14th International Symposium on Polymer Electrolytes, Geelong, Australia

Wohlfarth, A. (2014) Transport and Stability Issues of Anion Exchange Membranes, Poster, 14th International Symposium on Polymer Electrolytes, Geelong, Australia

Wohlfarth, A. (2013) Polyelectrolytes for Fuel Cells and Batteries, Vortrag, MIT Forum on Materials for Sustainable Energy, Boston, USA

Wohlfarth, A.; Fuchs, A.; Kreuer, K-D.; Maier, J., (2012) WO Patent 2012059222, Alkaline single ion conductors with high conductivity and transference number and methods for preparing the same

Kreuer, K.D.; Wohlfarth, A. (2012) Limits of Proton Conductivity, *Angewandte Chemie*

Atanasov, V.; Bürger, M.; Wohlfarth, A.; Schuster, M.; Kreuer, K.D.; Maier J. (2012) Highly sulfonated poly(phenylene sulfones): optimization of the polymerization conditions, *Polymer Bulletin*

Wohlfarth, A. (2012) Single Alkaline (Li⁺, Na⁺) Ion Conducting Polyelectrolytes for Battery Applications, Vortrag, 63rd Annual Meeting of the International Society of Electrochemistry, Prague, Czech Republic

Wohlfarth, A. (2012) Solvation and mobility in lithium-polyelectrolytes for battery applications, Vortrag, GDCh Electrochemistry, München

Wohlfarth, A. (2012) Ion solvation and mobility in lithium-polyelectrolytes for battery applications, Poster, 9th International Symposium on Polyelectrolytes, Lausanne, Switzerland

Wohlfarth, A. (2012) Single Alkaline (Li⁺, Na⁺) Ion Conducting Polyelectrolytes for Battery Applications: Solvation and Dissociation Issues, Poster, Bunsentagung, Leipzig

Zhang, W.; Juho B.; Wohlfarth, A.; Franzén, J. A (2011) Stereodivergent Strategy for the Preparation of Corynantheine and Ipecac Alkaloids, *Chemistry – A European Journal*

Kreuer, K.D.; Wohlfarth, A.; de Araujo, C. C.; Fuchs, A.; Maier, J. (2011) Single Alkaline-Ion (Li⁺, Na⁺) Conductors by Ion Exchange of Proton-Conducting Ionomers and Polyelectrolytes, *ChemPhysChem*

Pfaffenhuber C.; Weichert K.; Wohlfarth, A.; Kreuer, K.D.; Maier, J. (2011) Novel semi-solid electrolytes for Li-based batteries, *MPG-FKF Annual Report*

Wohlfarth, A. (2011) Single Alkaline-Ion (Li⁺, Na⁺) Conductors by Ion Exchange of Proton-Conducting Ionomers and Polyelectrolytes, Vortrag, 18th International Conference on Solid State Ionics, Warsaw, Poland

Bender, J.; Wohlfarth, A.; Hoch, C.; (2010) New Alkali Metal-rich Oxometallates, *Zeitschrift für Naturforschung Sektion B*

Hoch, C.; Bender, J.; Wohlfarth, A.; Simon, A. (2009) The Suboxometallates A₉MO₄, *Zeitschrift für Anorganische und Allgemeine Chemie*